

Table of Contents

Chapter		Page	
I.	INTRODUCTION AND OVERVIEW	1	1/A7
II.	EXPERIMENTAL METHODOLOGY AND PROCEDURES	3	1/A9
II.A.	Heat Transfer with Full-Coverage Film Cooling . .	3	1/A9
II.B.	Stanford Experimental Program	5	1/A11
II.C.	Experimental Facility	6	1/A12
II.D.	Heat-Flux Data Acquisition	7	1/A13
II.D.1.	Spanwise-averaged data	7	1/A13
II.D.2.	Local heat flux data	8	1/A14
III.	HEAT TRANSFER FOR THREE INJECTION GEOMETRIES	11	1/B4
III.A.	Temperature Parameter	11	1/B4
III.B.	Mass Flux Ratio	11	1/B4
III.C.	Initial Conditions	13	1/B6
III.D.	Number of Rows of Holes	14	1/B7
III.E.	Hole Spacing	15	1/B8
III.F.	Concluding Remarks	16	1/B9
IV.	LOCAL HEAT FLUX DATA	20	1/B13
IV.A.	Experimental Test Conditions	20	1/B13
IV.A.1.	Presentation of the data	20	1/B13
IV.A.2.	Symmetry of the data	22	1/C3
IV.A.3.	Comparison of third and fifth blowing row data	22	1/C3
IV.A.4.	Low-M data	24	1/C5
IV.A.5.	High-M data	25	1/C6
IV.A.6.	Comparison to spanwise-averaged data . .	26	1/C7
IV.C.	Concluding Remarks	27	1/C8
V.	NUMERICAL PREDICTION PROGRAM	34	1/D7
V.A.	Introduction	34	1/D7
V.B.	The STANCOOL Program	34	1/D7
V.C.	Injection Model	36	1/D9
V.C.1.	Model development	36	1/D9
V.C.2.	STANCOOL injection model	37	1/D10
V.D.	Turbulence-Augmentation Model	40	1/D13
V.D.1.	Model development	40	1/D13
V.D.2.	STANCOOL turbulence model	41	1/D14
V.E.	Summary and Constants for the Model	43	1/E2
V.F.	Prediction of the Data Bases	44	1/E3
References	69	1/G1

A	MODIFYING STAN5 TO OBTAIN STANCOOL	71	1/G3
B	PREVIOUSLY UNREPORTED SLANT-INJECTION DATA	87	2/A7
B.1.	Data with 11 rows blowing, heated starting length	89	2/A9
B.1.a.	Initial profiles of temperature and velocity	89	2/A9
B.1.b.	M = 0.20; $\theta \approx 1$	90	2/A11
	M = 0.20; $\theta \approx 0$	91	2/A13
	M = 0.20; $\theta \approx 1$, $\theta = 0$ by superposition	92	2/B1
B.1.c.	M = 0.6; $\theta \approx 1$	93	2/B3
	M = 0.6; $\theta \approx 0$	94	2/B5
	M = 0.6; $\theta \approx 1$, $\theta = 0$ by superposition	95	2/B7
B.1.d.	M = 0.75; $\theta \approx 1$	96	2/B9
	M = 0.75; $\theta \approx 0$	97	2/B11
	M = 0.75; $\theta \approx 1$, $\theta = 0$ by superposition	98	2/B13
B.1.e.	M = 0.90; $\theta \approx 1$	99	2/C1
	M = 0.90; $\theta \approx 0$	100	2/C3
	M = 0.90; $\theta \approx 1$, $\theta = 0$ by superposition	101	2/C5
B.1.f.	M = 1.33; $\theta \approx 1$	102	2/C7
	M = 1.33; $\theta \approx 0$	103	2/C9
	M = 1.33; $\theta \approx 1$, $\theta = 0$ by superposition	104	2/C11
B.2.	Data with 6 rows blowing, heated starting length	105	2/C13
B.2.a.	Initial profiles of temperature and velocity	105	2/C13
B.2.b.	M = 0.4; $\theta \approx 1$	106	2/D1
	M = 0.4; $\theta \approx 0$	107	2/D3
	M = 0.4; $\theta \approx 1$, $\theta = 0$ by superposition	108	2/D5
B.2.c.	M = 0.9; $\theta \approx 1$	109	2/D7
	M = 0.9; $\theta \approx 0$	110	2/D9
	M = 0.9; $\theta \approx 1$, $\theta = 0$ by superposition	111	2/D11

item 830-H-4

NAS 1.2613219

JAN 31 1980

NASA Contractor Report 3219

COMPLETED

ORIGINAL

**Full-Coverage Film Cooling on Flat,
Isothermal Surfaces: A Summary
Report on Data and Predictions**

M. E. Crawford, W. M. Kays, and R. J. Moffat

CONTRACT NAS3-14336
JANUARY 1980

NASA

116

NASA Contractor Report 3219

Full-Coverage Film Cooling on Flat, Isothermal Surfaces: A Summary Report on Data and Predictions

M. E. Crawford, W. M. Kays, and R. J. Moffat
Stanford University
Stanford, California

Prepared for
Lewis Research Center
under Contract NAS3-14336



National Aeronautics
and Space Administration

**Scientific and Technical
Information Office**

1980

Table of Contents

Chapter	Page
I. INTRODUCTION AND OVERVIEW	1
II. EXPERIMENTAL METHODOLOGY AND PROCEDURES	3
II.A. Heat Transfer with Full-Coverage Film Cooling . .	3
II.B. Stanford Experimental Program	5
II.C. Experimental Facility	6
II.D. Heat-Flux Data Acquisition	7
II.D.1. Spanwise-averaged data	7
II.D.2. Local heat flux data	8
III. HEAT TRANSFER FOR THREE INJECTION GEOMETRIES	11
III.A. Temperature Parameter	11
III.B. Mass Flux Ratio	11
III.C. Initial Conditions	13
III.D. Number of Rows of Holes	14
III.E. Hole Spacing	15
III.F. Concluding Remarks	16
IV. LOCAL HEAT FLUX DATA	20
IV.A. Experimental Test Conditions	20
IV.A.1. Presentation of the data	20
IV.A.2. Symmetry of the data	22
IV.A.3. Comparison of third and fifth blowing row data	22
IV.A.4. Low-M data	24
IV.A.5. High-M data	25
IV.A.6. Comparison to spanwise-averaged data . .	26
IV.C. Concluding Remarks	27
V. NUMERICAL PREDICTION PROGRAM	34
V.A. Introduction	34
V.B. The STANCOOL Program	34
V.C. Injection Model	36
V.C.1. Model development	36
V.C.2. STANCOOL injection model	37
V.D. Turbulence-Augmentation Model	40
V.D.1. Model development	40
V.D.2. STANCOOL turbulence model	41
V.E. Summary and Constants for the Model	43
V.F. Prediction of the Data Bases	44
References	69

A	MODIFYING STAN5 TO OBTAIN STANCOOL	71
B	PREVIOUSLY UNREPORTED SLANT-INJECTION DATA	87
B.1.	Data with 11 rows blowing, heated starting length	89
B.1.a.	Initial profiles of temperature and velocity	89
B.1.b.	M = 0.20; $\theta \approx 1$	90
	M = 0.20; $\theta \approx 0$	91
	M = 0.20; $\theta \approx 1$, $\theta = 0$ by superposition .	92
B.1.c.	M = 0.6; $\theta \approx 1$	93
	M = 0.6; $\theta \approx 0$	94
	M = 0.6; $\theta \approx 1$, $\theta = 0$ by superposition .	95
B.1.d.	M = 0.75; $\theta \approx 1$	96
	M = 0.75; $\theta \approx 0$	97
	M = 0.75; $\theta \approx 1$, $\theta = 0$ by superposition .	98
B.1.e.	M = 0.90; $\theta \approx 1$	99
	M = 0.90; $\theta \approx 0$	100
	M = 0.90; $\theta \approx 1$, $\theta = 0$ by superposition .	101
B.1.f.	M = 1.33; $\theta \approx 1$	102
	M = 1.33; $\theta \approx 0$	103
	M = 1.33; $\theta \approx 1$, $\theta = 0$ by superposition .	104
B.2.	Data with 6 rows blowing, heated starting length .	105
B.2.a.	Initial profiles of temperature and velocity	105
B.2.b.	M = 0.4; $\theta \approx 1$	106
	M = 0.4; $\theta \approx 0$	107
	M = 0.4; $\theta \approx 1$, $\theta = 0$ by superposition .	108
B.2.c.	M = 0.9; $\theta \approx 1$	109
	M = 0.9; $\theta \approx 0$	110
	M = 0.9; $\theta \approx 1$, $\theta = 0$ by superposition .	111

Chapter I

INTRODUCTION AND OVERVIEW

The study of full-coverage film cooling using flat surfaces was carried out between July, 1971, and December, 1977, under Contract NAS3-14336. The study was divided into two principal phases: experimental studies of the heat transfer and hydrodynamics and analysis of the data using integral and differential means.

To date, five comprehensive data reports in the form of NASA Contractor Reports have been issued [1,2,3,4,5], which document all of the experimental data except that contained in the present report. Also during this program, the Stanford boundary layer program was revised into a program called STAN5 and documented as a NASA Contractor Report [6].

The experimental methodology and procedures are described in Chapter II. Heat transfer with full-coverage film cooling is defined in a manner analogous to transpiration cooling, and the superposition approach to film cooling is described. The objectives of the experimental data program and experimental facility are then outlined, and the methods for acquisition of spanwise-averaged and local heat-flux data are described.

A summary of the heat transfer data is contained in Chapter III, covering normal-, 30° slant-, and $30^\circ \times 45^\circ$ compound-angled injection geometries and hole-spacing-to-hole-diameter ratios of 5 and 10. Included are the effects of injection temperature (θ , temperature parameter), mass flux ratio (M), boundary-layer upstream initial conditions, number of rows of holes, and hole spacing.

Chapter IV documents an investigation of the local heat flux distribution carried out on the 30° slant-angled injection test section. Data were acquired for two mass flux ratios at ten locations around an injection site. Full-coverage and recovery region heat transfer data for six rows of holes were also acquired as a part of the local heat flux study (see Chapter III).

A differential prediction program, STANCOOL, is described in Chapter V, and a user's guide on how to modify STAN5 to obtain STANCOOL is given in Appendix A. The chapter includes a description of the background

development work and the final versions of the injection model and turbulence-augmentation model. The chapter also contains recommended model constants and sample predictions. STANCOOL was the outgrowth of the analytical work described in NASA Contractor Reports [1,3,4].

Appendix B contains heat transfer data for six and eleven rows of film cooling and slant-angled injection. The data were acquired with an initial momentum thickness Reynolds number of about 3000 and a heated starting length. Mass flux parameter values for the six-row data were nominally 0.4 and 0.9, and for the eleven-row data they were 0.2, 0.6, 0.75, 0.9, and 1.25. The eleven-row data complement the flat plate and 0.4 data in Reference 3 to form a complete data set.

Chapter II

EXPERIMENTAL METHODOLOGY AND PROCEDURES

A. Heat Transfer with Full-Coverage Film Cooling

A conventional means for describing convective heat transfer from a surface (on a flux basis) is via the rate equation

$$\dot{q}'' = h(T_{\infty}^* - T_w) \quad (1)$$

where T_{∞}^* is the mainstream temperature*, T_w is the wall temperature, and h is the local heat transfer coefficient.

The bulk of two- and three-dimensional film-cooling research to date has used a modified form of Eqn. (1) with T_{∞} being replaced by T_{aw} , the temperature an adiabatic wall would attain downstream of the last coolant injection location. The heat transfer coefficient is replaced by h_o , the coefficient that would exist for the same Reynolds number but without injection. Much of the early experimental research involved obtaining distributions of T_{aw} for various geometries and injection conditions. When T_{aw} is properly non-dimensionalized, an expression called "effectiveness" obtains. It ranges numerically from 0 to 1 and reflects the degree to which the downstream surface is protected by the upstream coolant injection (i.e., it will be 0 for no protection, and it will be 1 if the coolant causes the downstream surface heat flux to be reduced to zero). The development of the theory leading to this approach to film-cooling heat transfer is summarized by Eckert [7].

The conventional meaning of effectiveness as the sole indicator of surface protection from high heat flux is not valid in the region where the actual heat transfer coefficient, h , differs appreciably from h_o . This variation occurs in the region near a hole or a row of holes and is due to the effects of the coolant injection on the hydrodynamic boundary layer. Surface heat flux with film cooling is a two-parameter problem requiring information on both h and effectiveness.

* For a flow Mach number greater than about 0.25, a mainstream recovery temperature or adiabatic wall temperature should be used.

The Stanford film-cooling research program has adopted Eqn. (1) to describe heat transfer with full-coverage film cooling, without reference to "effectiveness." All effects of film cooling are carried in h . This approach was first described by Choe et al. [8]. Its focal point is the linearity of the constant-property thermal energy equation, which would govern the Stanford film-cooling experiments. A non-dimensional temperature parameter is defined

$$\theta = \frac{T_{\infty} - T_j}{T_{\infty} - T_w} \quad (2)$$

where T_j is the coolant injection temperature. Using superposition theory on the linear thermal energy equation yields a calculation equation for h ,

$$h(\theta) = h(\theta_0) - \theta \cdot [h(\theta_1) - h(\theta_0)] \quad (3)$$

Calculation of h for a given injection temperature requires information on h for two values of the temperature parameter, for the same value of M .

Use of Eqn. (1) for film cooling permits an easy comparison of heat transfer coefficients with and without film cooling, because both coefficients have the same temperature-driving potential. Eqn. (1) can also be used to describe transpiration cooling heat transfer; hence it is simple to compare full-coverage film cooling with transpiration cooling (transpiration is a $\theta = 1$ condition, since the transpired coolant leaves the surface at the same temperature as the surface). The comparison of h with film cooling to the h of an uncooled surface or transpiration-cooled surface can be made on a Stanton number basis. Correlations for St_0 (without film cooling) and St with transpiration cooling can be found in Ref. 9.

With a given full-coverage film-cooling geometry, the film-cooling Stanton number depends on both the hydrodynamic and the thermal characteristics of the coolant and mainstream flow, and on the surface thermal boundary condition. Hydrodynamic characteristics are described by the coolant-to-mainstream mass flux ratio (blowing ratio), based on the flow area of one hole,

$$M = \frac{(\rho U)_j}{(\rho U)_{\infty}} \quad (4)$$

where (ρU) is the mass density-velocity product and the subscripts ∞ and j denote mainstream and coolant conditions. The thermal characteristics of the coolant, mainstream, and surface are defined by θ , the temperature parameter given in Eqn. (2). The initial condition of the boundary layer, at the start of the film-cooling region, can be represented by its momentum thickness Reynolds number, $Re_{\delta_2} = U_{\infty} \delta_2 / \nu$ and its enthalpy thickness Reynolds number, $Re_{\Delta_2} = U_{\infty} \Delta_2 / \nu$.

B. Stanford Experimental Program

The objective of the Stanford studies has been to amass sufficient data to support development of analytical methods for predicting heat and momentum transfer with full-coverage film cooling. The boundary layer on a full-coverage surface is periodic across the span and is three-dimensional. For a given full-coverage geometry, the Stanton number should depend on the following parameters: θ , M , and initial Re_{δ_2} and Re_{Δ_2} ; Prandtl number, Mach number, and Eckert number for the coolant and mainstream; mainstream turbulence, surface rotation and curvature, and mainstream pressure gradients.

The Stanford experimental program focused upon three parameters for each geometry tested: θ , M , and upstream boundary layer conditions. Three geometries were investigated, all using flat surfaces with eleven rows of holes in each surface. The hole angles corresponded to normal-angled injection (90 degrees to the surface), slant-angled injection (30 degrees to the surface in the downstream direction), and compound-angled injection (30 degree slant injection that was skewed 45 degrees from the spanwise direction). The holes were spaced five diameters apart in the spanwise and streamwise directions.

The θ parameter was controlled by using one constant temperature for the surface and another for the mainstream, while varying the secondary injection temperature. Values chosen were: $T_j = T_{\infty}$, θ_0 ($\theta = 0$), and $T_j = T_w$ defining θ_1 ($\theta = 1$). The M parameter was controlled by varying the injection velocity, using a constant mainstream velocity. The injection temperature was kept within 15 K of the surface temperature to eliminate density effects, and M varied from 0 (a baseline data points without blowing) to about 1.5. The upstream initial conditions were set

by controlling the hydrodynamic and thermal boundary layer development over the preplate. The momentum thickness Reynolds number, Re_{δ_2} , varied from 500 to 3000, and Re_{Δ_2} varied from 500 to 2000. The ratio of hole diameter to momentum thickness varied from 10 at the low initial momentum Reynolds number down to 2 at the high values.

C. Experimental Facility

The experimental program was carried out in a closed-loop wind-tunnel facility. The tunnel floor consisted of a preplate, a test section, and an instrumented afterplate, with all plates capable of being heated to a temperature 15 K above that of the mainstream. A secondary air loop of the wind tunnel delivered air, heated or cooled, to the discrete-hole test section. Fig. 1 shows a schematic of the wind tunnel.

The main air loop of the wind tunnel was driven by a blower which delivered air through a delivery duct, oblique header, heat exchanger, screen pack, and contraction nozzle, and into the tunnel duct. The duct was 51 cm wide, 20 cm high, and 2.5 m long. Flow left the tunnel duct through a plenum box that supplied both the secondary blower and the primary blower. Velocity could be varied in steps from 7 m/s to 35 m/s, and the velocity was held constant along the test section and afterplate by adjustment of the flexible top wall of the tunnel.

The secondary air loop of the wind tunnel provided heated, measured air to the injection hole. The flow was delivered via eleven individual ducts, one for each row of holes, each containing a hot-wire anemometer type of flow measurement device.

Copper plates, 0.5 cm deep by 45 cm wide by 6 cm long in the flow direction, formed the test surface, with the first plate blank (the upstream guard plate) and the eleven downstream plates containing alternate rows of nine holes and eight holes, each 1.03 cm in diameter. The holes were spaced on 5 diameter centers, in both the spanwise and flow directions, and formed a staggered array. Heater wires were glued into two grooves machined into the back side of each plate. The plates were supported by an aluminum frame across their ends, and phenolic standoff along their spans (to minimize conduction heat loss from the plates and to isolate the plates from each other). Four iron-constantan thermocouples were installed

from the back side of each plate, with each thermocouple located midway between two adjacent holes. Low-conductivity air-delivery tubes extended back from the plate surface, and one tube in each row contained an iron-constantan thermocouple. The cavity was loosely packed with insulating material and closed with bottom plates. Both the frame and bottom plates were heated to minimize conduction loss from the plates. The test-plate power system delivered stabilized AC power to each plate, metered by inserting a wattmeter into the circuit. The reading was corrected for calibration and circuit-insertion losses. Uncertainty in plate power measurement was felt to be 0.3 w.

The preplate and afterplate of the test surface were identical in design, and each was formed of 48 copper plates, each 2.6 cm long in the flow direction. Twenty-four plates were supported by rectangular copper tubes which passed hot water for plate-temperature control. The plates were arranged such that the downstream half of the preplate and the upstream half of the afterplate were heated. Calibrated heat flux meters were located in the afterplate and were used to obtain Stanton number data for the flow as it recovers from the blowing region effect. Uncertainty in afterplate heat flux measurements was estimated at 3 percent.

D. Heat-Flux Data Acquisition

1. Spanwise-averaged data

Heat-flux measurements were obtained in the film-cooling region using a steady-state energy-balance technique. The electrical power delivered to a plate containing a row of holes was measured, and all energy losses from the plate other than by convection from the working surface were accounted for as accurately as possible. Energy-loss modes were modeled in the data-reduction program as radiation from the plate top surface, conduction between the plate and frame, conduction between adjacent plates, and convection between the plate hole area and the injectant. The resulting average heat flux for the plate was then defined as $\dot{q}_{s-a}'' = (E-L)/A_{tot}$, where E is the energy supplied to the plate, L is the sum of the energy-loss modes other than by forced convection, and A_{tot} is the total plate area. Since the plate had holes spaced P apart across the span and the injectant boundary condition was spanwise periodic, the area for heat flux

can be interpreted as that associated with one hole. This is depicted in Fig. 2. Accuracy for the Stanton number data is estimated using a root-sum square uncertainty analysis to be ± 2.5 percent for the $\theta = 1$ data and ± 5 percent for the $\theta = 0$ data. The larger uncertainty for the latter data reflects the uncertainty tied to the plate-injectant convective loss constant.

2. Local heat flux data

Measurements of local heat flux were made in the full-coverage region with a ten-junction RdF Microfoil Heat Flow Sensor. The sensor was fabricated for three laminated sections with its sensing element in the middle laminate. The outer laminates served as protective covers. The sensing element was a thermopile made of $0.51 \mu\text{m}$ thermoelectric alloy foil materials, butt-welded to form the junctions. In the middle laminate was a chromel-alumel thermocouple to measure the sensor temperature. Dimensions of the laminated sensor were 0.025 cm thick by 0.5 cm wide by 1.9 cm long. Local heat flux data for each test were obtained at ten locations within an area around a hole, as indicated on the data figures in the next section. The sensor was attached to the heat transfer surface using a 3-M Scotch Brand Tape No. 415, with the leads trailing in the downstream direction. After installation of the sensor on the plate (for a particular location), the plate was allowed to return to steady-state conditions before a measurement was recorded. Uncertainty for the heat-flux measurements was estimated to be ± 4 percent.

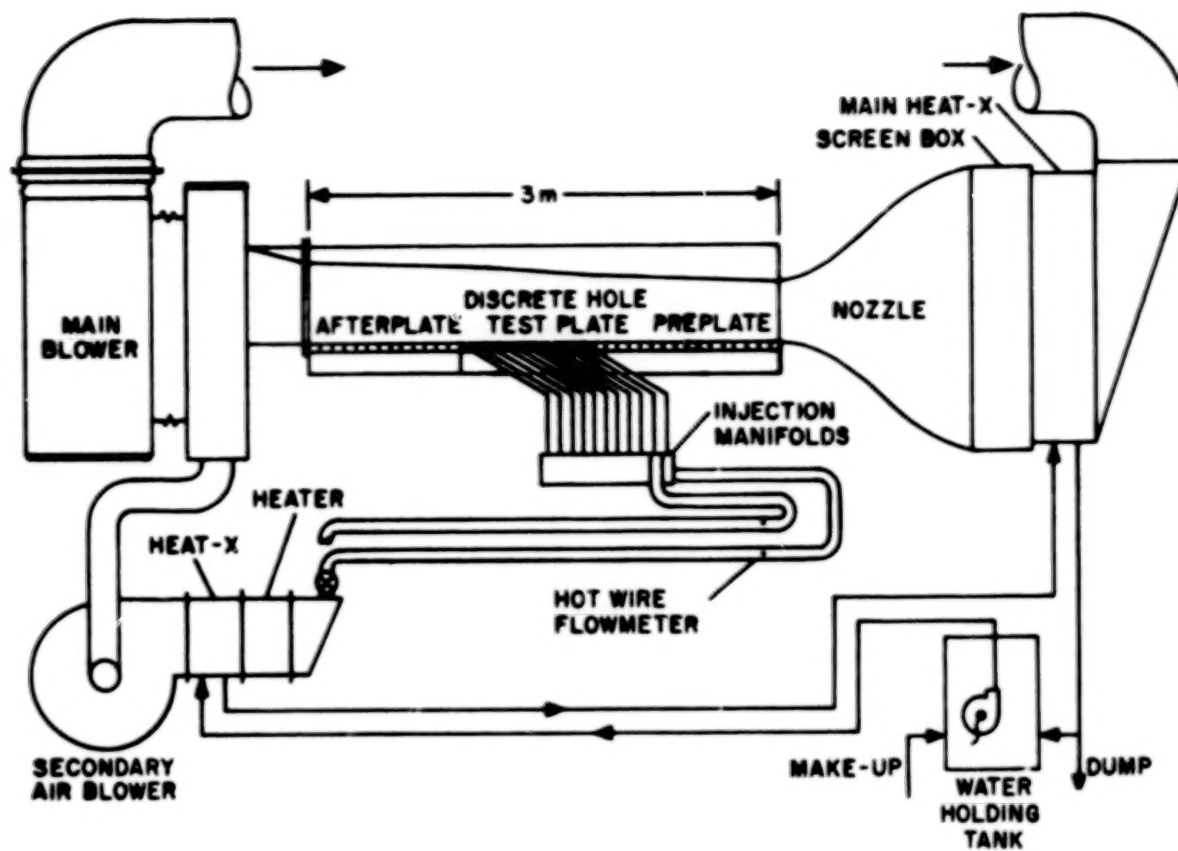


Fig. 1. Schematic of the full-coverage test apparatus

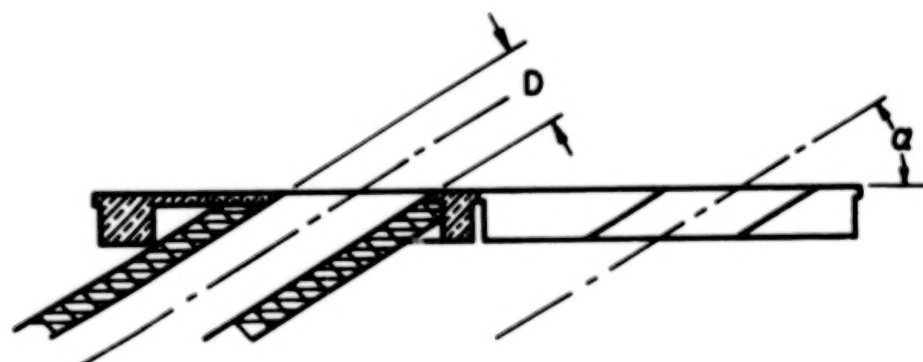
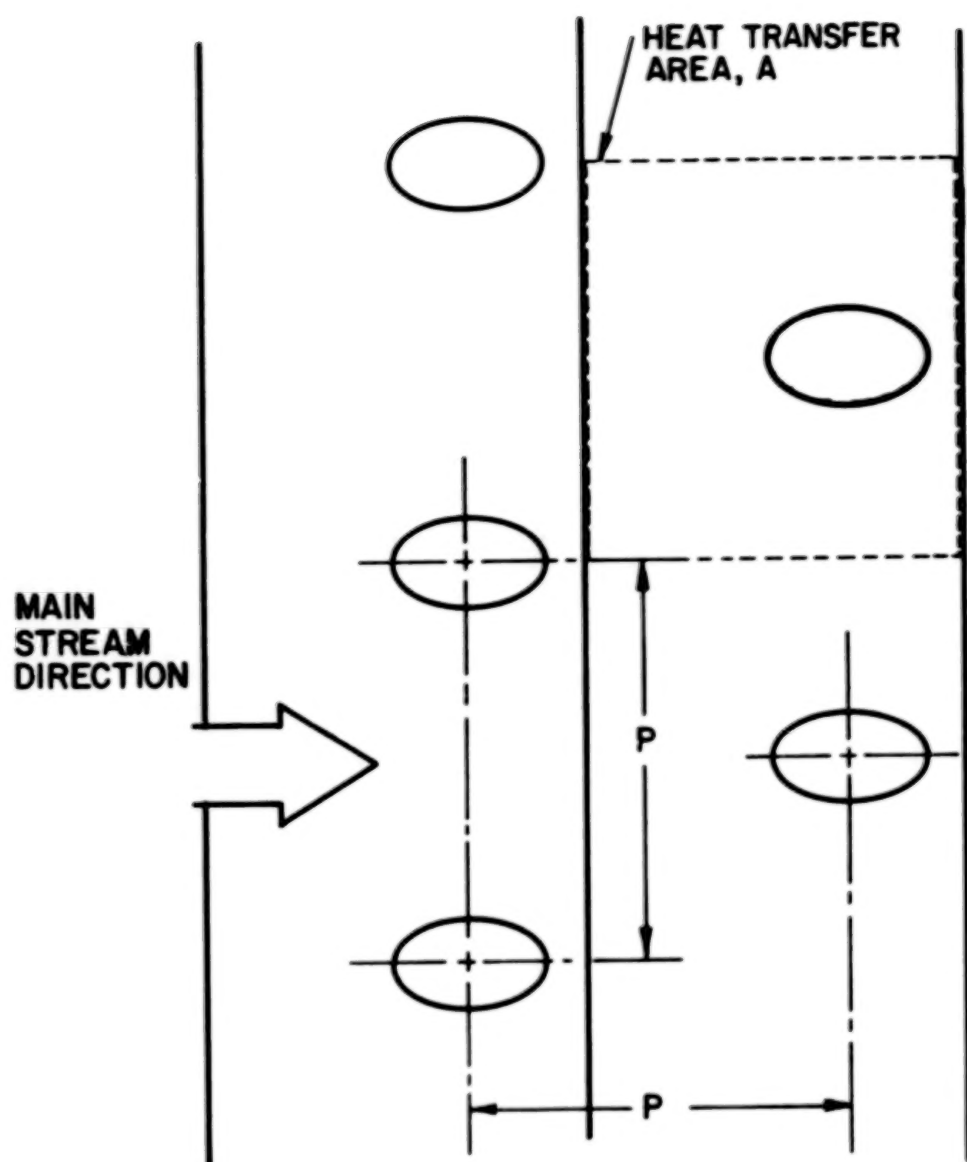


Fig. 2. The test-plate geometry.

Chapter III

HEAT TRANSFER FOR THREE INJECTION GEOMETRIES

A. Temperature Parameter

For a given mass flux ratio and upstream initial conditions, the heat transfer coefficient is a linear function of the temperature parameter, θ . Eqn. (3) describes this dependence. Eqn. (3) will apply for all conditions in which the thermal energy equation remains linear. The reader is referred to References 1 and 3, which experimentally confirm the superposition approach for obtaining heat transfer coefficients with θ greater than unity. Superposition with film cooling and large temperature differences has been confirmed by Ville and Richards [10]. Metzger and his co-workers [11] use superposition to obtain their film-cooling effectiveness data.

For the Stanford film-cooling studies, data were taken for $\theta \approx 0$ and $\theta \approx 1$. The data were then superpositioned-adjusted to $\theta = 0$ and $\theta = 1$ for presentation of the data. The $\theta = 0$ heat-transfer coefficient is the appropriate value for use with the effectiveness approach to film cooling [8,11], and the $\theta = 1$ data can be compared with transpiration data. For advanced gas-turbine application, the θ range for a given M is 1.25 to 1.75 [10].

The actual effect of θ on the Stanton number is described in the following sections. The important point is that, with superposition, only two data bases are required, and the heat transfer coefficient for a given θ follows from Eqn. (3). This is experimentally very convenient and simple, and it allows other data bases to be analytically produced for testing computer programs that model full-coverage film cooling.

B. Mass Flux Ratio

The effect of mass flux ratio on Stanton number for the three injection geometries can best be seen by plotting St versus M for different streamwise locations in the full-coverage region. Fig. 3 presents these data for the third, sixth, and tenth film-cooling rows. In the figure the

plotted data are $\theta = 0$ (open symbols) and $\theta = 1$ (shaded symbols), while the $\theta = 1.5$ line is obtained using Eqn. (3). Initial momentum and enthalpy thickness Reynolds numbers were about 3000 and 2000, respectively.

From the figure four major points are evident: (a) normal-angled injection results in a higher St than either slant- or compound-angle injection geometries; (b) both angled data sets show a minimum in St around $M = 0.4$ to 0.5 ; (c) in the initial cooling region (row 3), high blowing can cause the St to exceed the unblown value even at $\theta = 1.0$; and (d) past the initial cooling region, compound-angled injection provides the lowest heat transfer coefficient. By row 10 the surface heat flux with compound-angled injection is essentially zero in the M range from 0.4 to 0.6 .

In assessing the relative merits of injection geometries, the spanwise-averaged heat transfer performance should not be the only consideration. From an aerodynamic point of view it is advantageous to have the injectant enter the boundary layer with as much streamwise momentum as possible. Slant- and compound-angled injection has an advantage over normal-angled injection in this respect. A second point for consideration is the possibility of lateral and streamwise variations in local heat flux. The local heat flux data for slant-angled injection presented in Chapter IV and the flow visualization data of Colladay and Russell [12] indicate that compound-angled injection might result in more uniform heat flux.

The full-coverage film-cooling data indicate a minimum in Stanton number around $M = 0.4$ to 0.5 . This minimum is observable in both of the oblique data sets at high initial Reynolds numbers. (No high- M data were obtained with normal-angled injection. The minimum occurs with all three geometries at low initial Reynolds number -- to be discussed in the next section.) Above $M = 0.5$ (for these constant-property experiments) the jets of coolant apparently cause a region of disturbed flow with high heat transfer coefficient behind the jets, and the average Stanton number increases. Note that the $\theta = 0$ St could easily be approximated as a power-law function of M .

A point to be raised concerns which injection parameter is appropriate to describe high-velocity, variable-property turbine blade flows.

The present full-coverage film-cooling data show that a minimum Stanton number occurs but does not allow one to choose between associating with a mass ratio of 0.40 or a momentum ratio of 0.16. Some slot-film-cooling studies [13] use correlations based on M , and most transpiration cooling studies [9] use an area-averaged M value to reflect the percentage of coolant added to the sublayer of the boundary layer. On the other hand, variable property studies for effectiveness downstream of film-cooling injection [14] indicate that a momentum ratio should be considered. That ratio is also used to correlate jet-in-crossflow trajectory data.

C. Initial Conditions

Full-coverage data sets have been taken for three injection geometries with heated starting lengths and with momentum thickness Reynolds numbers of about 550 and 3000 (also at 1800 for compound-angled injection). In addition, a number of unheated starting-length data runs were made. Only the heated starting-length data will be discussed here. The step-wall temperature data will probably be useful for numerical modeling of the data and can be found in References 1, 3, and 5.

Figure 4 contains Stanton number data from the third, sixth, and tenth film-cooling rows for the 550 momentum and enthalpy thickness Re . These plots are similar to those in Fig. 3 for high initial Re . The tenth row low Re data are seen to lie between the third and sixth high Re data (closer to the sixth). In the initial film-cooling region (row 3), the heat transfer coefficients for the low initial Re are larger than for the high initial Re data, and, in the initial region, slant-angle injection provides better cooling than compound-angled injection.

The higher Stanton number for a lower initial Re is also a characteristic of two-dimensional boundary layer flows [9]. This suggests that the ratio of the film-cooled Stanton number for $\theta = 1$ to the unblown Stanton number, St_0 , might be independent of the initial conditions. The data in Figs. 3 and 4 were normalized by St_0 obtained at $M = 0$, and the ratios for both initial conditions were plotted in Fig. 5. Note the additional data for compound-angled injection. These were obtained at an initial momentum Re of 1800 and are added from Ref. 5 for completeness.

In Fig. 5 most of the data ratios for a given geometry, for both initial conditions, are within 10 percent of each other at every value of M .

The scatter is even less by the tenth row data. This suggests that for a hole spacing of five diameters, the full-coverage film cooling retains a boundary-layer-like character, and the major effect of the initial conditions is similar to that found in unblown boundary layers.

Where the St ratio data for a given M exhibits scatter, the higher St ratio comes from the lower initial Re data. This suggests that a higher turbulence level may be associated with the jets of coolant emerging into the thinner boundary layer. This increased turbulence effect is counteracted to some degree by the emerging jets remaining closer to the wall in a low Re boundary layer, thus providing better cooling for the near-wall region. For the low initial Re , the ratio of initial boundary layer thickness to jet diameter is about one, while for the high Re it is about five. The Stanton number ratio at a given M may be affected by the local boundary layer (or momentum) thickness. For these experiments the effect appears to be second order.

D. Number of Rows of Holes

The effect due to changing the number of rows of holes was studied for the slant-angled injection geometry. The data were taken for $P/D = 5$ and 6 and 11 rows of injection. The 11-row initial conditions are those described in Section B of this chapter. The six-row geometry was obtained by shutting off the first five rows of injection. The six-row initial conditions for the plate upstream of the first blowing row (plate 5) are given in Section A of Chapter IV. The two geometries had about the same initial Re_{δ_2} but different Re_{Δ_2} . Note the six-row data also served as the spanwise-averaged heat flux data for Chapter IV.

Two blowing ratios were used in the study: $M = 0.4$ and $M = 0.9$. Stanton number data were acquired using two injectant temperatures, $\theta \approx 0$ and $\theta \approx 1$, at each blowing ratio. Eqn. 3 was used to adjust the data to $\theta = 0$ and $\theta = 1$ for plotting. The data for $M = 0.4$ are shown plotted in Fig. 6 versus enthalpy thickness Reynolds number. Arrows on the figures indicate the first and last blowing rows. The six-row data are seen to be about 5 to 10 percent above the corresponding eleven-row data, but the trend is similar. Once blowing begins, the St data for $\theta = 1$ drop below the St_0 reference line, achieving a reduction in St of about

30 percent by the sixth row of holes. The downstream area past the last row of holes is called the recovery region. For the six-row geometry the recovery region St jumps up to within 10 percent of St_0 , indicating minimal downstream protection. The last data point is about 60 hole diameters downstream. The eleven-row recovery region data show the benefit of additional rows of cooling, since the Stanton number remains low in the recovery region.

For $\theta = 0$ the Stanton number lies above St_0 , but in the recovery region it quickly drops to within 4 or 10 percent of St_0 .

The thermal boundary layer growth is a strong function of the temperature parameter, θ , of the injection. For $\theta = 1$ the thermal boundary layer grows about as rapidly as the momentum boundary layer. For $\theta = 0$ the periodic injection of fluid having the same enthalpy as the mainstream retards the thermal boundary layer growth. The momentum boundary layer is the same for the two cases. Past the last row of holes the increased turbulence production ceases (see Yavuzkurt et al. [4]). Thus the mechanism for diffusing out the thick $\theta = 1$ thermal boundary layer for return to St_0 is reduced. The $\theta = 0$ thermal boundary layer has an enthalpy thickness much nearer the equilibrium value. Once the turbulent diffusivity drops, the boundary layer rapidly returns to near-equilibrium conditions.

Data for $M = 0.9$ are shown in Fig. 7. The effect of increased M on turbulent diffusivity in the near-wall region is very evident. The $\theta = 1$ data lie about 30 percent above the St_0 value for the same enthalpy thickness Reynolds number. Again, the six- and eleven-row data show similar trends. The six-row, $\theta = 1$ data were acquired with an M of 1.05, which may account for the slightly higher St . The effect of reduced turbulence production in the recovery region is seen in the rapid drop of the $\theta = 1$ data. The much thicker thermal boundary layer for eleven rows of holes causes the St to drop below St_0 .

E. Hole Spacing

Some data for each of the three injection geometries were taken at a pitch-to-diameter of 10, to provide additional data bases for modeling purposes. The $P/D = 5$ test sections were used, and $P/D = 10$ was obtained by plugging alternate holes and rows in the arrays with modeling

clay. The normal- and slant-angled data were acquired with low initial Re , and the compound-angled data were acquired with high initial Re . The data will not be presented here, but may be obtained from Refs. 1, 3, and 5. Comparison of $P/D = 5$ with $P/D = 10$ data for a given injection angle showed the following: (1) the St decrease below St_0 for $\theta = 1$ was much less for the wider hole spacing; (2) the data indicated a minimum in St for $\theta = 1$ and M about 0.4, with higher St for higher M ; and (3) in the recovery region downstream of the last row of holes, the St rapidly returned to St_0 , indicating much less recovery-region protection than with the same M and smaller P/D .

F. Concluding Remarks

Experimental heat transfer studies have been carried out for three injection geometries. Injection of wall-temperature fluid into the boundary layer causes the Stanton number to drop in a manner analogous to transpiration cooling. Unlike the latter situation, however, full-coverage film cooling displays a minimum in Stanton number for a mass flux ratio, M , of about 0.4 to 0.5. Increasing M above 0.4 results in an increasing Stanton number. Past the initial cooling region the compound-angled injection geometry provides the lowest Stanton number for a given N . Variation in initial conditions upstream of the blowing section has a second-order effect on the Stanton number distribution. Studies of six and eleven rows of holes for slant-angled injection show that the latter gives much better surface protection downstream of the last row of holes. With six rows, the Stanton number rapidly returns to the unblown value in the recovery region, whereas with eleven rows, it remains low longer. Studies of 5- and 10-diameter hole-spacing geometries showed the latter to provide much less surface protection. Of the three injection geometries, compound-angled injection seems to be preferable to slant- and normal-angled injection.

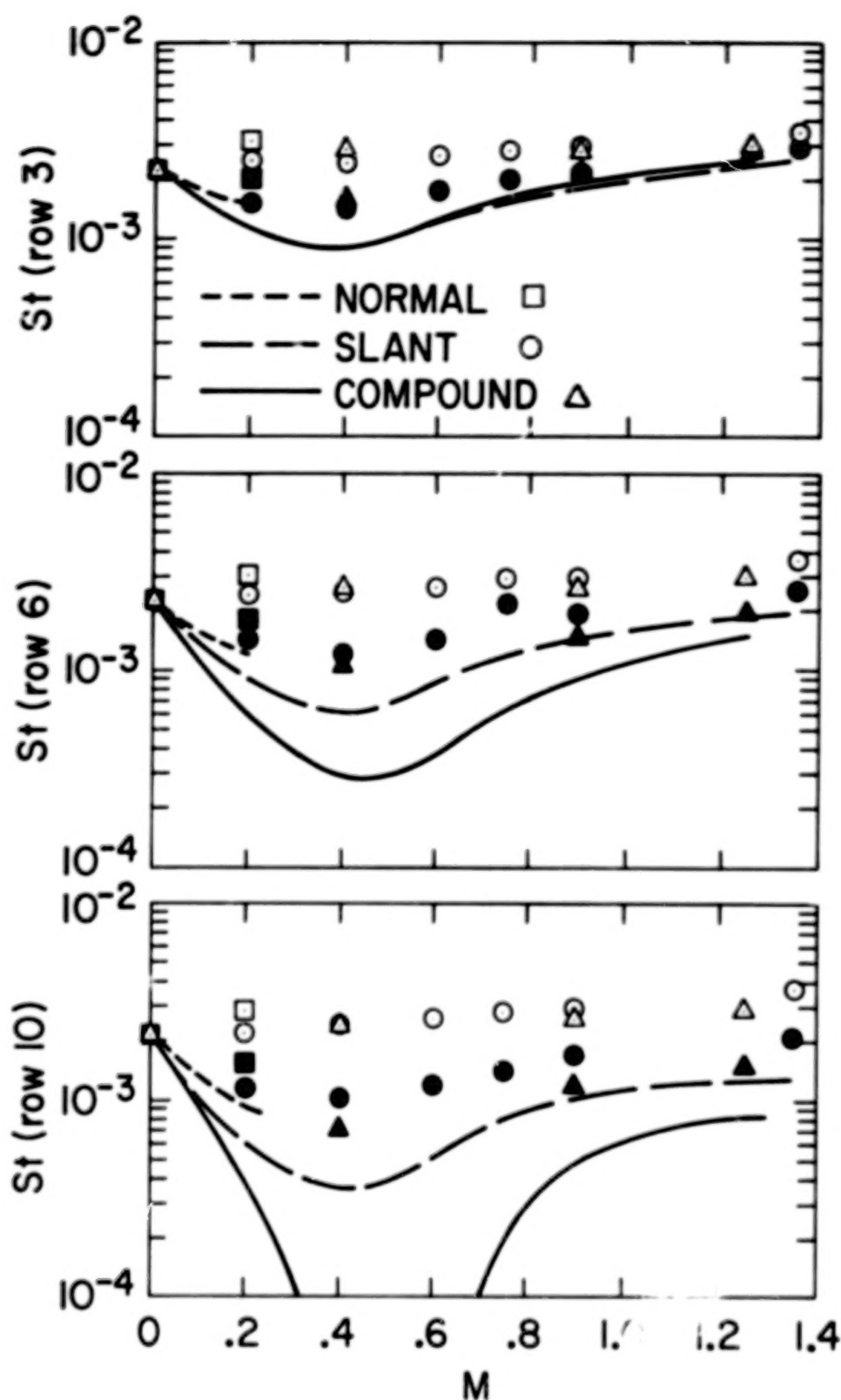


Fig. 3. Effect of mass flux ratio on Stanton number after 3, 6, and 10 rows of holes. Thick initial boundary layers. Data points are for $\phi = 0$ and $\phi = 1.0$, while lines are predictions for $\phi = 1.5$.

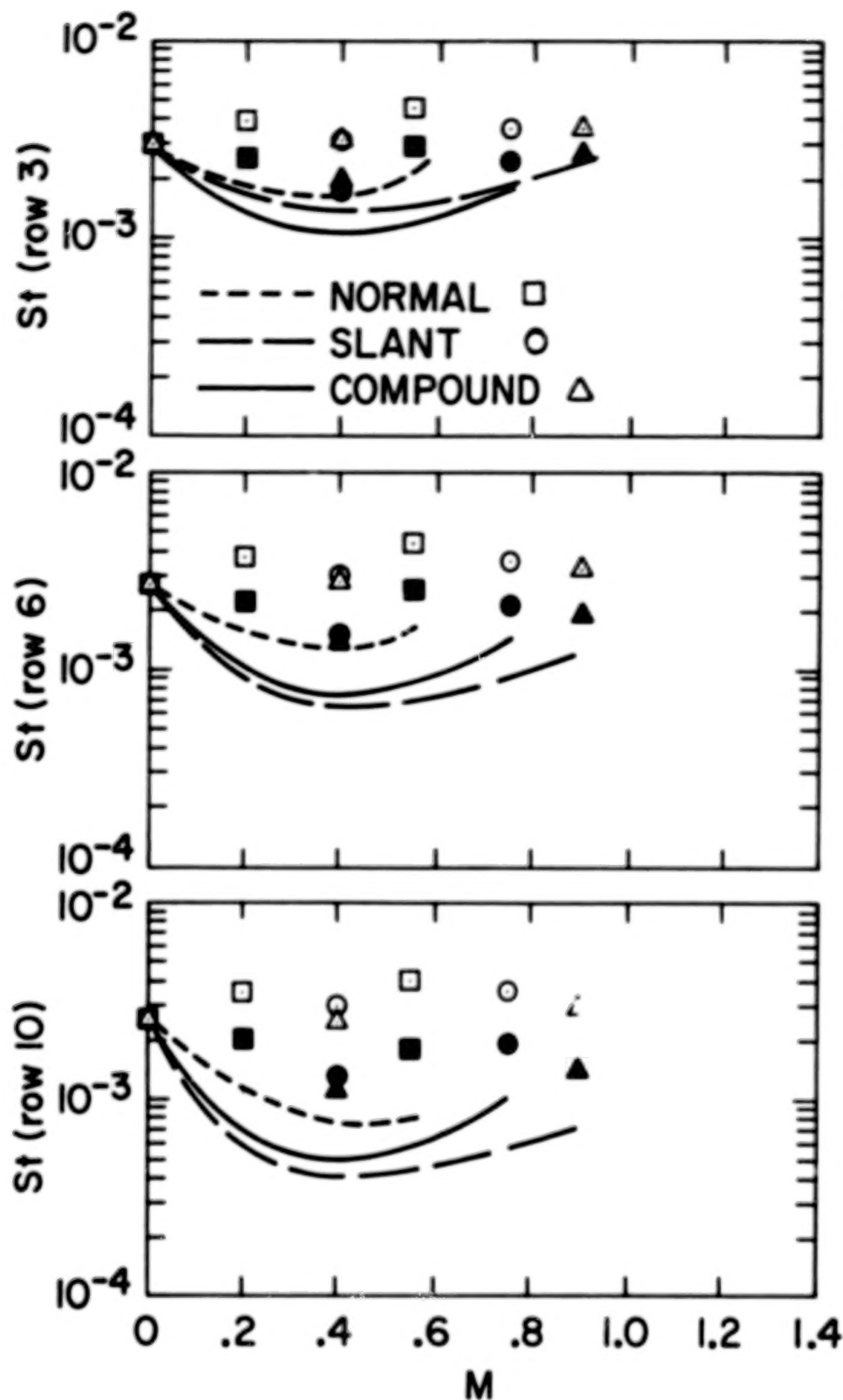


Fig. 4. Effect of mass flux ratio on Stanton number after 3, 6, and 10 rows of holes. Thin initial boundary layers. Data points are for $\theta = 0$ and $\theta = 1.0$, while lines are predictions for $\theta = 1.5$.

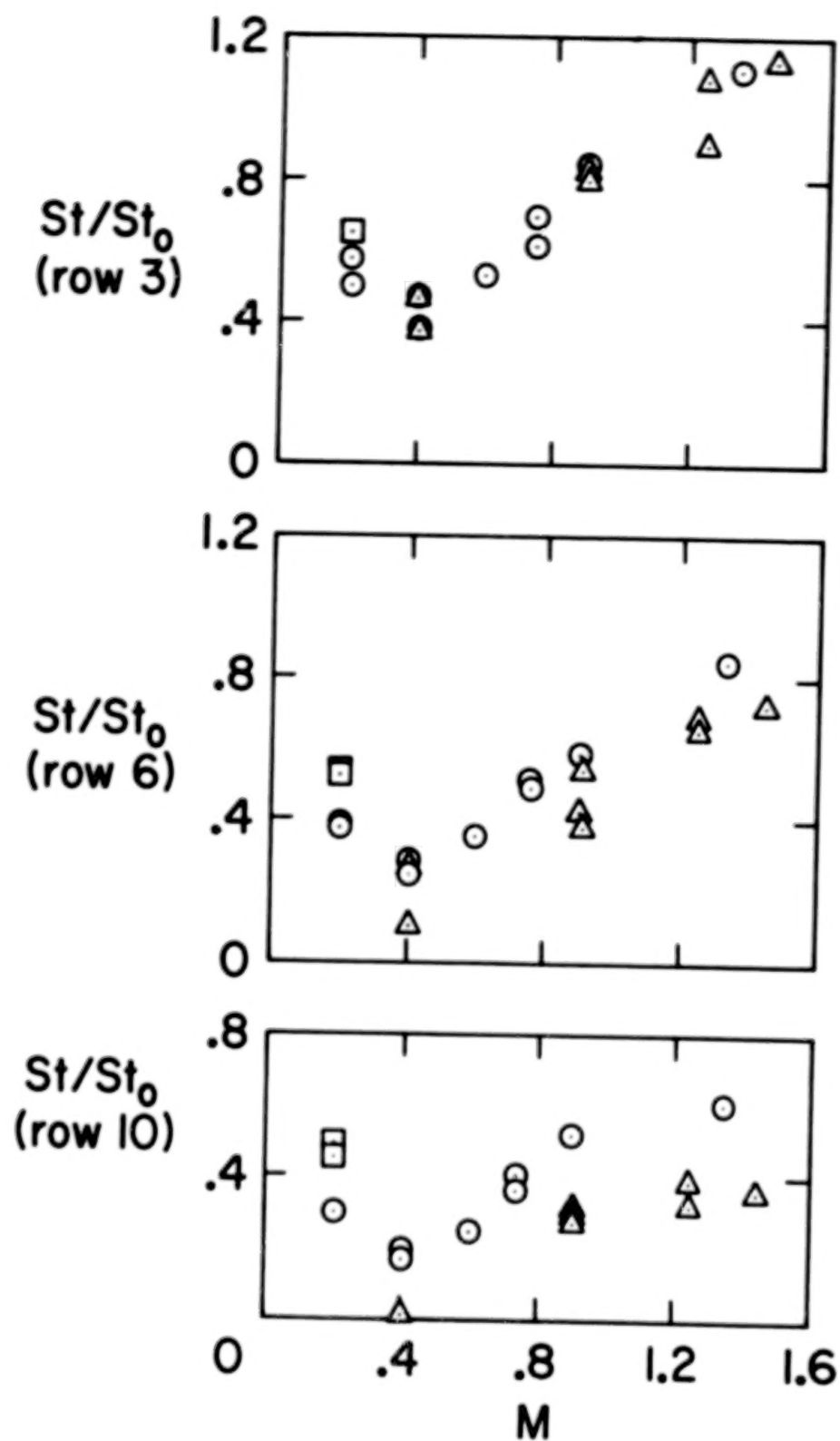


Fig. 5. Ratio of film-cooled to unblown Stanton numbers at $\theta = 1$ for various initial conditions. Symbols: \square , normal; \circ , slant; \triangle , compound angle.

Chapter IV

LOCAL HEAT FLUX DATA

A. Experimental Test Conditions

Local heat-flux data were acquired using the slant-angled test surface. Two blowing ratios were used in the study: $M = 0.4$ (a low- M data set) and $M = 0.9$ (a high- M data set). These blowing ratios were chosen based upon the initial findings of Crawford et al. [3], who reported that the full-coverage Stanton number for $\theta = 1$ reached a minimum around $M = 0.4$ to 0.6 and that the Stanton number increased for higher M . Based on these findings, $M = 0.4$ and 0.9 were also identified for the hydrodynamic study of the slant-angled injection flow field by Yavuzkurt et al. [4].

For the local heat flux tests, the first five blowing rows of the eleven-row test section were shut off, leaving six rows of cooling holes before the recovery region (afterplate). For both M data sets, spanwise averaged heat flux data, \dot{q}_{s-a}'' , were acquired first and then the local heat flux data, \dot{q}_{1-a}'' , were acquired in the third and the fifth blowing row.

Initial momentum and enthalpy thickness Reynolds numbers for the tests were about 3300 and 1400 (measured at the midpoint of the plate upstream of the first blowing row). The momentum profile had a displacement-to-momentum thickness ratio of 1.37 and a mainstream velocity of 16.3 m/s. The 99 percent momentum and thermal boundary layer thicknesses were about 2.8 cm and 1.7 cm. The wall and mainstream temperatures were about 34°C and 19°C. Air was used as the working fluid.

B. Results and Discussion

1. Presentation of the data

The local heat flux data are presented in tabular form (Table 1) and in graphical form (Figs. 8 through 11). For convenience of presentation, the data have been normalized using \dot{q}_{s-a}'' for the plate where the \dot{q}_{1-a}'' were obtained. The figures show the hole locations and heat flux locations

BLANK PAGE

BLANK PAGE

Table 1
Local-to-Spanwise-Averaged Heat Flux Ratios, $\dot{q}_{l-a}''/\dot{q}_{s-a}''$,
for 3rd and 5th Blowing Rows

HFM Position	M = .4 $\theta = 1.0$ (5th)	M = .4 $\theta = 0.15$ (5th)	M = .4 $\theta = 0.15$ (3rd)	M = .9 $\theta = 1$ (5th)	M = .9 $\theta = 1$ (3rd)	M = .9 $\theta = .15$ (5th)	M = 9 $\theta = .15$ (3rd)
1	.815	.804	.811	.838	.834	.897	.908
2	1.29	.907	.881	1.12	1.02	1.00	.838
3	.620	1.10	1.01	1.31	1.34	1.57	1.46
4	1.37	.937	.895	1.12	1.01	1.00	.838
5	.835	.804	.811	.810	.783	0.909	.862
6	1.24	1.01	1.01	1.17	1.06	0.991	1.01
7	1.26	.951	.853	1.09	1.06	0.921	.884
8	.710	.893	.853	.852	.809	1.17	1.06
9	1.35	.981	.866	1.10	1.02	0.932	.931
10	1.26	1.03	1.02	1.17	1.14	0.980	.990
\dot{q}_{s-a}'' (w/m ²)	480	700	734	736	813	882	883

(dashed lines) relative to the holes, drawn to scale. The spanwise and streamwise pitch is five hole diameters. Fig. 8 identifies the heat flux meter numbers. To avoid confusion, the data for meters 6 through 10 are shown shifted over one pitch distance on the figures. Data from row 5 are depicted as circles, and data from row 3 are depicted as diamonds. The connecting solid lines are for visual aid only.

2. Symmetry of the data

The data location pairs (1,5), (2,4), (6,10), and (7,9) on each figure are symmetric because of the staggered hole array, and their data should be similar. There are 28 pairs of data for various M and θ in Table 1. Of these, 22 pairs agree with 4 percent (e.g., comparing meter 1 with meter 5). The remaining pairs agree within 6 percent. This implies that the flow field is indeed symmetric about lines passing through the hole centers. To aid in the discussion that follows, the data from each pair have been averaged and are presented in Table 2. The values for the third blowing row are in parentheses

3. Comparison of third and fifth blowing row data

It appears that the major differences between the third row data and the fifth row data occur in the regions between holes. There are lanes about 1.5 hole-diameters wide which seem to run the length of the array. The lanes may be caused by the grid stagger, with a hole spacing greater than two. Meters 2, 4, 7, and 9, and to some extent 6 and 10, are in these lanes. The hydrodynamic boundary layer over the lanes for a given row of holes is influenced, in part, by the following events: (1) diversion of jets injected two rows upstream by the local jets; (2) lateral diffusion of the jets injected one row upstream; and (3) downwash of mainstream fluid that is being entrained due to the streamwise vorticity associated with the emerging jets.

The first event is the one most apt to change as the boundary layer develops over the initial rows of holes. This was observed in the flow visualization study by Colladay and Russell [12] and can be seen in the $\theta = 0$ Stanton number data of Crawford et al. [3]. The third blowing row is the first to have in-line jets upstream. From Table 2 the heat flux ratio increases between the third row lanes (2,4 and 7,9) and fifth blowing

Table 2
Averaged heat flux ratios,
5th row and (3rd row)

Location	1,5	2,4	3	6,10	7,9	8
M = 0.4, $\theta = 1$.83	1.33	.62	1.25	1.31	.71
M = 0.9, $\theta = 1$.82 (.81)	1.12 (1.02)	1.31 (1.34)	1.17 (1.10)	1.09 (1.04)	.85 (.81)
M = 0.4, $\theta = 0$.80 (.81)	.92 (.89)	1.10 (1.01)	1.02 (1.01)	.97 (.86)	.89 (.85)
M = 0.9, $\theta = 0$.90 (.89)	1.00 (.84)	1.57 (1.46)	.99 (1.00)	.93 (.91)	1.17 (1.06)

Table 3
Normalized 5th row data

Location	1,5	2,4	3	6,10	7,9	8
M = 0.4, $\theta = 1$.63	1.00	.47	.95	1.00	.54
M = 0.9, $\theta = 1$.74	1.00	1.18	1.05	1.00	.77
M = 0.4, $\theta = 0$.84	1.00	1.16	1.07	1.00	.94
M = 0.9, $\theta = 0$.94	1.00	1.64	1.03	1.00	1.22

row lanes. It is not clear whether this is an initial effect or whether the increase will continue with streamwise distance as a function of coolant addition. The Stanton number of Crawford suggest this is an initial region effect.

The data for lanes (2,4) and (7,9) in Table 2 are nominally the same. These data can be compared to the other local heat flux data for a given M and θ by averaging these two pairs and using their average to normalize the remaining local data. This procedure has been carried out and is given in Table 3 for the data on the fifth blowing row. The discussion which follows is based on this table.

4. Low-M data

The most significant feature of this data set is the 40 to 50 percent spanwise difference in heat flux for $\theta = 1$. The region downstream of the holes is well protected (i.e., low surface/heat flux) compared to the lanes between holes. The large difference in heat flux suggests potential thermal stress problems for low blowing ratios, especially with wide hole spacings.

Comparison of (1,5) data immediately upstream of a hole with (6,10) data laterally adjacent to the hole indicates that not much of the upstream injectant is diverting around the emerging jet. The (6,10) data are nearly the same as the lane value (7,9). On the other hand, it is also possible that the upstream jet is diverting but that the potential cooling effect of the diverted injectant is being masked by the local acceleration of the boundary layer as it diverts around and over the blockage caused by the emerging jet.

From Table 2 the three data locations 3, 8, and (1,5) have heat flux ratios for $\theta = 1$ of 0.62, 0.71, and 0.83. These data locations are in line with injection holes and about 2.5, 5.0, and 7.5 hole diameters downstream of an injection site. This sequence of data reflects the local recovery of the thermal and momentum boundary layers from injection as the jets of coolant spread and mix with the surrounding fluid. The monotonic sequence suggests that the jets are attached to the surface by 2.5 diameters downstream.

It is difficult to interpret the $\theta = 0$ (mainstream temperature injectant) data. The data share the same hydrodynamics as the $\theta = 1$ data, but the effects on the thermal profile of the boundary layer are markedly different. The $\theta = 1$ condition continues to "pump up" the thermal boundary layer to reduce the heat flux, whereas the $\theta = 0$ condition periodically "deflates" the thermal profile. The $\theta = 0$ data at the data location 3, 8, and (1,5) are 1.10, 0.89, and 0.80, with all the other locations having nominally unity ratios. This monotonic heat flux decrease suggests possibly a deceleration of the boundary layer as it approaches an emerging jet.

5. High-M data

One important feature of the high blowing-ratio data is the reduced spanwise variation in heat flux compared to the $M = 0.4$ data. For the high-M data and $\theta = 1$, the largest difference is about 25 percent, half the value of the low-M data. This indicates more lateral spreading and surface protection for high M . However, the spanwise-averaged heat flux for $M = 0.9$ is much higher than for $M = 0.4$. This implies there is a trade-off between increased St and reduced spanwise variation.

One factor affecting the trade-off is related to a second significant feature of the high-M data. For $\theta = 1$, the locations 3, 8, and (1,5) show values of 1.31, 0.85, and 0.82. This trend is different from the $M = 0.4$ data and indicates that the jet separates and then reattaches at about five diameters downstream. Presumably the separation region will be larger for higher M values. This suggests that, while the spanwise variations are, on the whole, reduced due to increased turbulent mixing, local heat flux variations will become more severe in the region behind the emerging jets as M increases. Strictly speaking, this conclusion applies only to 30-degree slant-angled injection.

Separation produces a low-pressure region which tends to entrain fluid. The very large heat flux for location 3 suggests the entrained fluid does not come from the adjacent wall layers. Presumably the interaction of the jet with the shear layer gives rise to streamwise vortices. These would aid entrainment by causing a downwash of outer-region fluid into the region around and under the separating jet. The data from locations (6,10) and (7,9) for $\theta = 1$ support this idea.

6. Comparison to spanwise-averaged data

Local heat flux data were acquired over an area of $P \times P$, where $P = 5D$. The data were found to vary as much as 50 percent over that area. With such a wide variation in local flux, it is worthwhile to compare the area-integral of the local heat fluxes, \dot{q}_{1-a}'' , with that of the spanwise-averaged heat flux, \dot{q}_{s-a}'' , obtained from the steady-state energy-balance technique. To obtain the area integral, the following area weights were assigned, based on the approximate area covered by the heat flux meter laminate.

$$\dot{q}_{avg}'' = \frac{1}{P} \left[\left(\frac{D}{2} \right) \left(\frac{P}{2} \right) (\dot{q}_1'' + \dot{q}_5'') + (D) \left(\frac{P}{2} \right) (\dot{q}_3'' + \dot{q}_8'') + \left(\frac{3D}{2} \right) \left(\frac{P}{2} \right) (\dot{q}_2'' + \dot{q}_4'') \right. \\ \left. + \left(\frac{3D}{2} \right) \left(\frac{P}{2} \right) \left(\frac{\dot{q}_6'' + \dot{q}_7''}{2} + \frac{\dot{q}_9'' + \dot{q}_{10}''}{2} \right) \right] \quad (5)$$

In Eqn. (5) the heat flux information for the area occupied by the holes (identical to the area occupied by meters 1 and 5) are omitted since no data were available. For $\theta = 1$ this is harmless, since the heat flux should be nearly zero for that area. For $\theta = 0$ this assumption is unfortunate, but there is no means of determining the heat flux for this area.

Local heat flux data in Table 1 were area-averaged using Eqn. (5), and the results are shown in Table 4. Several observations can be made. The $\theta = 1$ area-averaged heat flux, \dot{q}_{avg}'' , and the plate-energy-balance heat flux, \dot{q}_{s-a}'' , agree extremely well for both blowing ratios. There appears to be less agreement for row 3 data compared to row 5 data for both temperature ratios. For $\theta = 0$, the $M = 0.4$ locally averaged data are about 15 percent lower, and the $M = 0.9$ data are about 10 percent lower than their respective spanwise-averaged values. The discrepancy for $\theta = 0$ apparently reflects the lack of accounting of the high surface heat flux in the area immediately surrounding the hole. The larger discrepancy for low M appears to agree with the observation that the injected fluid is immediately turned in the downstream direction after leaving the cooling hole, causing a locally high heat flux behind the hole, while the high M fluid leaves the surface and reattaches farther downstream.

C. Concluding Remarks

The major conclusion from the local heat flux data is that there exist regions on a full-coverage array that have local heat fluxes 20 to 50 percent higher than the average. The high-flux region tends to be located in the lanes between the staggered holes, at least when the hole spacing is greater than 2, and is especially evident for low blowing ratios. Apparently, the coolant does not spread laterally to protect the lanes. For the higher blowing ratios, spreading of the jet is more evident, but the region immediately behind the holes is insufficiently cooled (for 30° slant-angled injection). This suggests that a pitch-to-diameter ratio of 5 is too large for low blowing ratios, but that low-to-moderate blowing ratios would have less behind-hole cooling problems. Compound-angled injection may not have as great a behind-hole cooling problem for higher blowing ratios, but no data are available as yet. The compound-angle injection would also permit more lane coverage for the area between holes.

Table 4

Comparison of Area-Average Local Heat
Flux Data with Spanwise-Averaged Data

	\dot{q}_{avg}''	\dot{q}_{s-a}''	$\dot{q}_{avg}''/\dot{q}_{s-a}''$
M = 0.4, $\theta = 1$ (5th row)	479(w/m ²)	480(w/m ²)	1.00
M = 0.9, $\theta = 1$ (5th row)	717	736	0.97
(3rd row)	750	813	0.92
M = 0.4, $\theta = 0$ (5th row)	600	700	0.86
(3rd row)	599	734	0.82
M = 0.9, $\theta = 0$ (5th row)	821	882	0.93
(3rd row)	775	883	0.88

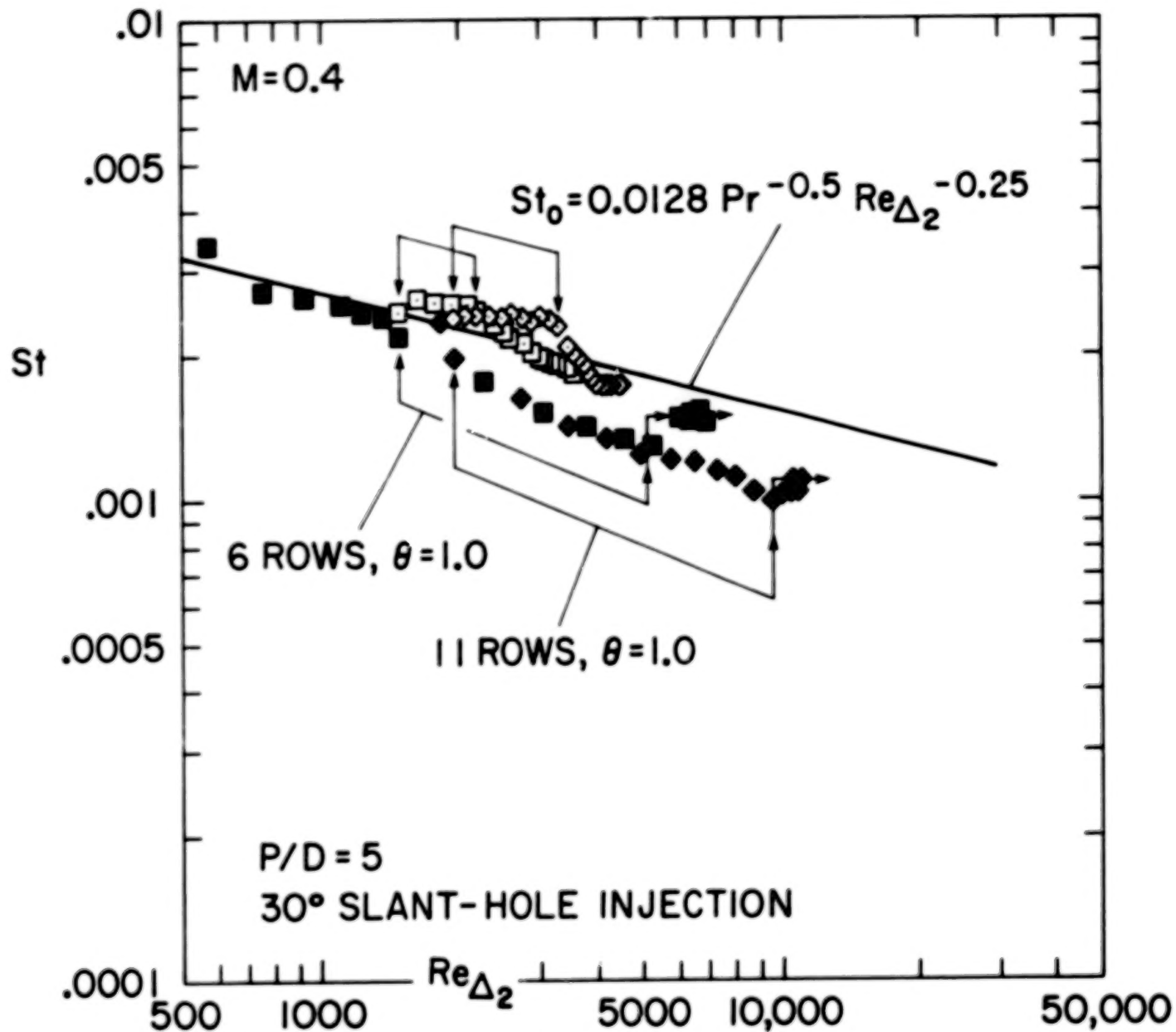


Fig. 6. Spanwise-averaged Stanton numbers for 6 and 11 rows of cooling with $M = 0.4$. Open symbols are $\theta = 0$, closed symbols are $\theta = 1$. Initial momentum thickness Reynolds number ≥ 3000 .

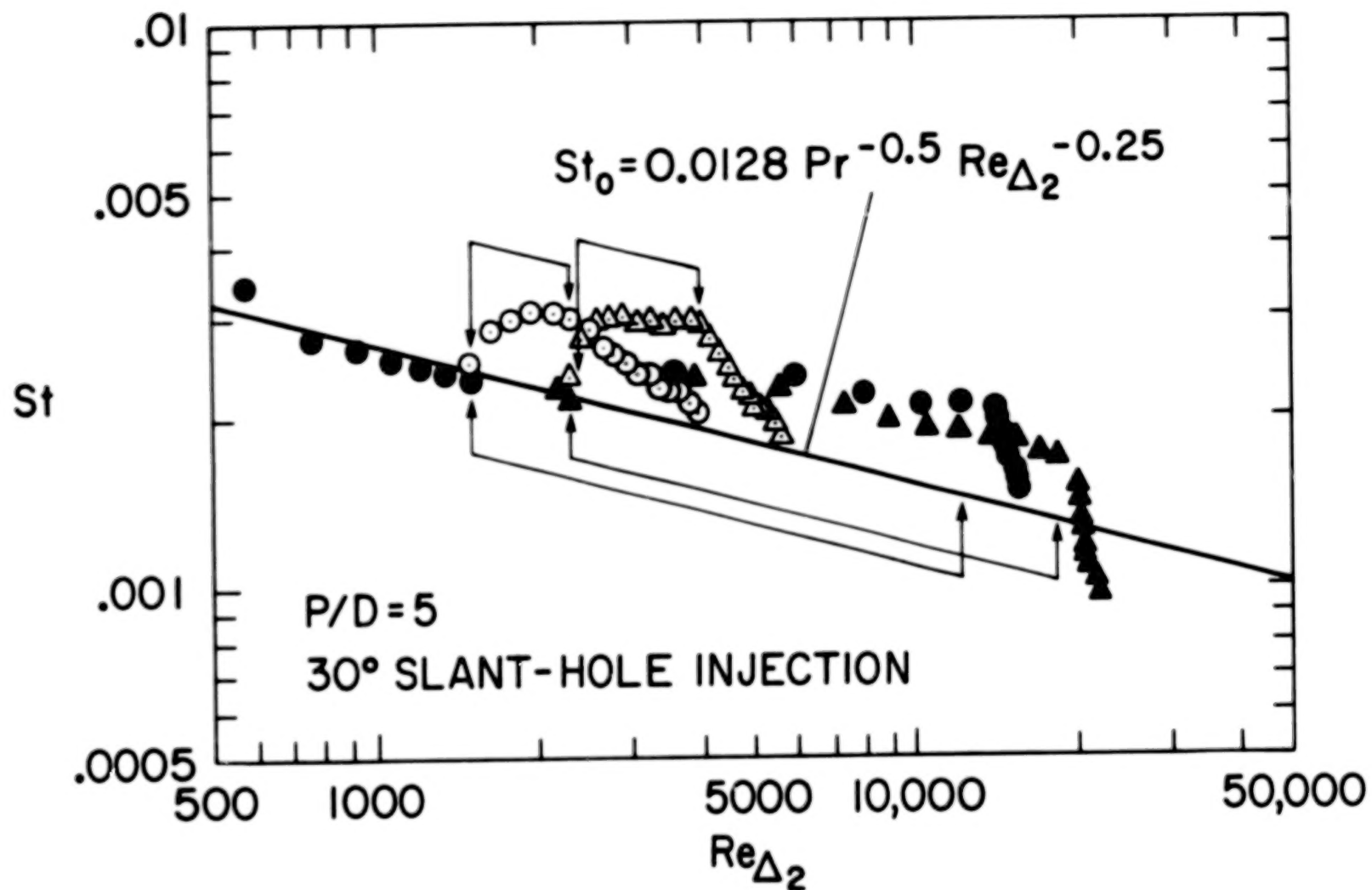


Fig. 7. Spanwise-averaged Stanton numbers for 6 and 11 rows of cooling with $M \approx 0.9$. Open symbols are $\theta = 0$, closed symbols are $\theta = 1.0$. Initial momentum thickness Reynolds number ≈ 3000 .

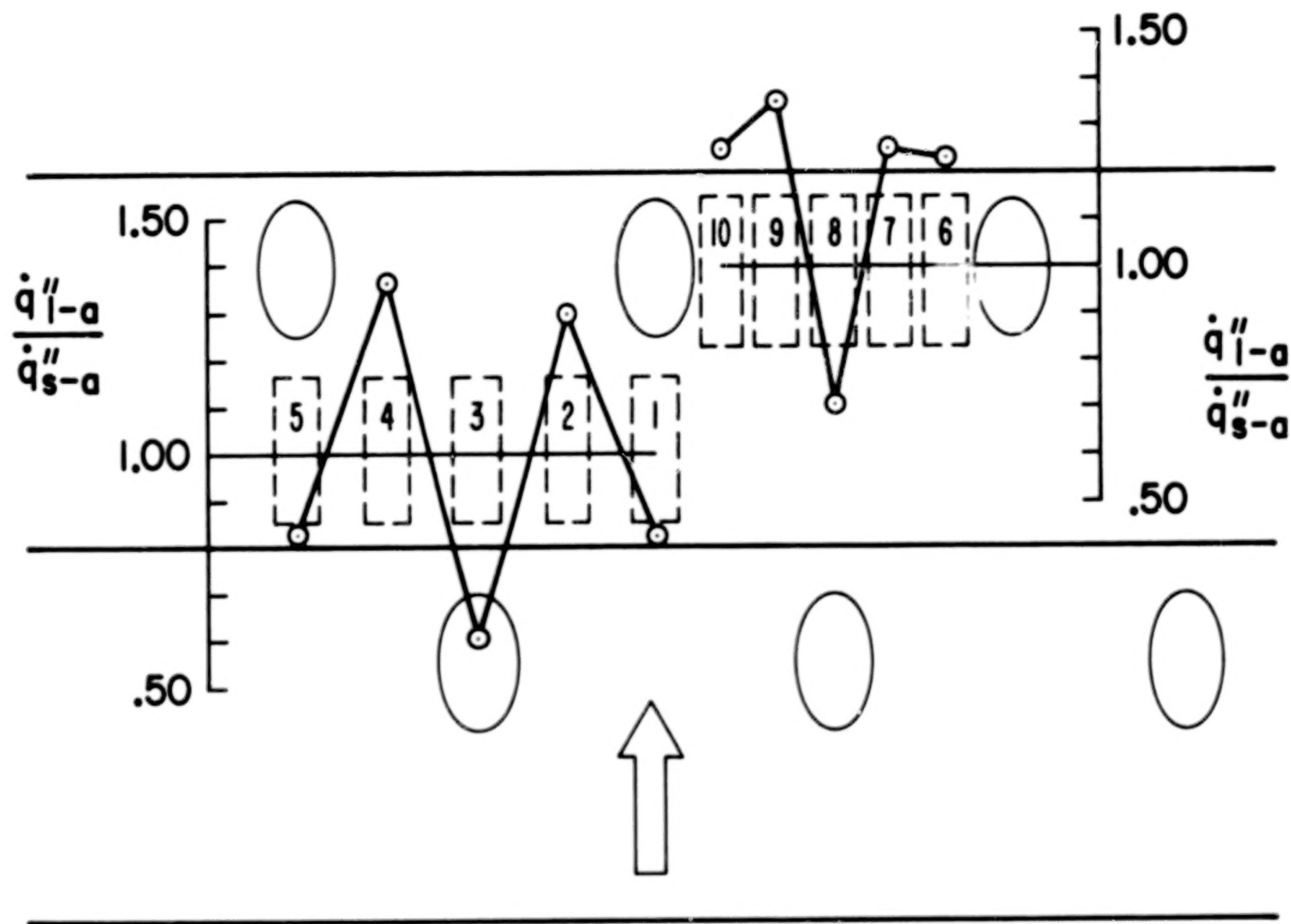


Fig. 8. Local heat flux ratios for $M = 0.4$ and $\theta = 1.0$.

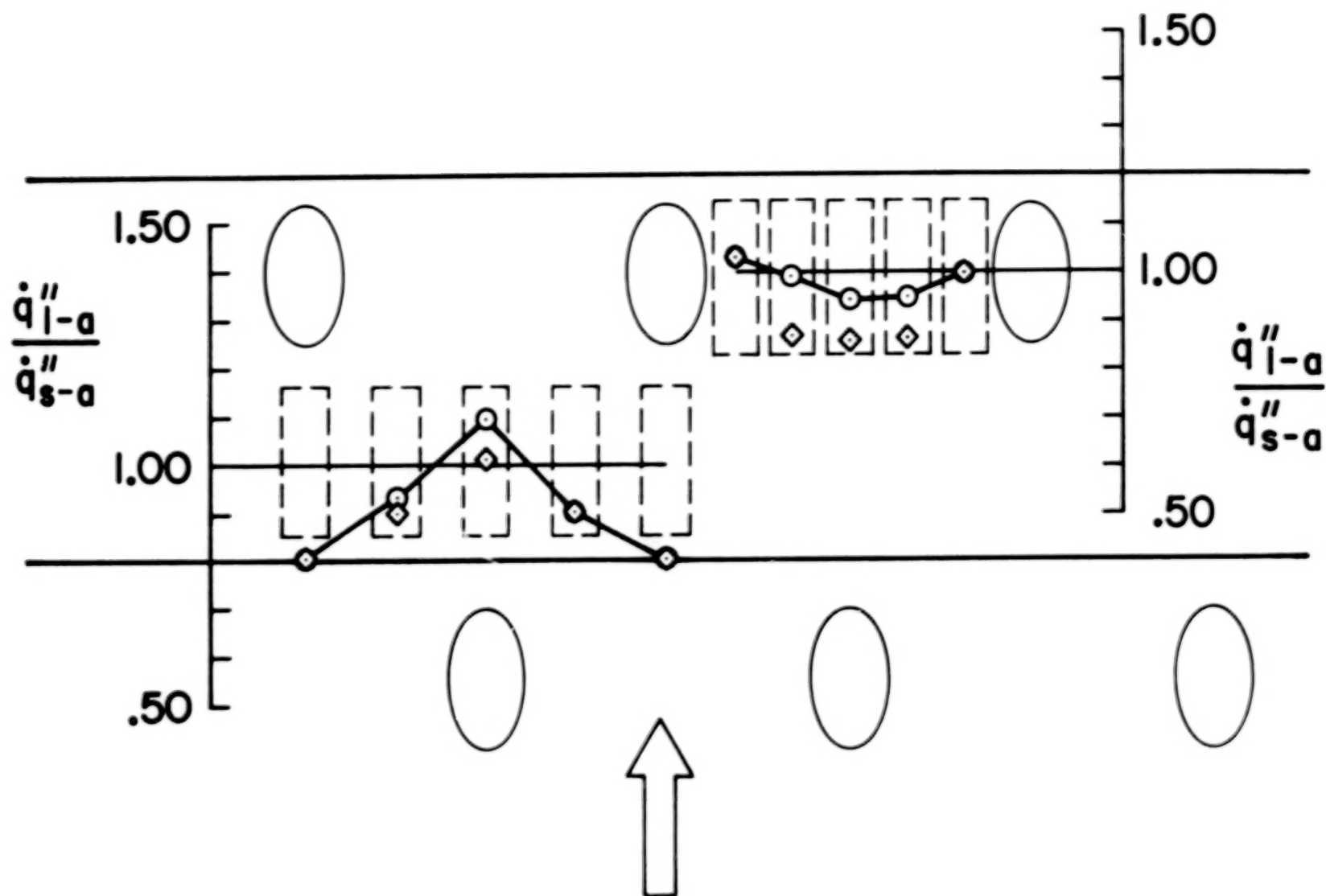


Fig. 9. Local heat flux ratios for $M = 0.4$ and $\theta = 0.15$.

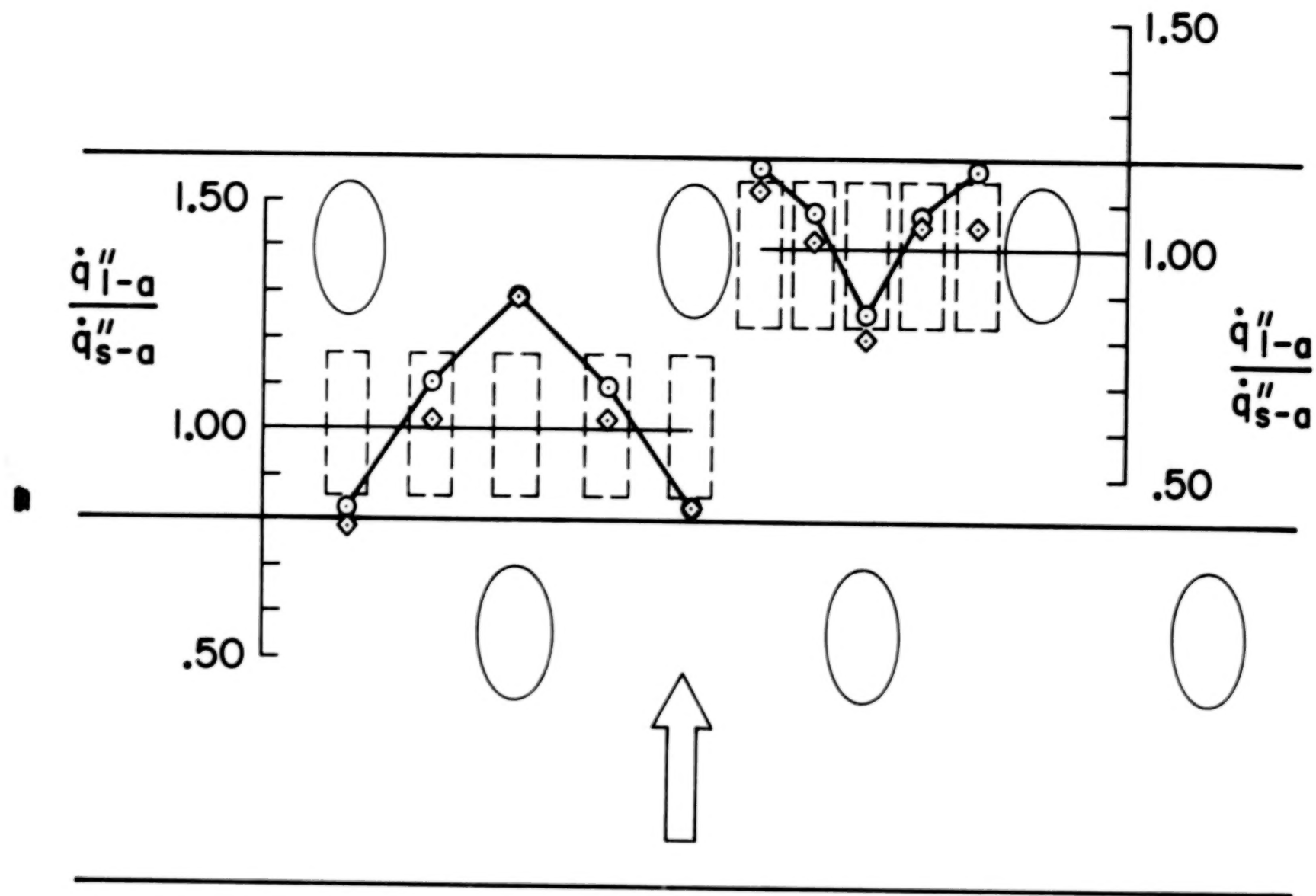


Fig. 10. Local heat flux ratios for $M = 0.9$ and $\theta = 1.0$.

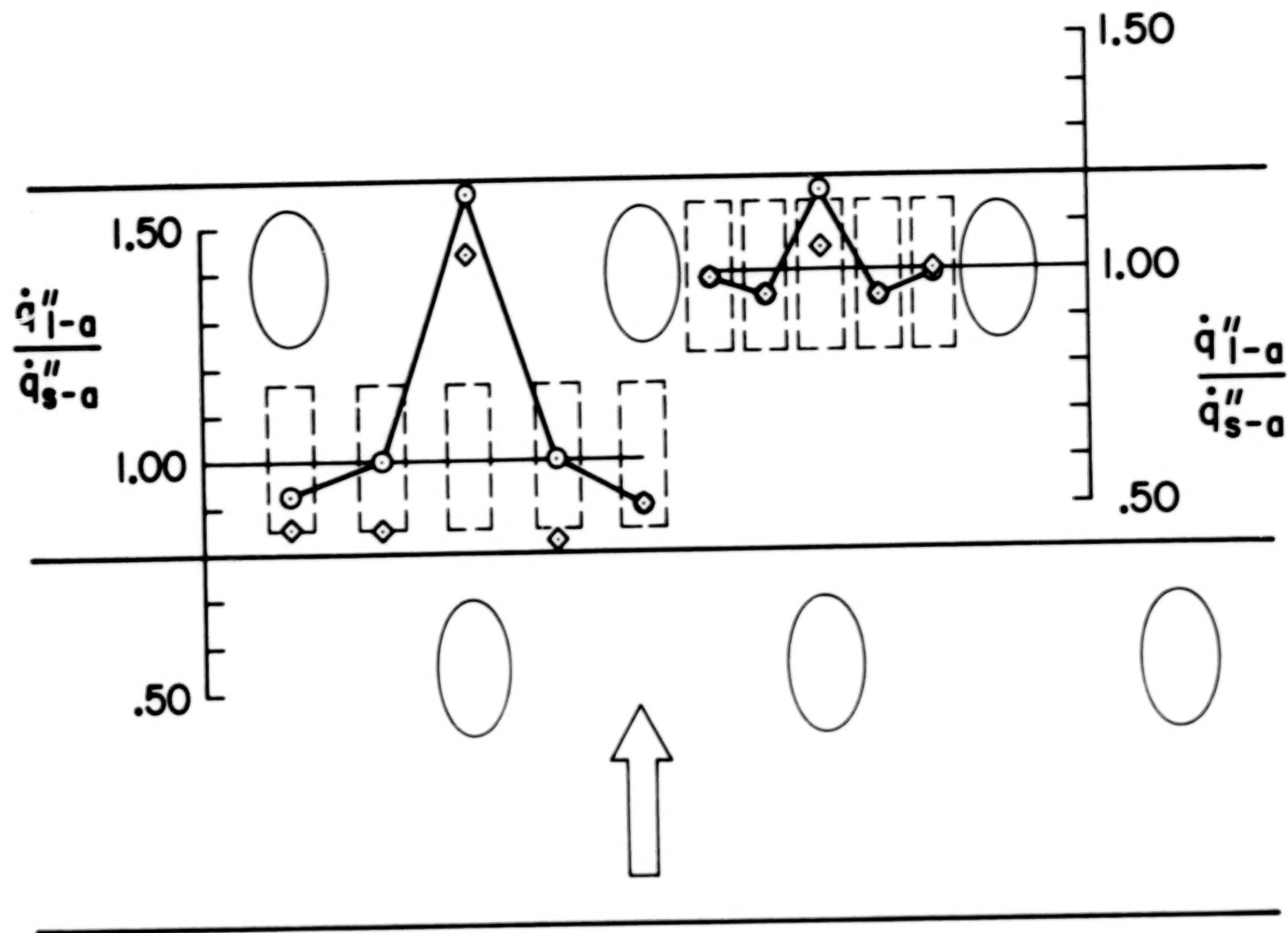


Fig. 11. Local heat flux ratios for $M = 0.9$ and $\theta = 0.15$.

Chapter V

NUMERICAL PREDICTION PROGRAM

A. Introduction

The intent of the analysis part of the Stanford film-cooling research was to incorporate the Stanford experimental data base into a program that could predict heat transfer. Both integral and two-dimensional (2-D) methods were studied in detail. The integral method showed promise for normal-angled injection at low to moderate M [1], but for slant-angled injection [3] the $\theta = 0$ data had a trend completely different from the normal injection data, and it was not amenable to simple correlation. Thus, the integral method was abandoned.

Choice of a 2-D finite-difference boundary layer method in preference to a 3-D method was based upon several factors. First, the general flow field is boundary layer in nature, and the departures from 2-D behavior are spanwise periodic. This permits defining spanwise-averaged velocity and temperature quantities which are continuous in the flow direction. This approach has been developed in detail by Choe [1] and Herring [15]. Second, the primary data used in development of the method was intended to be the data acquired in the experimental phase of this program. The construction of the apparatus is such that the data are inherently spanwise-averaged Stanton numbers representing the area-averaged effects of injection from a row of holes. The third criterion relates to the program's utility as a design tool, which requires short execution times and small computer-core requirements. Recently, Launder and his colleagues [16,17] have had success with a 3-D elliptic/parabolic boundary layer program coupled to a two-equation model of turbulence, but their success has been limited to low to moderate M .

B. The STANCOOL Program

The differential method that has been developed consists of a 2-D boundary layer program, STAN5, with added routines to model coolant injection and turbulence augmentation. The resulting program is called STANCOOL.

The program solves the boundary layer equations by a marching process in the streamwise direction. Fluid is injected into the calculational boundary layer by stopping the program when a row of holes is encountered and inserting the injectant into the stream tubes between the wall and a carefully chosen "jet penetration point" within the boundary layer. The jet-boundary layer interaction is modeled by augmenting the Prandtl mixing length. Two constants are required, in addition to the accepted constants for predicting flow over a flat, slightly rough plate.

The boundary layer equations being solved are those described in the STAN5 documentation report [6] for flow over a flat surface.

$$\frac{\partial}{\partial x} (\rho U) + \frac{\partial}{\partial y} (\rho V) = 0 \quad (6)$$

$$\rho U \frac{\partial U}{\partial x} + \rho V \frac{\partial U}{\partial y} = -g_c \frac{dP}{dx} + \frac{\partial}{\partial y} \left(\mu_{\text{eff}} \frac{\partial U}{\partial y} \right) \quad (7)$$

$$\rho U \frac{\partial I^*}{\partial x} + \rho V \frac{\partial I^*}{\partial y} = \frac{\partial}{\partial y} \left[\mu_{\text{eff}} \frac{\partial I^*}{\partial y} + \frac{\mu_{\text{eff}}}{g_c J} \left(1 - \frac{1}{Pr_{\text{eff}}} \right) \frac{\partial}{\partial y} \left(\frac{U^2}{2} \right) \right] \quad (8)$$

where $I^* = I + U^2/2g_c J$. The effective viscosity and effective Prandtl number are defined in terms of an eddy viscosity, ϵ_m , and the turbulent Prandtl number, Pr_t .

$$\mu_{\text{eff}} = \rho(\nu + \epsilon_M) \quad (9)$$

$$Pr_{\text{eff}} = \frac{1 + (\epsilon_M/\nu)}{\frac{1}{Pr} + \frac{\epsilon_M}{\nu} \cdot \frac{1}{Pr_t}} \quad (10)$$

Eddy diffusivity for momentum is modeled by the Prandtl mixing length.

$$\epsilon_M = l^2 \left| \frac{\partial U}{\partial y} \right| \quad (11)$$

The mixing-length distribution used in the program is described in the section on turbulence augmentation. The turbulent Prandtl number is presumed to follow the flat-plate variation described in Ref. 6: for air, it is 1.72 at the wall and drops to 0.86 in the outer region.

Boundary conditions for the 2-D flow equations are

$$U(x,0) = 0$$

$$V(x,0) = 0$$

$$\lim_{y \rightarrow \infty} U(x,y) = U \text{ (constant)}$$

$$I^*(x,0) = I_0^* \text{ (constant)}$$

$$\lim_{y \rightarrow \infty} I^*(x,y) = I_\infty^* \text{ (constant)}$$

C. Injection Model

1. Model development

The injection model is a calculational technique for inserting coolant into the boundary layer each time the marching process encounters a row of holes. Three candidate injection models were examined: transpiration at the wall, slot-type injection parallel to the wall, and distributed injection.

Testing of these models was carried out using the same turbulence model. The procedure was to find the injection and turbulence model constants that allowed prediction of the $\theta = 1$ Stanton number data for a given set of initial conditions, and test the $\theta = 0$ case. The predictions were deemed successful when the same injection and turbulence model constants predicted the $\theta = 0$ and $\theta = 1$ Stanton number data.

The first injection model to be tested was the transpiration model developed by Choe [1]. This model uniformly distributes the injectant over the area around the injection holes. It was found to be a successful model for low M but failed for $M = 0.4$.

A slot-type model was then developed to more accurately simulate the way the coolant is injected into the boundary layer. This model extended the range of successful predictions to $M = 0.6$, but failed for still higher M . The empirical constant for this model was the slot height, or jet-penetration point, and the injectant was distributed equally between the wall and the slot height. Physically, as M increases, the slot height should increase to model the fact that the jets of coolant penetrate

farther into the boundary layer. However, as the height was increased, the momentum effects that should have been associated with large M diminished due to the model requirement for uniform injectant distribution. An attempt was made to allow the slot of injectant to reside above the wall for high M , but this resulted in even poorer heat transfer predictions. Evidently, for moderate to high M , turbulent mixing and jet-boundary layer interaction combine to distribute some of the injectant in the near-wall region, even though the bulk of the coolant does arrive at or near the penetration point. These facts suggested examining a distributed injection model.

2. STANCOOL injection model

In constructing the distributed injection model, consideration was taken of the physical process occurring when the jets enter the boundary layer. The jet-in-crossflow discussion by Abramovich [18] and the film-cooling flow-visualization study of Colladay and Russell [12] were used as guides.

For low M the jets do not penetrate but are immediately "knocked over" by pressure and drag forces on the emerging jets, as a consequence of the boundary layer flow. For higher M , the jets leave the surface entirely and are turned in the downstream direction by pressure and shear forces which overcome the jet's resistance to change of direction. In either case, as a jet emerges into the boundary layer the shear layer at the injectant-boundary layer interface promotes entrainment of boundary layer fluid into the jet, and eventually the injectant becomes diffused into the existing boundary layer.

The injection process and entrainment diffusion process are modeled together. As a jet passes through the stream tubes that comprise the boundary layer, drag forces are presumed to "tear off" some of the injectant. The injectant that is shed into a given stream tube is then accelerated by drag forces. Shedding commences at the wall and continues until the total amount shed equals the injectant mass flowrate per unit width of film-cooled surface. The point where shedding is complete is named the penetration distance.

Equations that describe the model are obtained from one-dimensional mass, momentum, and thermal energy balances on the element of injectant bounded between two stream surfaces. This element is shown in Fig. 12. For flow between these surfaces,

$$\dot{m}_{\text{new}} = \dot{m}_{\text{old}} + \dot{\delta m} \quad (12)$$

where \dot{m}_{old} is the flow rate upstream and $\dot{\delta m}$ is the injectant that is shed into the stream tube (on a rate basis). From a momentum balance consideration,

$$(\dot{m}_{\text{old}} + \dot{\delta m})\bar{U}_{\text{new}} = \dot{m}_{\text{old}}\bar{U}_{\text{old}} + \dot{\delta m}U_j \cos \alpha \quad (13)$$

where \bar{U}_{old} is the mass-averaged velocity of the upstream fluid and U_j is the velocity of the injectant. The U_j velocity is assumed not to vary with u . This is the simplest way to preserve overall momentum within the boundary layer (i.e., $\sum \dot{\delta m}U_j \cos \alpha = \dot{m}_j U_j \cos \alpha$, where $U_j = M\rho_\infty U_\infty / \rho_j$).

The drag forces that "tear off" the injectant are assumed to accelerate $\dot{\delta m}$ from its initial velocity up to the new stream-tube velocity,

$$F_D = \dot{\delta m}(\bar{U}_{\text{new}} - U_j \cos \alpha) \quad (14)$$

The drag forces can be defined in terms of a drag coefficient for convenience,

$$F_D = C_D \frac{1}{2} \rho A_j (\bar{U}_{\text{old}})^2 \quad (15)$$

where A_j is the cross-sectional area of the jet, $(D \cdot \delta y) / \sin \alpha$ for a stream tube that is δy in width (proportional to $\delta \psi$).

By introducing the definition $\dot{m}_{\text{old}} = \rho \bar{U}_{\text{old}} (\delta y \cdot P)$, where P is the distance between adjacent jets, and combining with the above equations, the ratio of the mass shed from the coolant jet to the existing mass between the stream tubes (on a rate basis) can be written as

$$\frac{\dot{\delta m}}{\dot{m}_{\text{old}}} = \left[\frac{2(P/D)}{C_D} \left(1 - \frac{U_j \cos \alpha}{\bar{U}_{\text{old}}} \right) - 1 \right]^{-1} \quad (16)$$

A mass-averaged velocity ratio can be formed by rearranging Eqn. (16):

$$\frac{\bar{U}_{\text{new}}}{\bar{U}_{\text{old}}} = \left[1 + \left(\frac{\dot{\delta m}}{\dot{m}_{\text{old}}} \right) \frac{U_j \cos \alpha}{\bar{U}_{\text{old}}} \right] \left(1 + \frac{\dot{\delta m}}{\dot{m}_{\text{old}}} \right)^{-1} \quad (17)$$

From energy balance considerations

$$\bar{I}_{\text{new}}^* (\dot{m}_{\text{old}} + \dot{\delta m}) = \dot{m}_{\text{old}} \bar{I}_{\text{old}}^* + \dot{\delta m} I_j^* \quad (18)$$

where \bar{I}_{old}^* is the mass-averaged stagnation enthalpy of the upstream fluid and I_j^* is that of the injectant (assumed not to vary with y to satisfy overall energy conservation). A mass-averaged enthalpy ratio can be formed by rearranging Eqn. (18):

$$\frac{\bar{I}_{\text{new}}^*}{\bar{I}_{\text{old}}^*} = \left[1 + \left(\frac{\dot{\delta m}}{\dot{m}_{\text{old}}} \right) \frac{I_j^*}{\bar{I}_{\text{old}}^*} \right] \left(1 + \frac{\dot{\delta m}}{\dot{m}_{\text{old}}} \right)^{-1} \quad (19)$$

In the prediction program, the injection model, based on the analysis given above, is contained in a subroutine, and it is invoked whenever a row of holes is encountered. The empirical input is the mass shed ratio, defined as

$$\frac{\dot{\delta m}}{\dot{m}_{\text{old}}} = \text{DELMR} = f(M, P/D, \alpha) \quad (20)$$

The DELMR expression is used in lieu of Eqn. (17), for simplicity. With this as input, the routine processes each flow tube from the wall outward. The velocities are adjusted according to Eqn. (17) to conserve momentum. The stagnation enthalpies are adjusted according to Eqn. (19). The injection process is terminated at the stream tube, where

$$\dot{m}_j = \rho_j U_j \frac{\pi D^2}{4P} = \sum_i \text{DELMR} \cdot \dot{\delta \psi}_i \quad (21)$$

Note the introduction of P to put the flow rate on a per-unit depth basis (consistent with the dimensions of ψ). The y location where flow injection is terminated is PD , the penetration distance.

D. Turbulence-Augmentation Model

1. Model development

The turbulence model accounts for the effects of coolant injection on the turbulent transport terms by altering the eddy viscosity. Three turbulence models were studied: mixing-length augmentation tied to the transpiration injection model, to the distributed injection model, and to a turbulence kinetic energy (TKE) model.

Development and testing of the augmented mixing-length model for use with transpiration was carried out by Choe [1] for normal-angled injection. He made detailed pitot tube surveys of the spanwise distribution of the velocity field within the full-coverage region. From a set of ten profiles between $-P/2$ and $+P/2$ he constructed a spanwise-averaged profile. He then integrated the momentum equation, using an analogy between wall friction and heat transfer, and obtained an average shear-stress distribution through the boundary layer. A mixing-length distribution was determined using the velocity profile derivatives and the shear stress distribution. The mixing-length distribution was found to be nearly identical to that of a 2-D boundary layer in the near-wall region and near the free stream, but in the central part of the boundary layer it was higher. The augmented mixing length was modeled by a one-parameter curve fit to the experimental distribution.

Crawford [3] carried out the same velocity profile study for the slant-angled injection and found the same augmented mixing-length profile as did Choe. The Crawford model is similar to Choe's, but the model parameter describing the peak in augmentation is directly tied to the distributed injection model.

A turbulence kinetic energy model was investigated in hopes of circumventing some of the recovery region problems encountered with the Crawford model [3]. Yavuzkurt et al. [4] carried out a detailed velocity and Reynolds stress study of the flow field over the slant-angled injection test section and in its recovery region. He developed a very successful TKE model for recovery region predictions, solving the TKE equation with a length-scale model developed from experimental data. Efforts were then made to develop a similar length-scale model for the full-coverage region,

but with only marginal success. Rather than use different schemes in the full-coverage and recovery regions, the Choe-type model, as modified by Crawford, was adopted.

2. STANCOOL turbulence model

The eddy diffusivity for momentum is modeled by algebraically augmenting the Prandtl mixing length using

$$\frac{\ell}{\delta} = \left(\frac{\ell}{\delta}\right)_{2-D} + \left(\frac{\ell}{\delta}\right)_a \quad (22)$$

where the "2-D" subscript refers to the 2-D mixing length and the "a" denotes the departure due to the jet-boundary layer interaction. The 2-D mixing-length distribution is that used in STAN5:

$$\ell_{2-D} = \begin{cases} \kappa y D & , \quad \kappa y < \lambda \delta \\ \lambda \delta & , \quad \kappa y \geq \lambda \delta \end{cases} \quad (23)$$

where D is the Van Driest damping function,

$$D = 1 - \exp(-y^+/A^+) \quad (24)$$

In the above equation, κ is the von Karman constant; λ is the outer layer length-scale constant; δ is the 99 percent boundary layer thickness, $y^+ = y\sqrt{\tau_w/\rho}/\nu$; and A^+ is the Van Driest damping constant. A^+ was about 22 to 23 in the full-coverage region, and it was 25 in the recovery region. The smaller A^+ in the film-cooling region reflected the effect of surface roughness due to the holes. The A^+ transition was handled according to the first-order lag equation described by Crawford and Kays [6].

Augmentation of the 2-D mixing length is depicted in Fig. 13. The curve represents a departure from the 2-D distribution, with a maximum located at PD/δ . The augmented mixing-length distribution is a curve fit to Fig. 13, and it is superimposed on the 2-D distribution according to Eqn. (22).

$$\ell_{\max,a} = \lambda_{\max,a} \cdot \delta \cdot F \quad (25)$$

where F is an exponential function that decays the $\lambda_{\max,a} \cdot \delta$ product on either side of PD/δ .

$$F = 2.718 \left(\frac{y}{PD} \right)^2 \exp[- (y/PD)^2]$$

The mixing-length augmentation is a maximum in the vicinity of the injection site, and it decreases in the downstream direction. A model for this decay was developed by Yavuzkurt [4], based on his hydrodynamic studies of the recovery region, downstream of the last row of holes. He found that the augmented turbulence decayed with a time constant proportional to the boundary layer thickness. To model this decay the $(\ell/\delta)_{\max,a}$ in Eqn. (25) is replaced by an effective value, $(\ell/\delta)_a$; and $\lambda_{\max,a}$ is replaced with

$$\lambda_{\text{eff}} = \lambda_{\max,a} \cdot \exp[- (x'/\delta)/2] \quad (27)$$

where x' is the streamwise distance, measured from the point of injection, and the time constant for decay is two boundary-layer thicknesses.

In the prediction program, the mixing length is computed using

$$\ell = \left\{ \begin{matrix} \kappa y \\ \lambda \delta \end{matrix} \right\} + \lambda_{\text{eff}} \cdot F \cdot \delta \quad (28)$$

and in the near-wall region the mixing length is damped by multiplying it by Eqn. (24). The empirical input to the turbulence-augmentation model is

$$\lambda_{\max,a} = \text{ALAM} = f(M, P/D, \alpha) \quad (29)$$

and λ_{eff} is computed using this input variable and Eqn. (27). The x' is zero at each injection location and increases linearly in the downstream direction.

The success of this turbulence-augmentation model is due partly to its being directly tied to the injection model through PD , the penetration distance. In the turbulence model, PD was arbitrarily assigned to coincide with the mixing-length maximum; in retrospect, perhaps it should have been the outermost edge of the mixing-length perturbation, because

for large M , where PD/δ approaches unity, half the augmentation is located in the potential core. This problem was discovered only after the model had been used for most of the low-to-moderate M predictions. To overcome this problem for high M or for thin initial boundary layers, PD/δ was never allowed to exceed 0.8 (arbitrarily fixed).

E. Summary and Constants for the Model

The STANCOOL program is basically the STAN5 boundary layer program with an appended subroutine COOL that contains the injection model. The turbulence-augmentation model resides within the existing subroutine AUX. Boundary conditions for the program consist of specifying the wall temperature and free-stream velocity at various x locations (usually constants, independent of x).^{*} The initial conditions are experimentally obtained velocity and temperature profiles upstream of the first row of cooling holes. A three-by-eleven array contains x locations and the M and θ parameter values for the eleven rows of film-cooling holes.

Program STANCOOL commences integration upstream of the first row of holes. When the program encounters a row of holes, it stops and the velocity and temperature profiles are augmented according to Eqns. (17) and (19), with $(\dot{\delta m}/\dot{m}_{old})$ being replaced by DELMR, the input injection constant. Injection commences at the surface and proceeds outward, stream tube by stream tube, until $\sum \dot{\delta m} = \dot{m}_j/P$. The final stream tube y location is PD , the penetration distance. With PD determined, the exponential function F (Eqn. (26)) is determined for the augmented mixing length. Integration is restarted, and at each integration point downstream, λ_{eff} is computed according to Eqn. (27), with $\lambda_{max,a}$ being replaced by ALAM, the input turbulence constant. The total mixing length is determined using Eqn. (28). For each row of holes this series of steps is repeated.

The input injection and turbulence augmentation constants were determined for each heated starting length, $P/D = 5$ data set contained in Refs. 1, 3, and 5, and in Appendix B (with the exception of $M = 1.5$ at momentum Reynolds number = 1800, compound-angled injection). Figs. 14 and

^{*} For low-velocity, constant-property flows the stagnation enthalpy and temperature variable are interchangeable.

15 show these constants and the recommended correlations. The user must provide DELMR and ALAM as input values to STANCOOL. Multiple points for a given M indicate different initial conditions. In Fig. 14 the DELMR constant is seen to be almost independent of initial conditions except for compound-angled injection at $M = 0.4$. For this case the DELMR constants were 0.45, 0.27, and 0.11 for initial momentum Reynolds numbers of 2700, 1800, and 500. The DELMR constant was shown to be completely independent of the thermal initial condition in Ref. 3. In Fig. 15 the important point is the 20 to 25 percent increase in ALAM for a low initial Reynolds number and normal- and slant-angled injection. The criterion for when the constants successfully predicted the data is discussed in the next section.

F. Prediction of the Data Bases

It is difficult to identify the physical criteria which should be used to assess the merits of a numerical prediction program. Candidates include: heat transfer and friction coefficients, temperature and velocity profiles, and profiles related to the turbulence within the flow field. Ideally one would like a numerical program capable of reproducing all attributes of the flow field for any prescribed geometry and initial and boundary conditions. For simple shear flows we are approaching this realization. When even the best programs are applied to complex flows (of which film-cooled boundary layers are a class), the predictions often deviate from the experimental data in one way or another and the programs must be specialized to yield satisfactory predictions. One should probably not use the word prediction, but instead call the process interpolation. One should not use a specialized program beyond the limits of the geometry and initial and boundary conditions of the data bases used to develop it.

The program reported here is a specialized program made by modifying a well-tested boundary layer program to include an injection model for introducing coolant, and by introducing a turbulence-augmentation model for simulating the shear layer interaction within the boundary layer. There is no claim that this program will predict the detailed attributes of the flow field. It was intended only to develop a program to replicate

the spanwise-averaged Stanton number data bases available at Stanford. We would expect, however, that success in predicting these spanwise-averaged data would imply the possibility of at least limited success in modeling the gross aspects of the flow.

In Section II.B it was indicated that, for a given full-coverage geometry, the Stanton number should depend on θ , M , and upstream boundary conditions; Prandtl number, Mach number, and Eckert number effects for the coolant and mainstream; turbulence and pressure gradient conditions of the mainstream; and surface rotation and curvature. Based on experience with simple flows, including transpired turbulent boundary layers, one would expect the STANCOOL program to have at least limited success in extrapolating the predictions to the compressible, high-velocity, pressure-gradient conditions of a gas turbine engine. The effects of mainstream turbulence, rotation and curvature have not been included in STANCOOL. One point not yet answered is which should be used: the ratio of coolant-to-mainstream velocity, the mass flux ratio, or the momentum ratio. One of these is required in describing the DELMR and ALAM prediction constant correlations for compressible, high-velocity flows.

Initial success in development of the STANCOOL program was described in [3]. The results are summarized as follows. The injection model was tested at $M = 0.4$ and five initial conditions: unheated starting lengths with momentum Reynolds numbers of 1900, 2700, and 4800, and heated starting lengths with momentum/enthalpy Reynolds numbers of 2700, 1800 and 500, 500. The same value of DELMR successfully predicted all five data sets. In addition, all but the low Reynolds number case used the same ALAM. For low Re the value had to be increased about 20 percent. The prediction program was used to simulate film cooling with 24 rows of holes and slant-angled injection at $P/D = 5$. The predicted Stanton number trend was identical to that for 11 rows (i.e., constant St for $\theta = 0$ and a continued decreasing St for $\theta = 1$). Predicted velocity and temperature profiles with $M = 0.4$ were compared to pitot-tube and thermocouple experimental spanwise-averaged profiles. The predicted velocity profile was in qualitative agreement, and the $\theta = 0$ and $\theta = 1$ predicted temperature profiles were almost identical to the experimental profiles.

Three sets of predictions have been carried out for normal-angled injection with $P/D = 5$. The results are shown in Figs. 16 and 17. The initial and boundary conditions, as well as the superposition-adjusted $\theta = 0$ and $\theta = 1$ data are contained in [1]. The agreement between data and STANCOOL is excellent except for the initial film-cooling region for $\theta = 0$ with low initial Reynolds number (see Fig. 17).

Ten sets of predictions have been carried out for slant-angled injection. The experimental data are contained in Appendix B and in [3]. Several predictions of the unheated starting length data sets are also contained in [3]. Figs. 18 through 23 show predictions for similar initial conditions, with $P/D = 5$ and M as a parameter. The predictions for low M are excellent. By $M = 0.6$, the $\theta = 1$ recovery region predictions begin to deviate substantially from the experimental values. Again there is a slight underprediction for $\theta = 0$ in the initial film-cooling region.

Figures 24 and 25 are for low initial momentum Reynolds number and $P/D = 5$ and $P/D = 10$. Except for the high- M recovery region at $\theta = 1$, the agreement between prediction and data is excellent. The effect of Eqn. (26) on damping ALAM can be seen by comparing the two figures.

Compound-angled injection data from [5] have been predicted, and they are given in Figs. 26 through 32. On the whole, these predictions are much less satisfactory. Surprisingly, the $M = 0.4$ data were the most difficult to predict, and no single value of DELMR could be found for the three different initial conditions (Figs. 25, 29, and 32). Recovery region predictions for $\theta = 1$ were inadequate at high M , and the initial blowing region predictions deviated by about 10 percent at high M . It is interesting to note, though, that the DELMR and ALAM values correlated reasonably well, as shown in Figs. 14 and 15.

The STANCOOL program has been successful in replicating most of the normal- and slant-angled injection data bases and has shown limited success for compound-angled injection. Recovery-region predictions at high M are also, at most, a limited success. Careful examination of the prediction graphs indicates prediction discrepancies in the initial film-cooling region for moderate to high M (and low M at low initial Reynolds number).

There are four distinct flow fields on the film-cooled surface:

(1) the initial film-cooling region; (2) the "asymptotic" film-cooling region (past the first few rows of holes); (3) the recovery region for low M ; and (4) the recovery region for moderate to high M . It is not surprising that STANCOOL adequately models regions (2) and (3) and not (1) and (4). Region (2), the asymptotic film-cooling region, is represented by the injection and turbulence-augmentation model. Region (3), the recovery region for low M , is indirectly modeled by the relatively fast decay of the augmented turbulence to its 2-D value and the fact that the recovery region profiles are not too different from the 2-D value.

For moderate to high M in the recovery region, the turbulence also quickly decays, but the velocity profiles are very flat and far from the 2-D value (Yavuzkurt, Ref. 4). This causes turbulence production that is less than the 2-D value and seems to be the primary cause for the continual drop in Stanton number in the recovery region. The depression of the mixing-length below its 2-D value for moderate to high M is not modeled in STANCOOL.

The initial film-cooling region represents the transition from 2-D flow to 3-D spanwise-periodic flow. This region is not modeled in STANCOOL. The transition region is fairly short (several rows) for normal- and slant-angled injection and high initial Reynolds number. The region is longer (five to six rows) for low initial Reynolds number (a thin boundary layer compared to the jet diameter). For compound-angled injection the transition region occupies at least six rows of film cooling, and the flow field is distinctly different from normal- and slant-angled injection because of its strong streamwise vorticity.

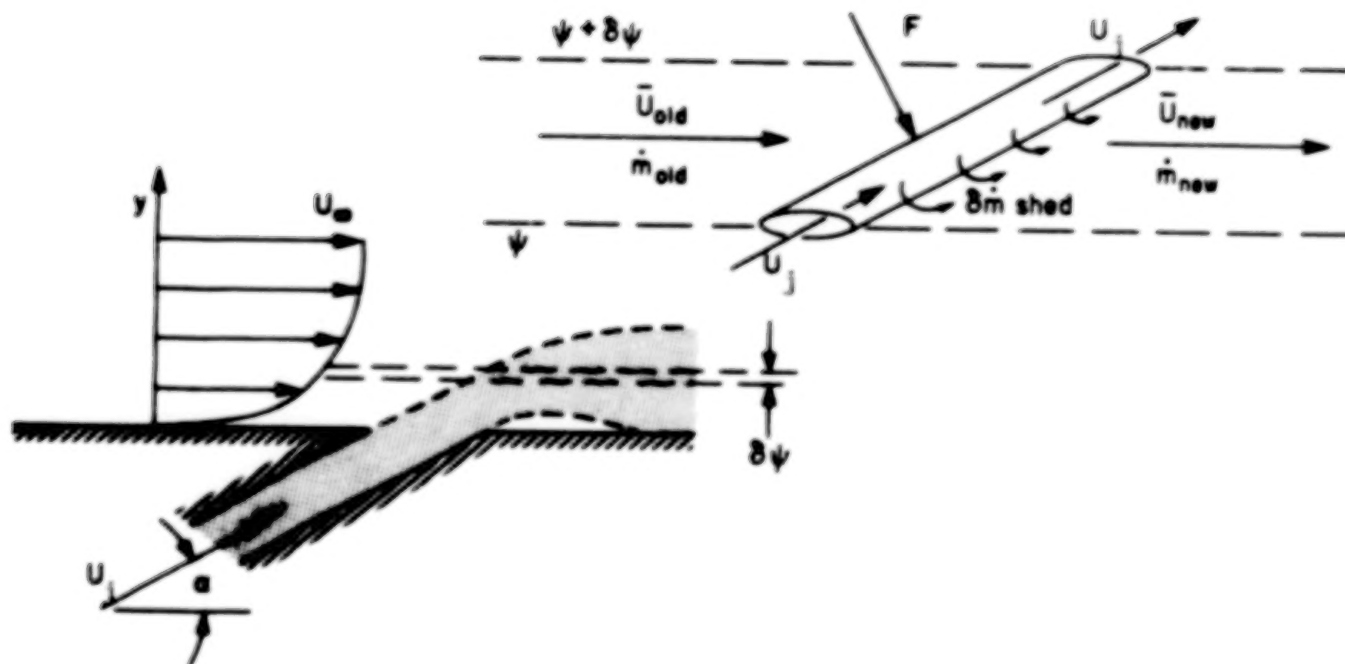


Fig. 12. Idealized representation of the injection process.

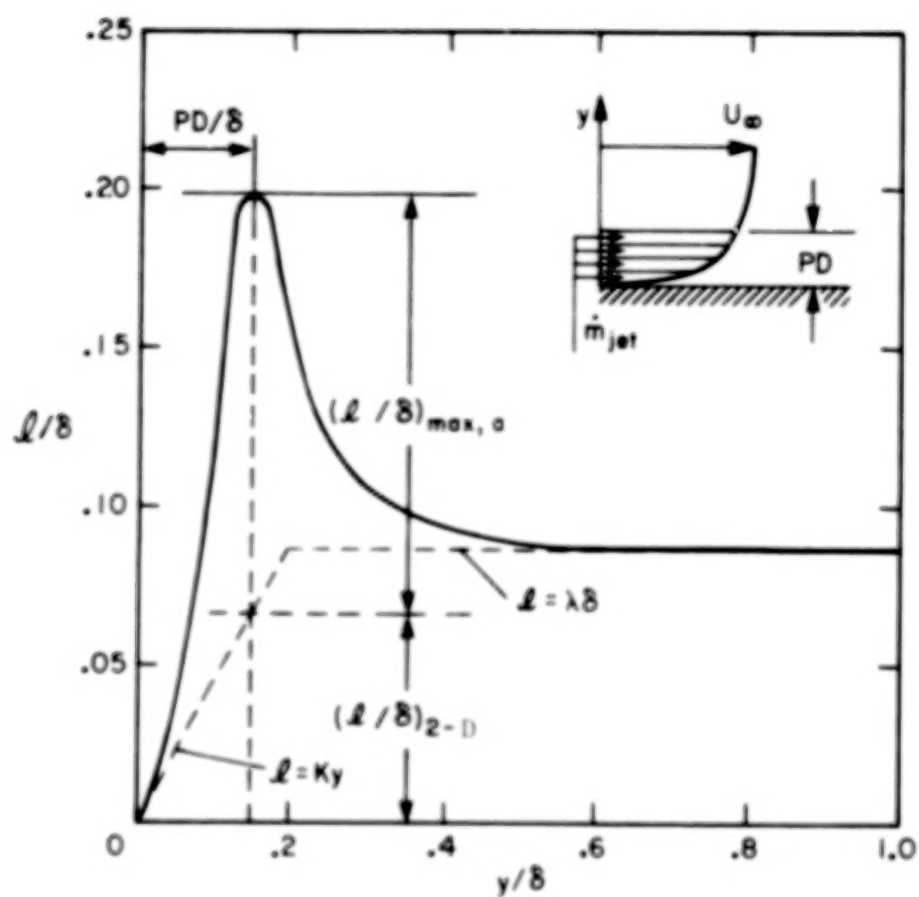


Fig. 13. Idealized representation of the distribution of mixing length in a full-coverge region.

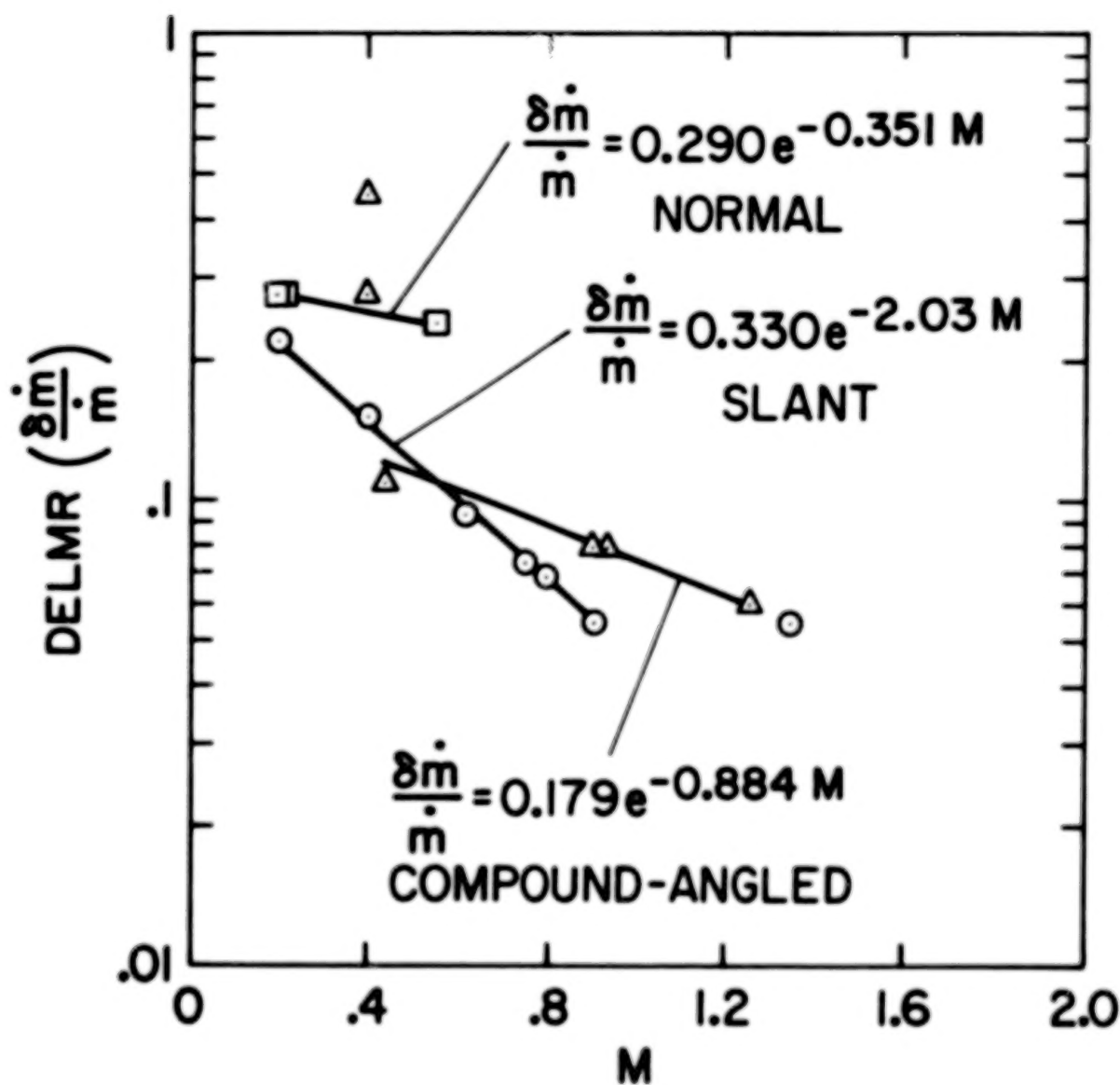


Fig. 14. The injection and parameter DELMR as a function of M for normal-, slant-, and compound-angle injection.

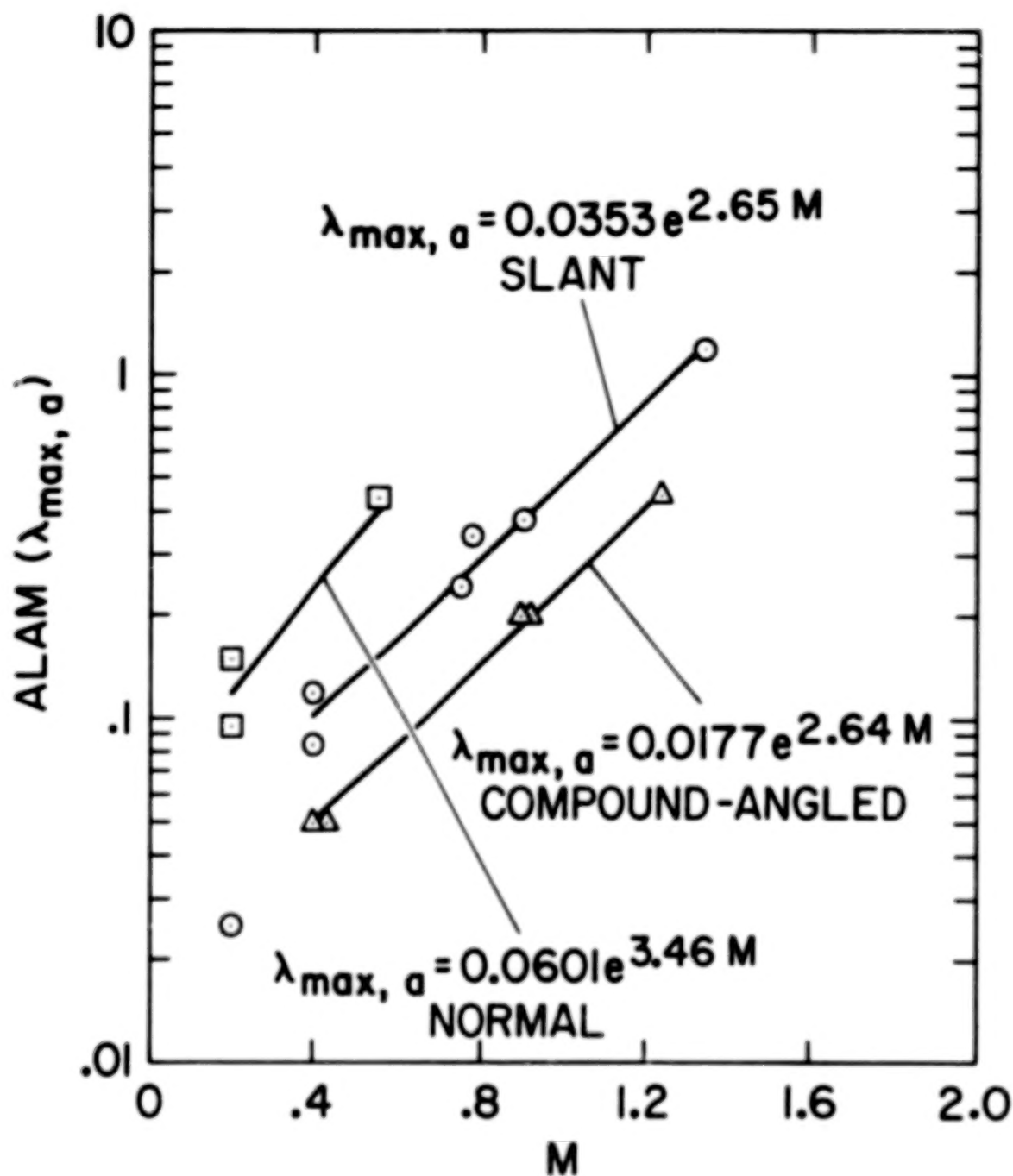


Fig. 15. The turbulence augmentation parameter ALAM ($\lambda_{\max, a}$) as a function of M for normal-, slant-, and compound-angle injection.

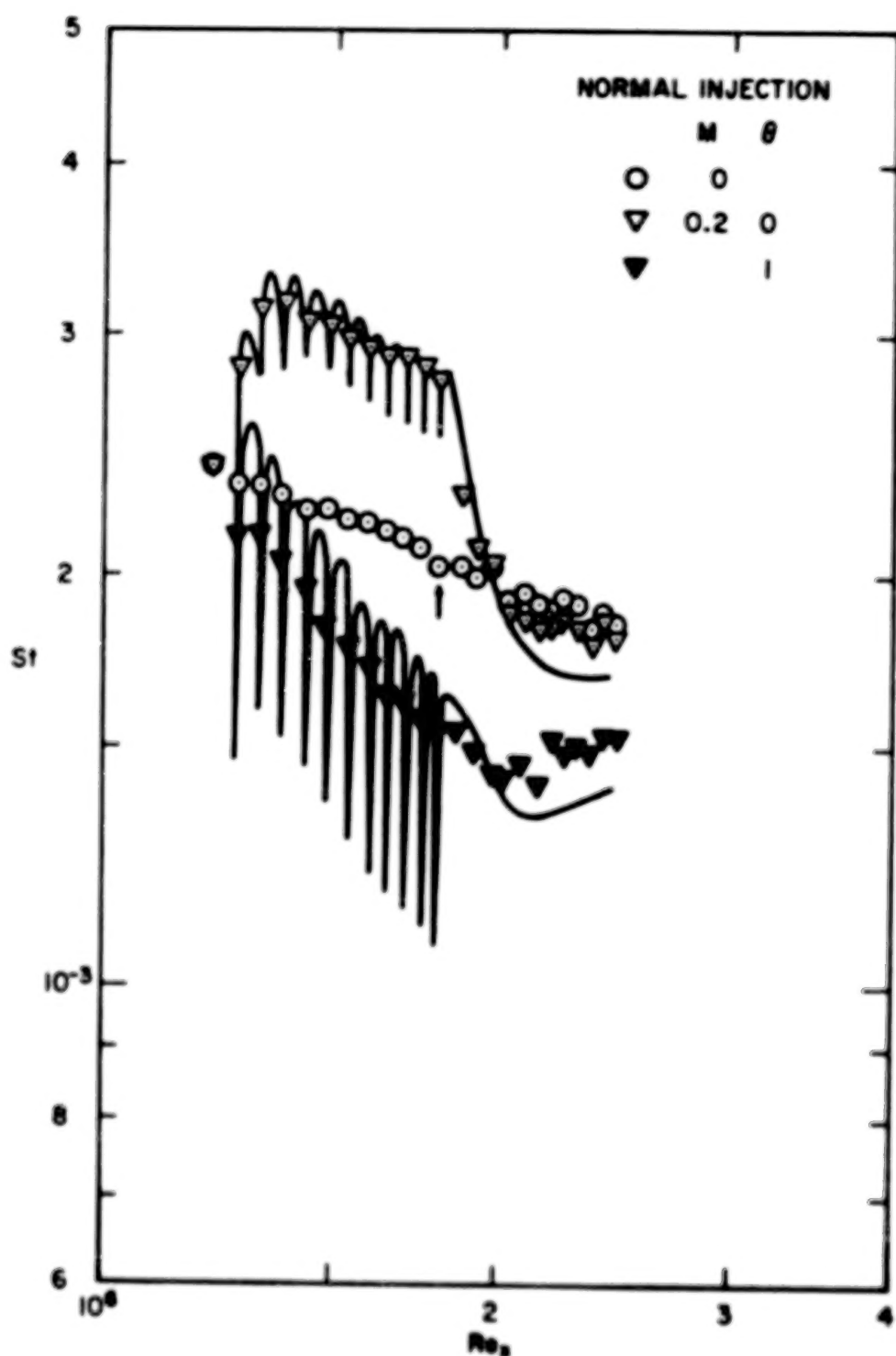


Fig. 16. Comparison of measured and predicted Stanton numbers for normal injection: $M = 0.2$, $P/D = 5.0$, with initial momentum and enthalpy thickness Reynolds numbers of 2800 and 1800, respectively.

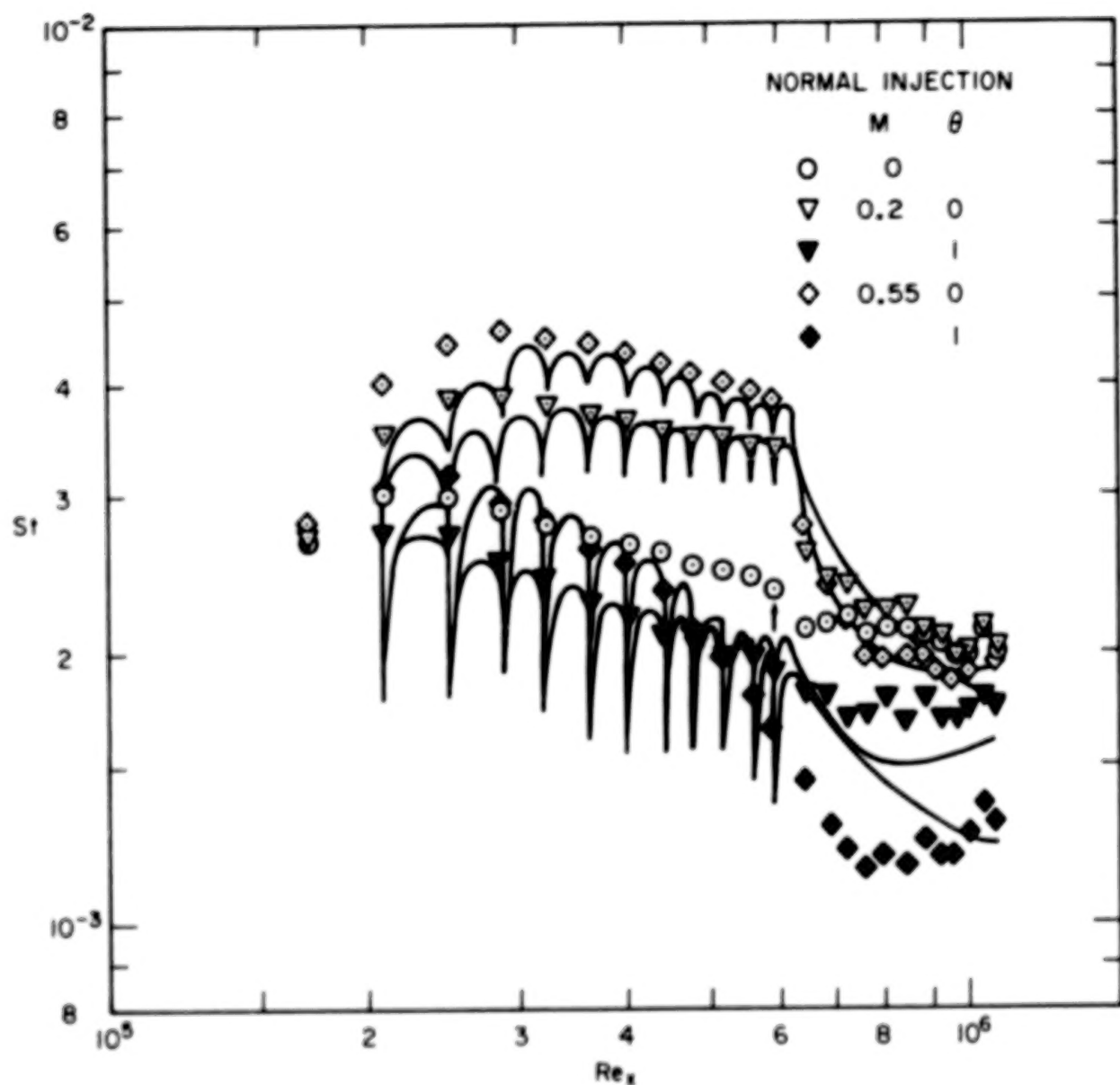


Fig. 17. Comparison of measured and predicted Stanton numbers for normal injection: $M = 0.2$ and 0.55 , $P/D = 5.0$, with initial momentum and enthalpy thickness Reynolds numbers of 550 and 600, respectively.

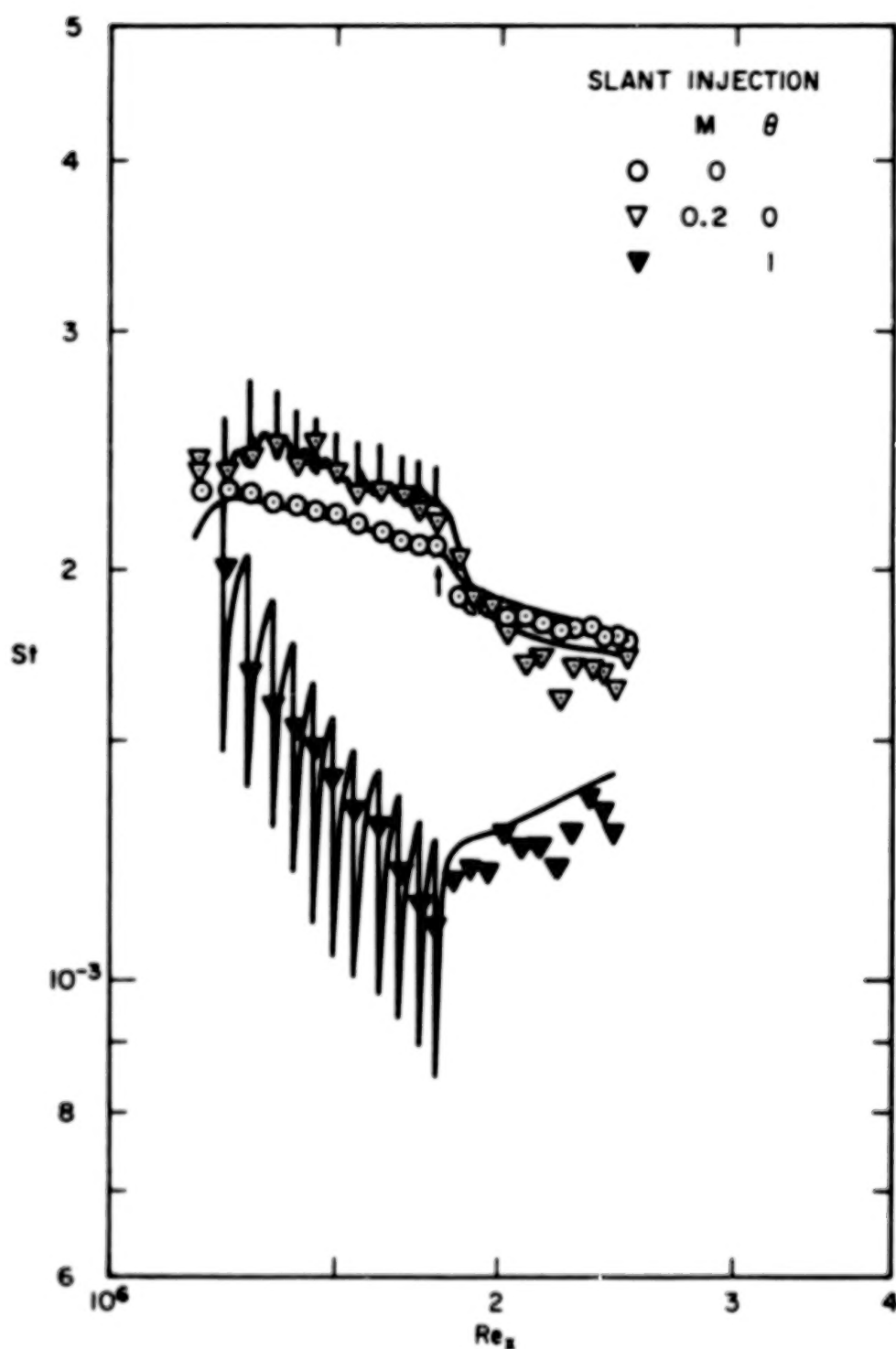


Fig. 18. Comparison of measured and predicted Stanton numbers for slant-angle injection: $M = 0.2$, $P/D = 5.0$, with initial momentum and enthalpy thickness Reynolds numbers of 3000 and 2100, respectively.

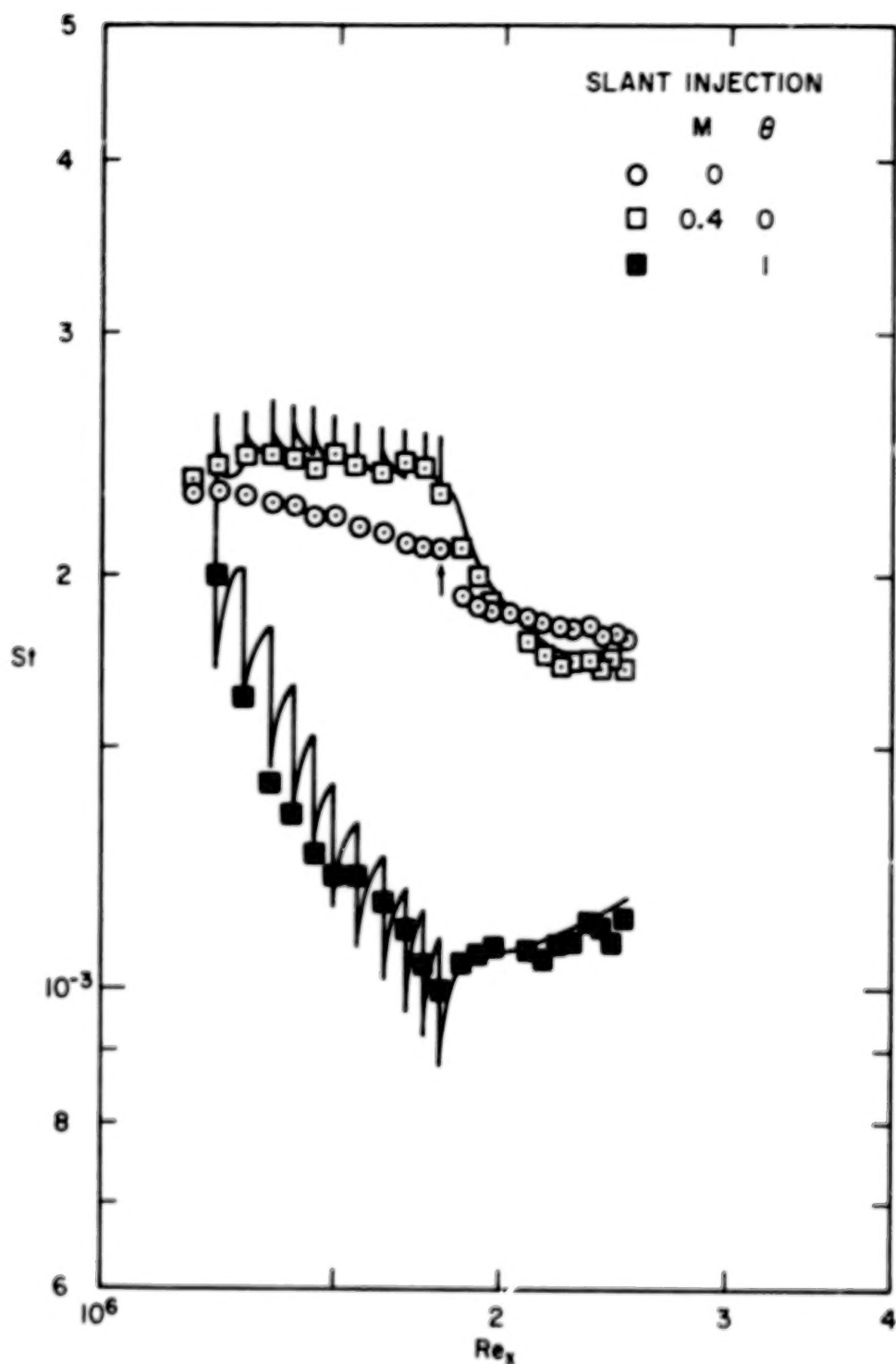


Fig. 19. Comparison of measured and predicted Stanton numbers for slant-angle injection; $M = 0.4$, $P/D = 5$, with initial momentum and enthalpy thickness Reynolds numbers of 3000 and 2100, respectively.

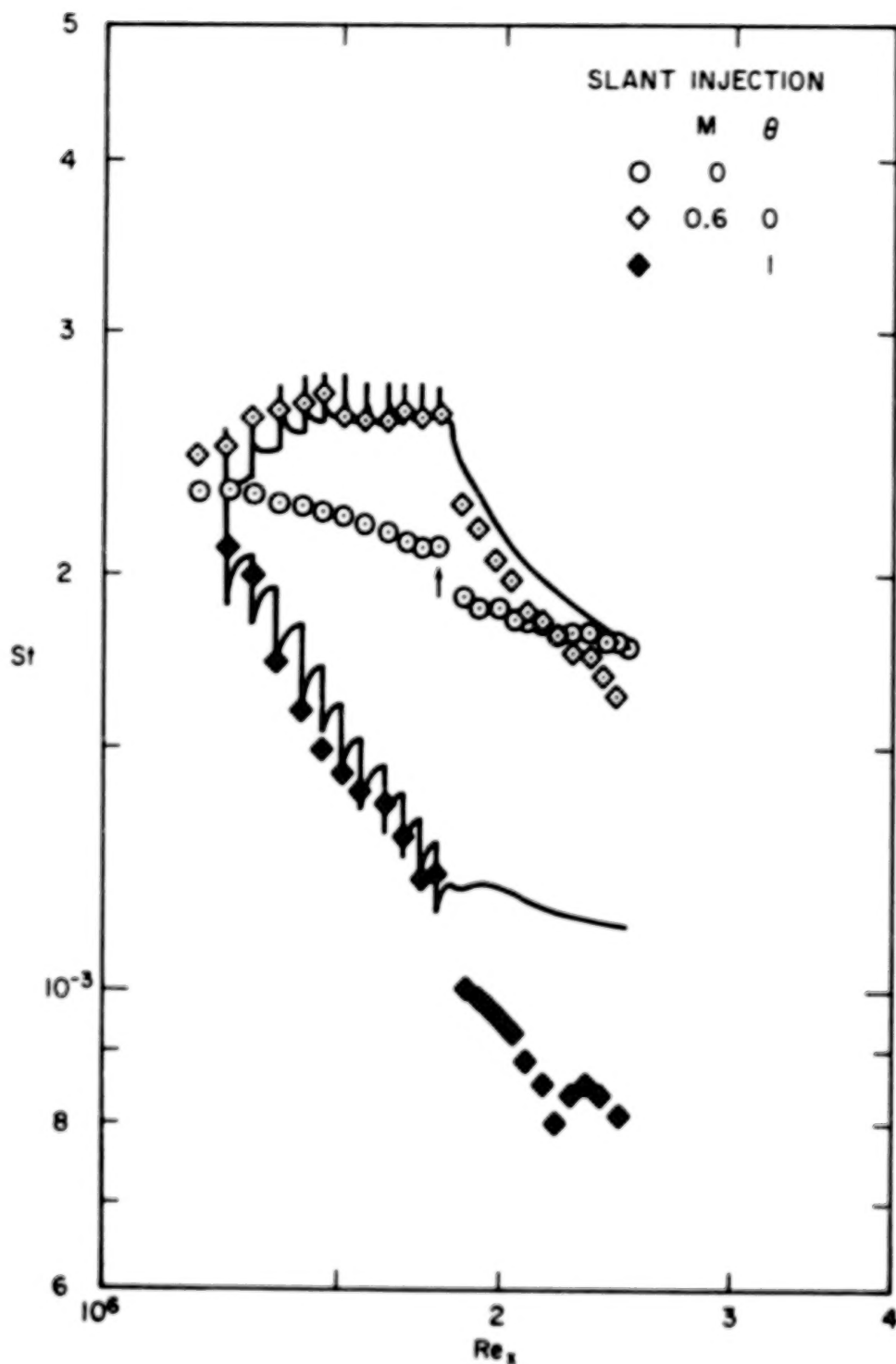


Fig. 20. Comparison of measured and predicted Stanton numbers for slant-angle injection: $M = 0.60$, $P/D = 5.0$, with initial momentum and enthalpy thickness Reynolds numbers of 3000 and 2100, respectively.

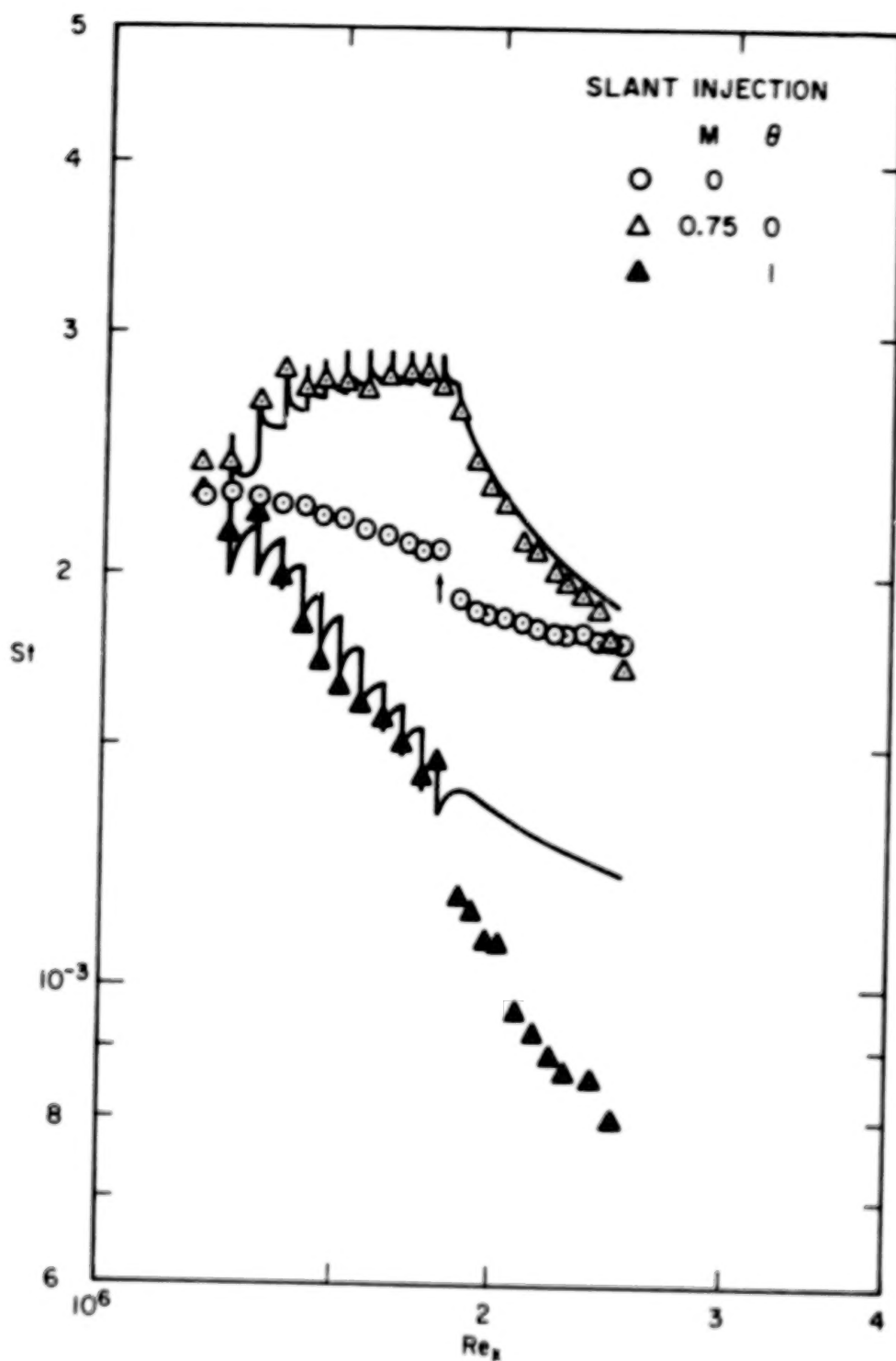


Fig. 21. Comparison of measured and predicted Stanton numbers for slant-angle injection: $M = 0.75$, $P/D = 5.0$, with initial momentum and enthalpy thickness Reynolds numbers of 3000 and 2100, respectively.

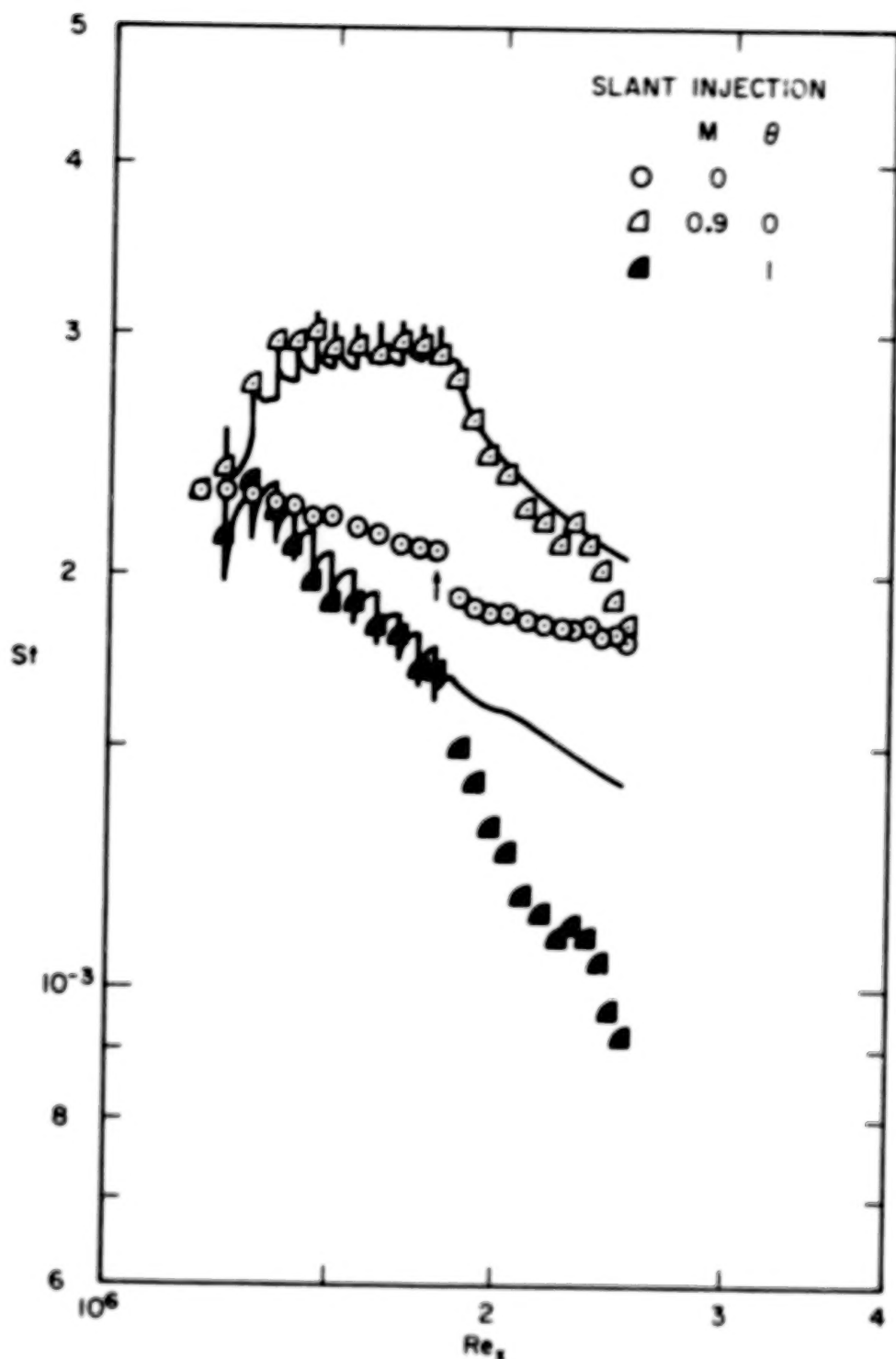


Fig. 22. Comparison of measured and predicted Stanton numbers for slant-angle injection: $M = 0.90$, $P/D = 5.0$, with initial momentum and enthalpy thickness Reynolds numbers of 3000 and 2100, respectively.

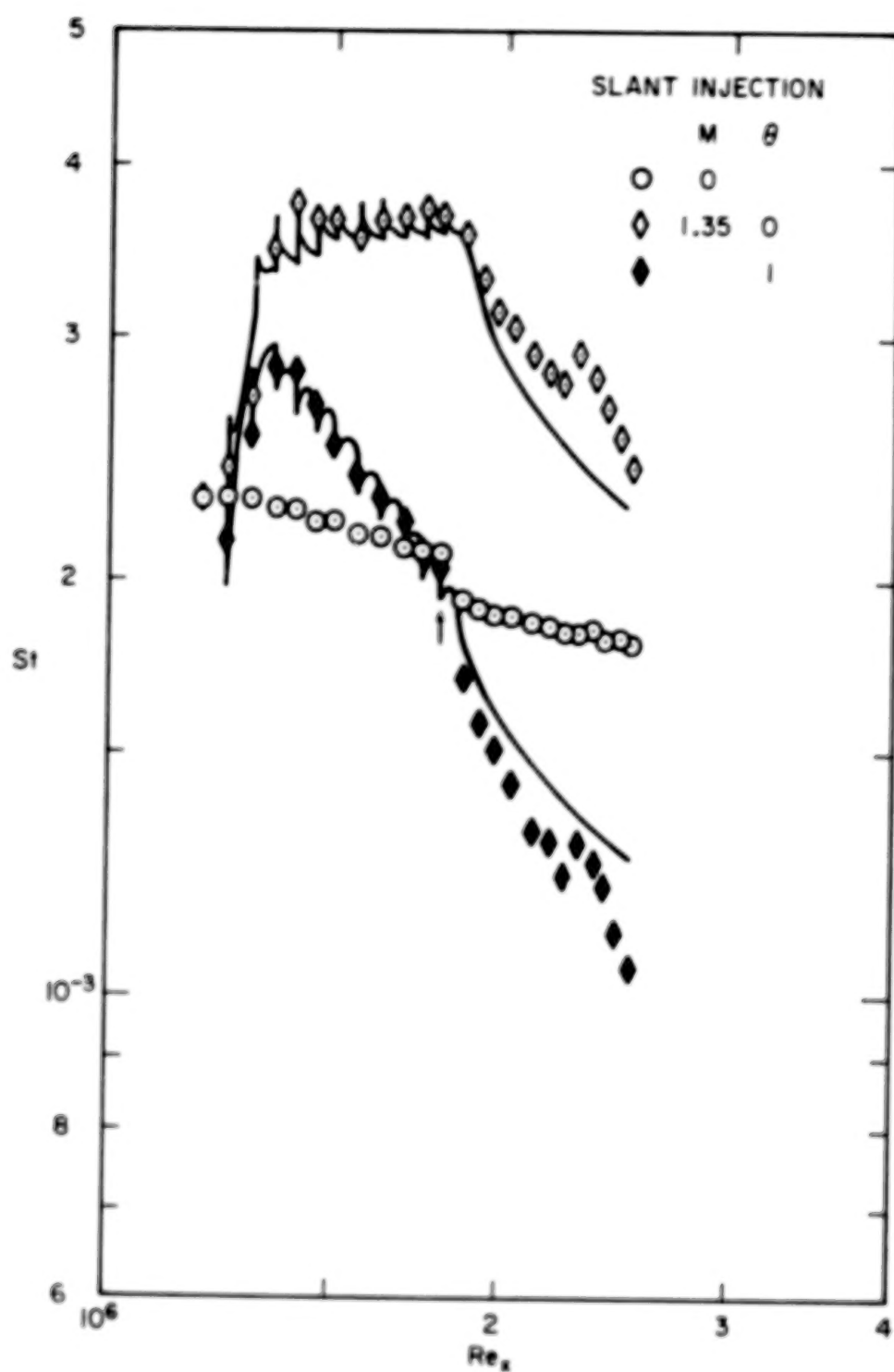


Fig. 23. Comparison of measured and predicted Stanton numbers for slant-angle injection: $M = 1.35$, $P/D = 5.0$, with initial momentum and enthalpy thickness Reynolds numbers of 3000 and 2100, respectively.

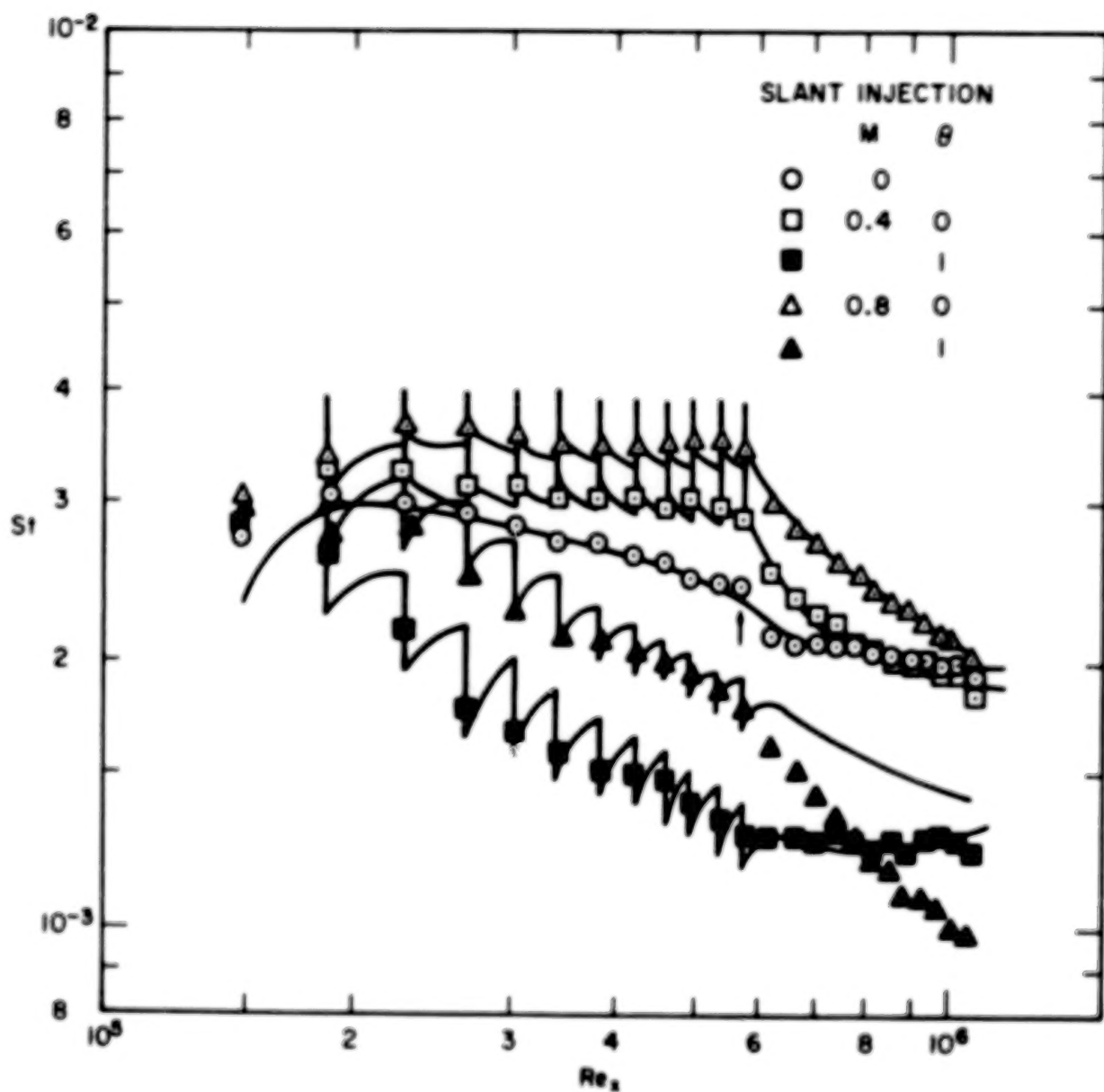


Fig. 24. Comparison of measured and predicted Stanton numbers for slant-angle injection: $M = 0.4$ and $M = 0.8$, $P/D = 5.0$, with initial momentum and enthalpy thickness Reynolds numbers of 500 and 500, respectively.

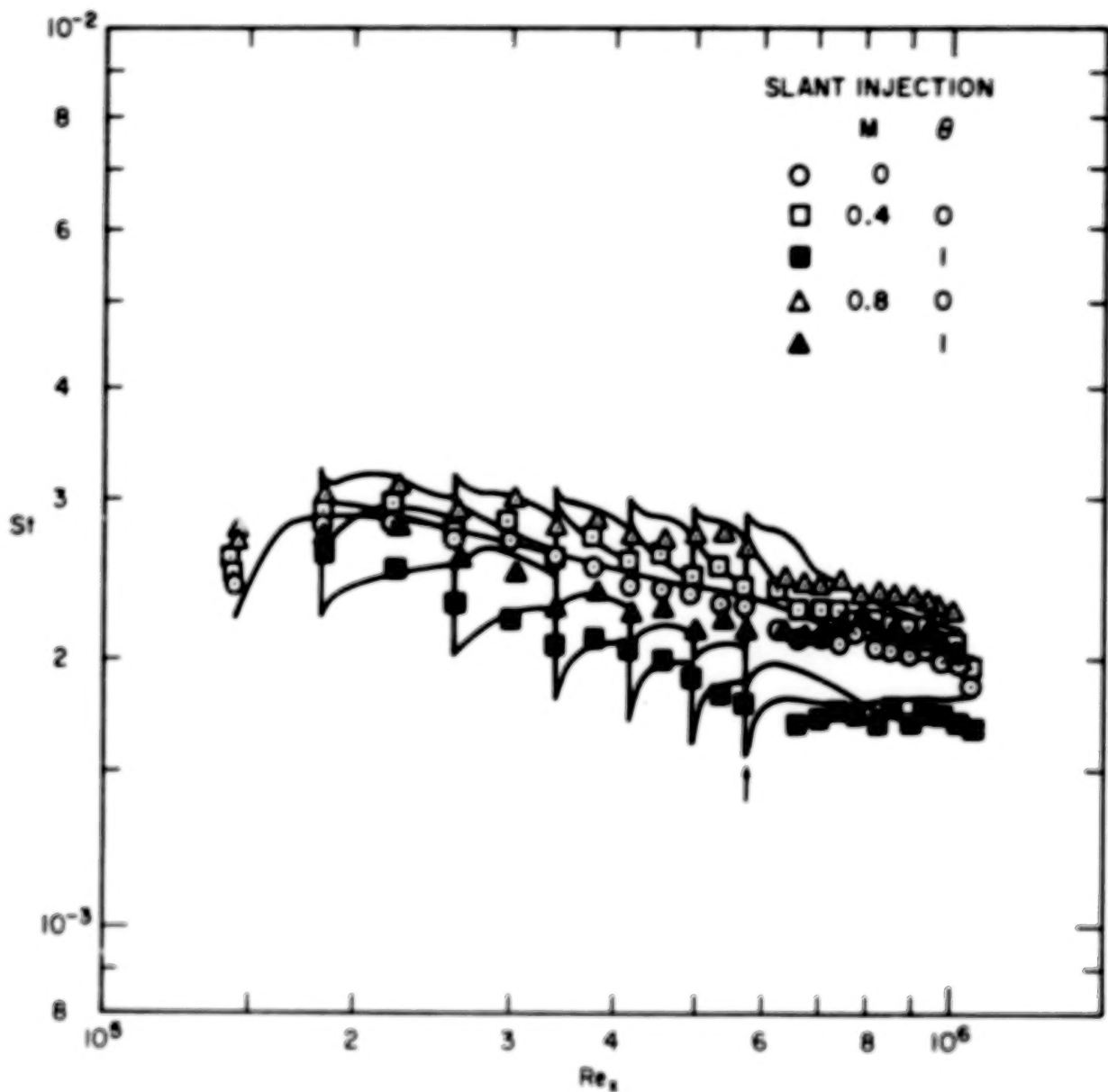


Fig. 25. Comparison of measured and predicted Stanton numbers for slant-angle injection: $M = 0.4$ and $M = 0.8$, $P/D = 10.0$, with initial momentum and enthalpy thickness Reynolds numbers of 500 and 500, respectively.

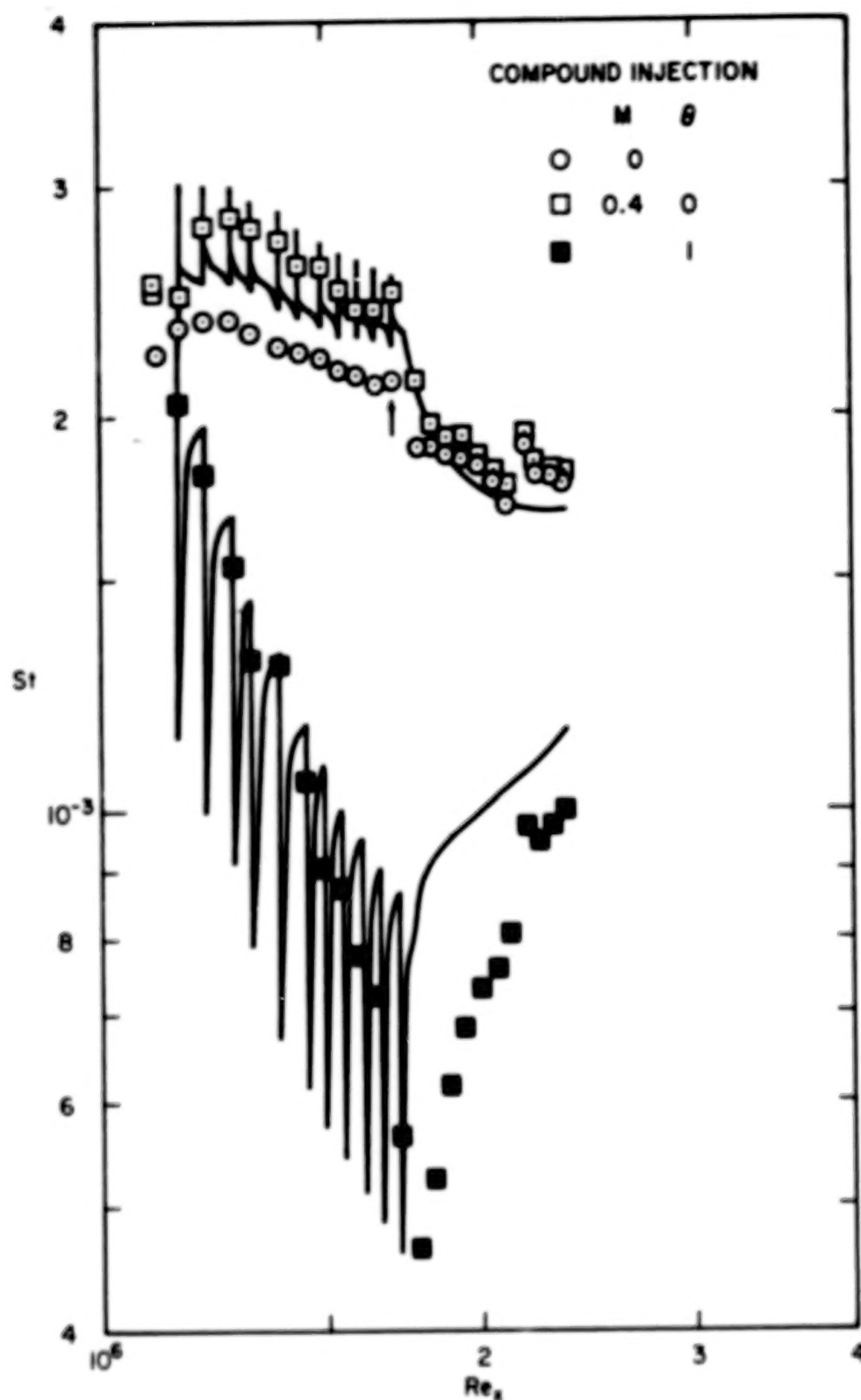


Fig. 26. Comparison of measured and predicted Stanton numbers for compound-angle injection: $M = 0.4$, $P/D = 5.0$, with initial momentum and enthalpy thickness Reynolds numbers of 2500 and 1800, respectively.

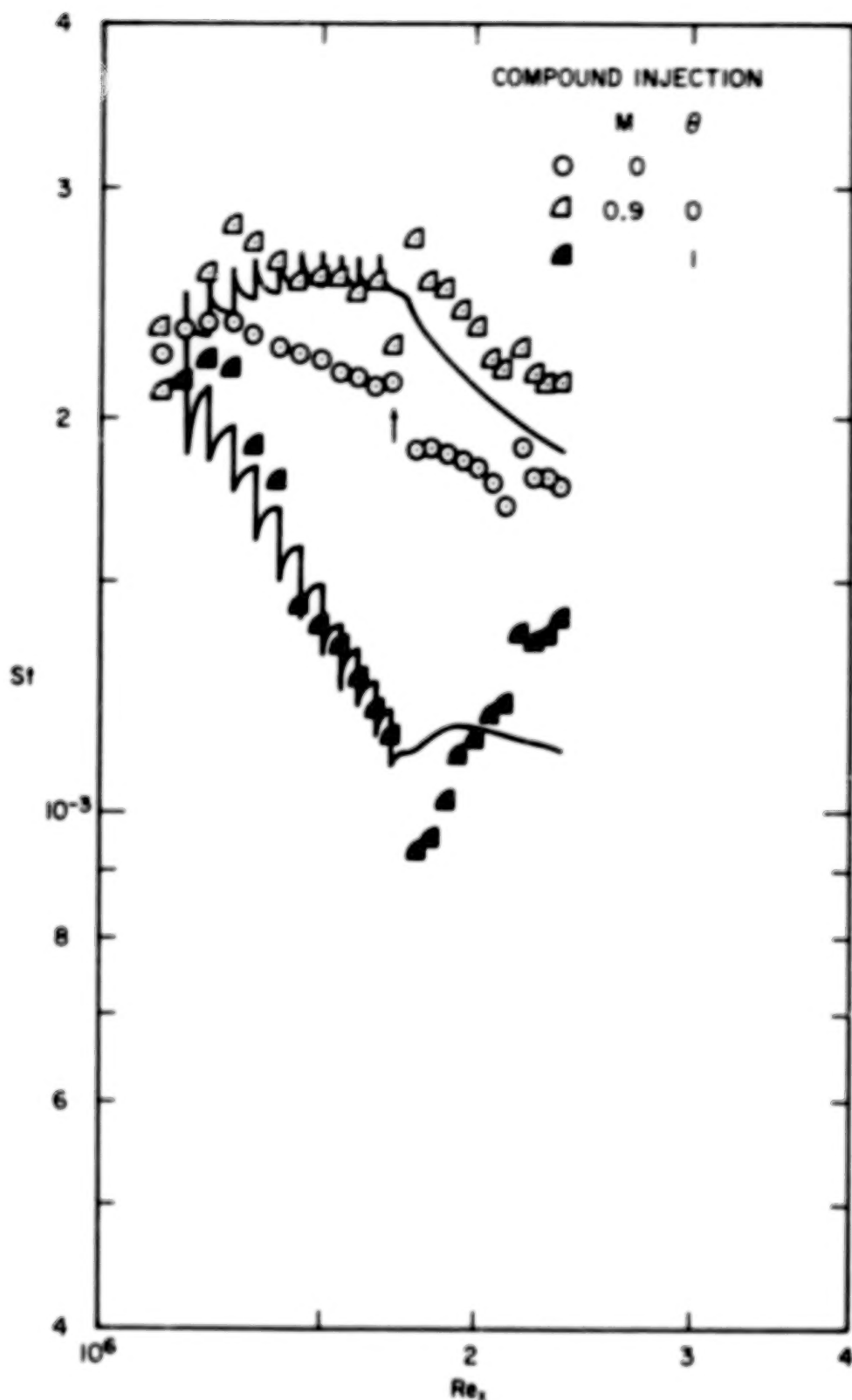


Fig. 27. Comparison of measured and predicted Stanton numbers for compound-angle injection: $M = 0.9$, $P/D = 5.0$, with initial momentum and enthalpy thickness Reynolds numbers of 2500 and 1800, respectively.

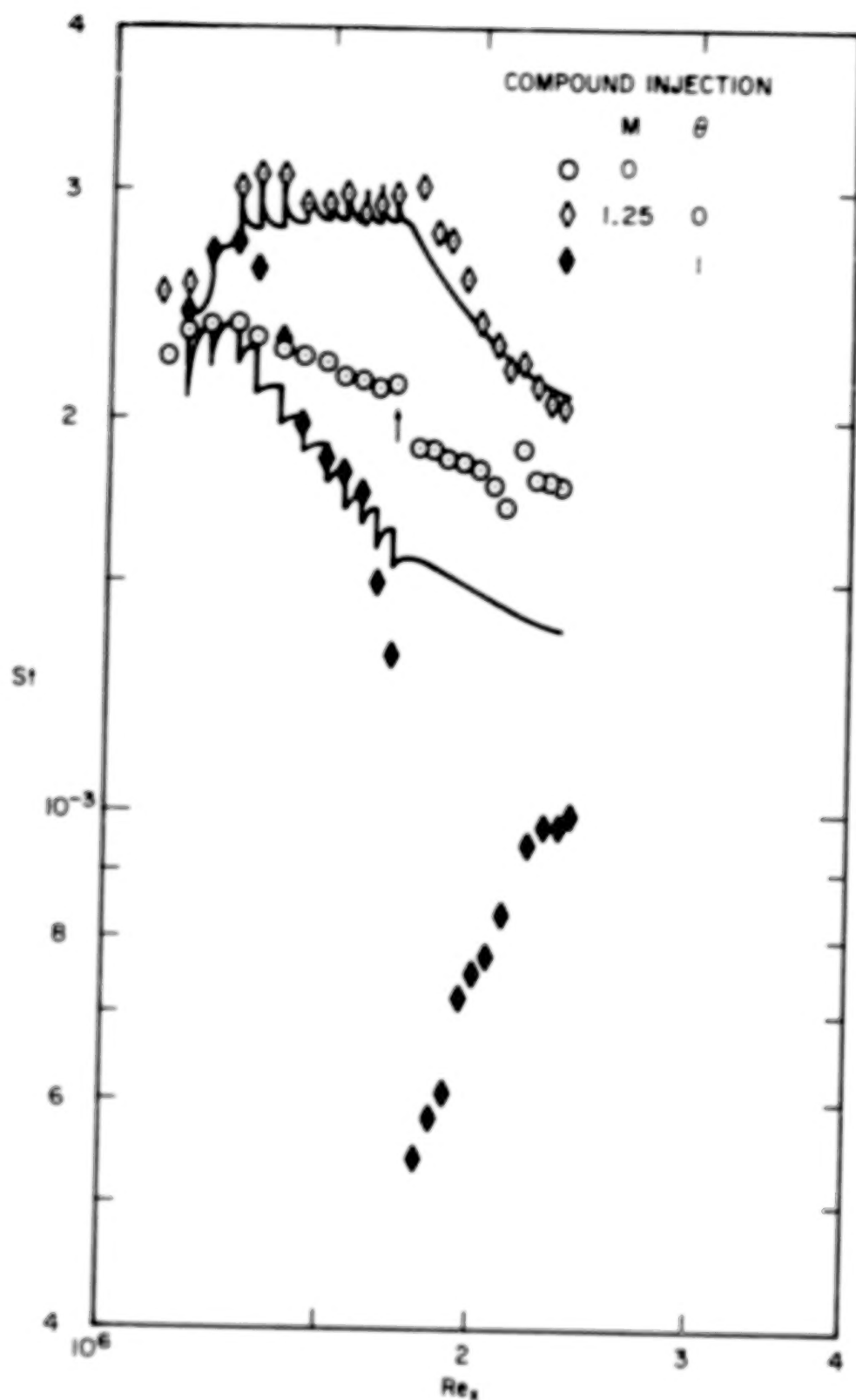


Fig. 28. Comparison of measured and predicted Stanton numbers for compound-angle injection: $M = 1.25$, $P/D = 5.0$, with initial momentum and enthalpy thickness Reynolds numbers of 2500 and 1800, respectively.

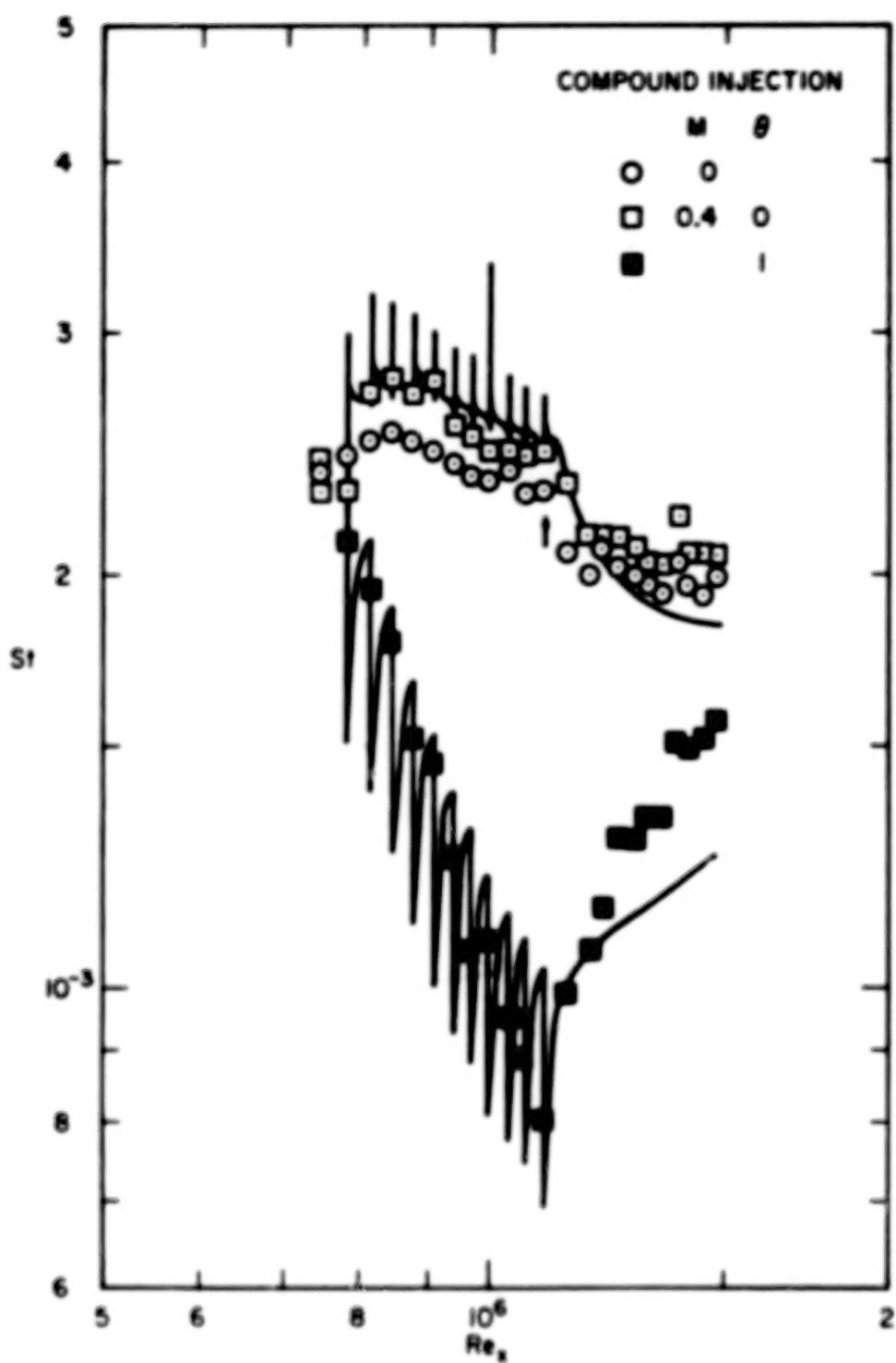


Fig. 29. Comparison of measured and predicted Stanton numbers for compound-angle injection: $M = 0.4$, $P/D = 5.0$, with initial momentum and enthalpy thickness Reynolds numbers of 1800 and 1400, respectively.

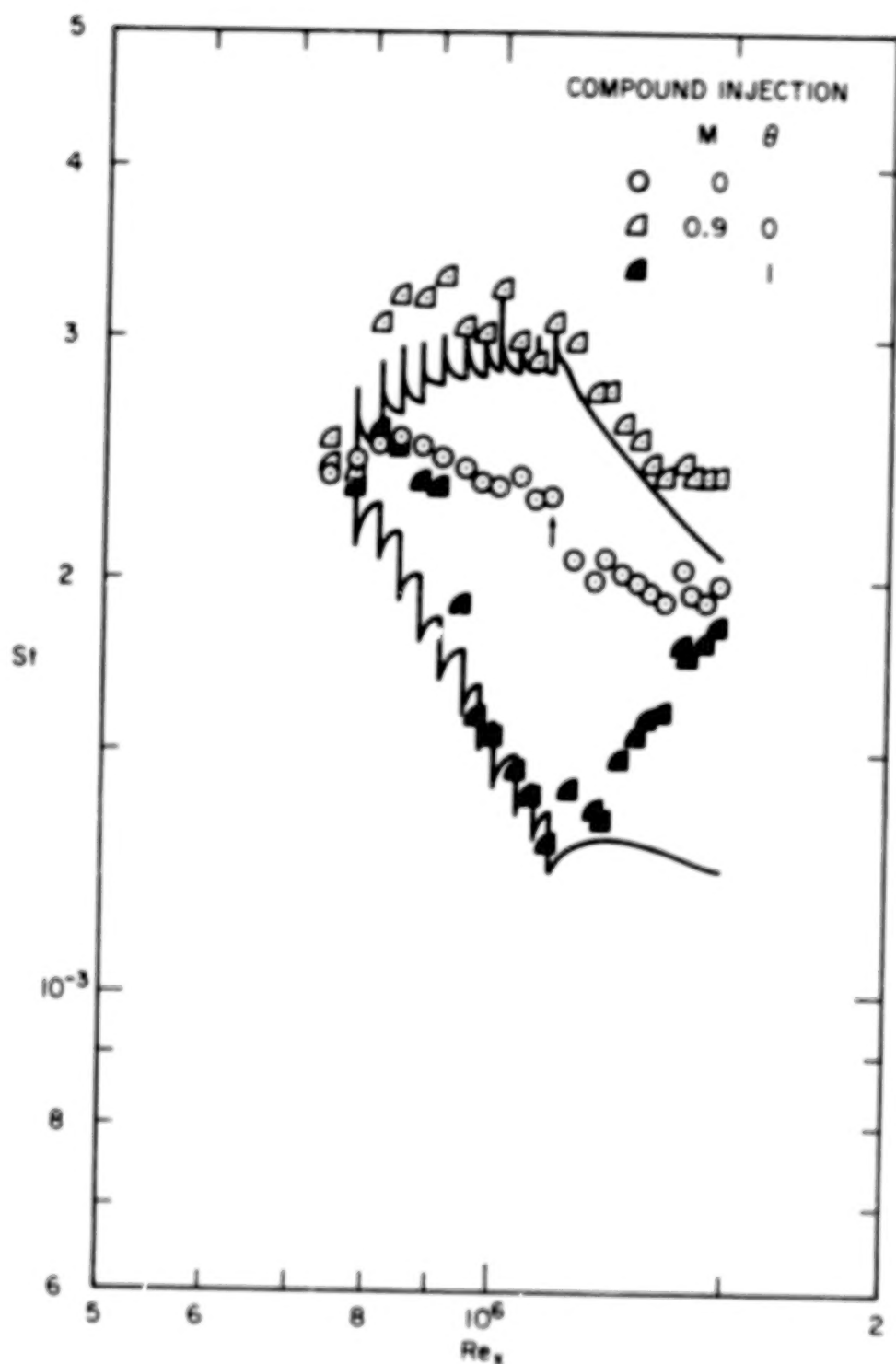


Fig. 30. Comparison of measured and predicted Stanton numbers for compound-angle injection: $M = 0.9$, $P/D = 5.0$, with initial momentum and enthalpy thickness Reynolds numbers of 1800 and 1400, respectively.

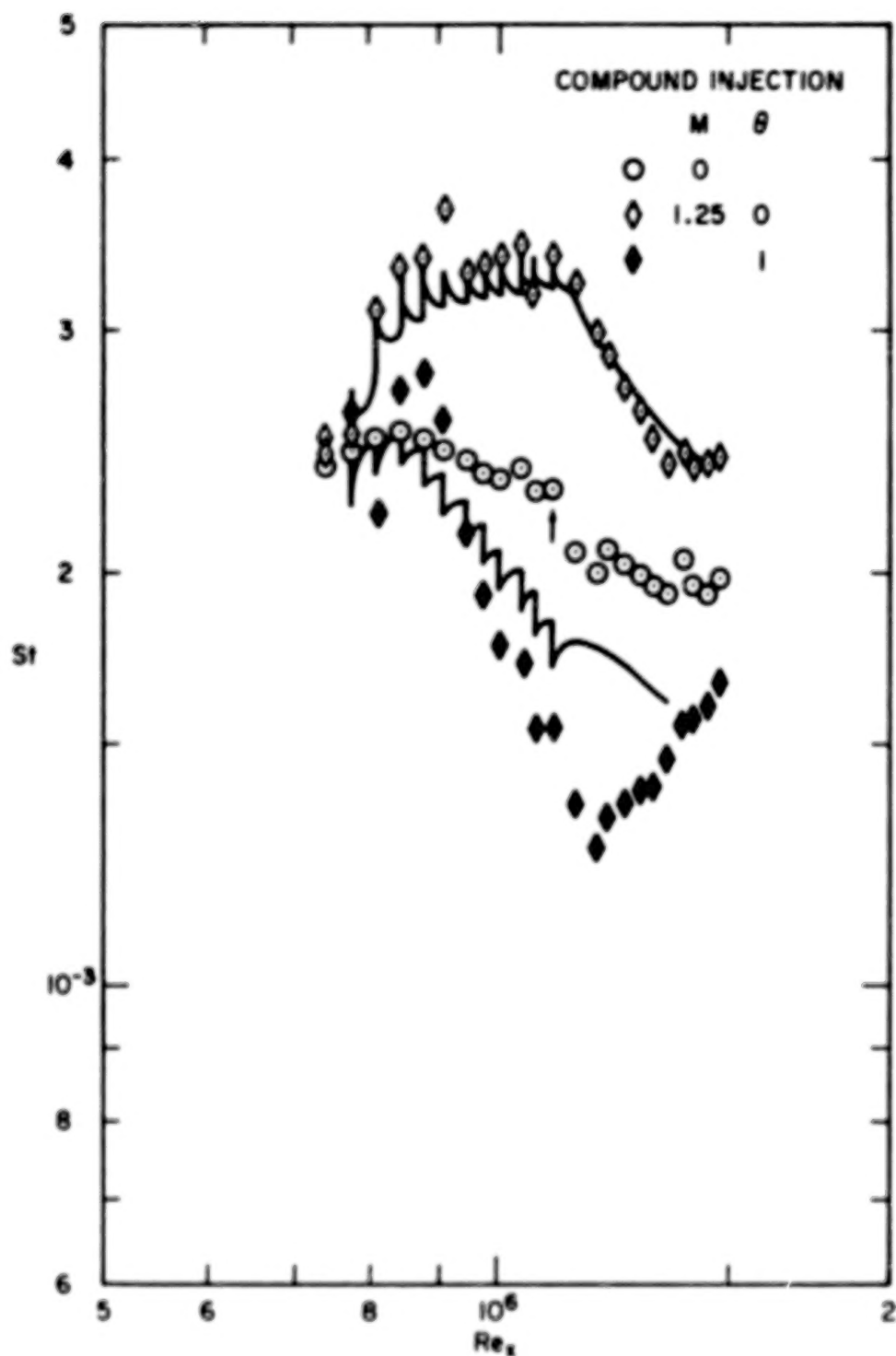


Fig. 31. Comparison of measured and predicted Stanton numbers for compound-angle injection: $M = 1.25$, $P/D = 5.0$, with initial momentum and enthalpy thickness Reynolds numbers of 1800 and 1400, respectively.

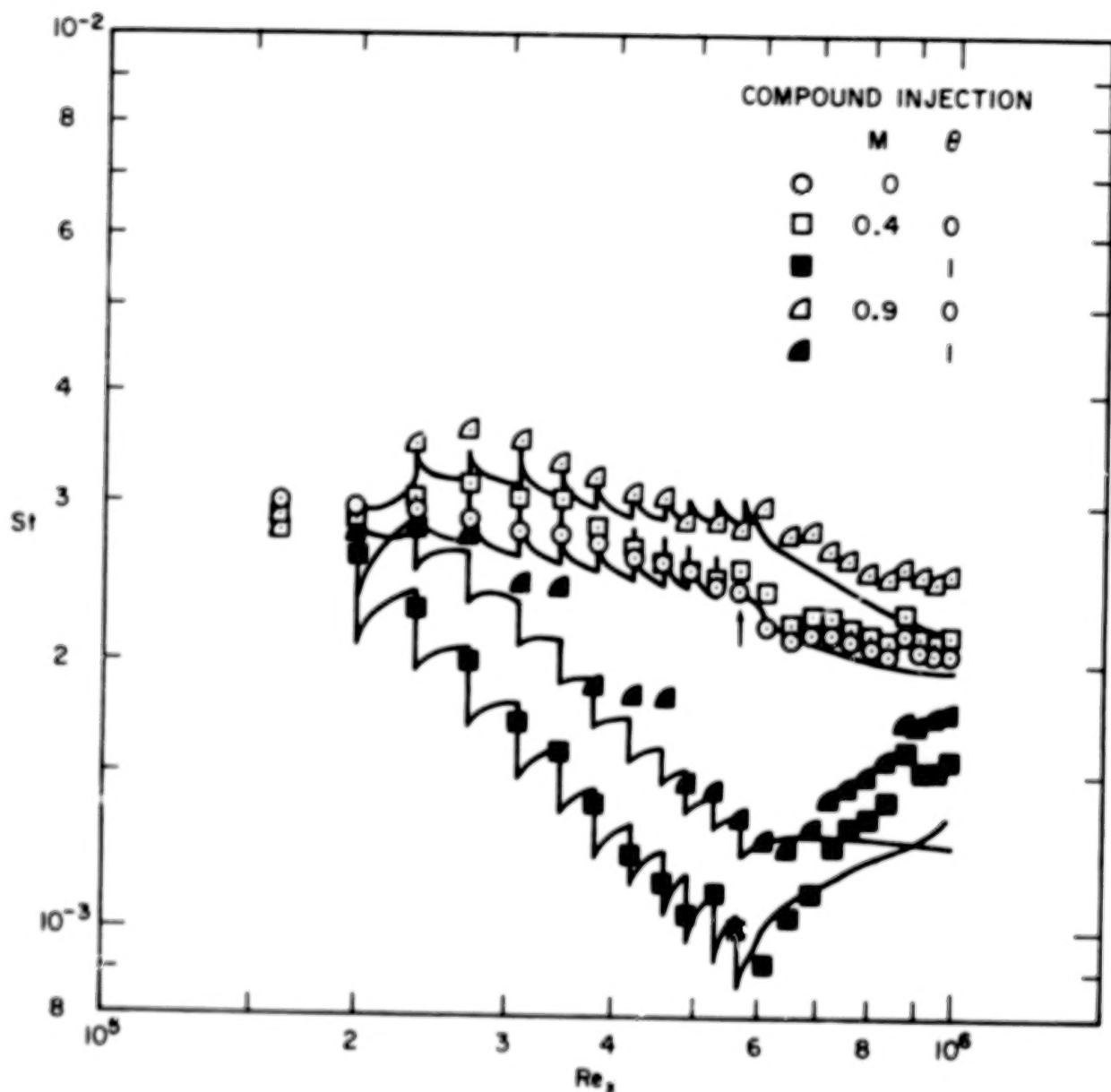


Fig. 32. Comparison of measured and predicted Stanton numbers for compound-angle injection: $M = 0.4$ and 0.9 , $P/D = 5.0$, with initial momentum and enthalpy thickness Reynolds numbers of 500 and 650, respectively.

References

1. Choe, M., Kays, W. M., and Moffat, R. J., "Turbulent Boundary Layer on a Full-Coverage, Film-Cooled Surface -- An Experimental Heat Transfer Study with Normal Injection," NASA Rep. CR-2642, 1976. (Also Stanford Univ., Dept. of Mech. Engrg., Report HMT-22).
2. Crawford, M. E. et. al., "Full-Coverage Film Cooling Heat Transfer Study-- Summary of Data for Normal-Hole Injection and 30° Slant-Hole Injection", NASA Rep. CR-2648, 1976.
3. Crawford, M. E., Kays, W. M., and Moffat, R. J., "Heat Transfer to a Full-Coverage, Film-Cooled Surface with 30° Slant-Hole Injection", NASA Rep. CR-2786, 1976. (Also Stanford Univ., Dept. of Mech. Engrg., Report HMT-25).
4. Yavuzkurt, S. et al., "Full-Coverage Film Cooling: 3-Dimensional Measurements of Turbulence Structure and Prediction of Recovery Region Hydrodynamics", NASA Rep. CR-3104, 1979. (Also Stanford Univ., Dept. of Mech. Engrg., Report HMT-27).
5. Kim, H. K., et. al., "Heat Transfer to a Full-Coverage, Film-Cooled Surface with Compound-Angle (30° and 45°) Hole Injection", NASA Rep. CR-3103, 1979. (Also Stanford Univ., Dept. of Mech. Engrg., Report HMT-28).
6. Crawford, M. E., and W. M. Kays, "STAN5 - A Program for Numerical Computation of Two-Dimensional Internal/External Boundary Layer Flows", NASA Rep. CR-2742, 1976. (Also Stanford Univ., Dept. of Mech. Engrg., Report HMT-23).
7. Eckert, E. R. G., "Film Cooling with Injection Through Holes", AGARD Conf. Proc. High Temperature Turbines, AGARD CP-73-71, 1971.
8. Choe, H., Kays, W. M., and R. J. Moffat, "The Superposition Approach to Film Cooling", ASME Paper 74-WA/HT-27, New York, 1974.
9. Kays, W. M., and R. J. Moffat, "The Behavior of Transpired Turbulent Boundary Layers", in Studies in Convection, Vol. 1, Academic Press, London, 1975.
10. Ville, J. P., and B. E. Richards, "The Measurement of Film Cooling Effectiveness on Turbine Components in Short Duration Wind Tunnels", AGARD Symposium on High Temperature Problems in Gas Turbine Engines, Ankara, Turkey, September 1977.
11. Metzger, E. E., Carper, H. J., and L. R. Swank, "Heat Transfer with Film Cooling Near Nontangential Injection Slots", J. Eng. Power, Vol. 90, p. 157, 1968.
12. Colladay, R. S., and L. M. Russell, "Streakline Flow Visualization of Discrete Hole Film Cooling for Gas Turbine Applications", J. Heat Transfer, Vol. 98, p. 245, 1976.

13. Goldstein, R. J., "Film Cooling", in Advances in Heat Transfer, Vol. 7, p. 321, 1971.
14. Pederson, D. R., Eckert, E. R. G., and R. J. Goldstein, "Film Cooling with Large Density Differences Between the Mainstream and the Secondary Fluid Measured by the Heat-Mass Transfer Analogy", J. Heat Transfer, Vol. 99, p. 620, 1977.
15. Herring, H. J., "A Method of Predicting the Behavior of a Turbulent Boundary Layer with Discrete Transpiration Jets", J. Eng. Power, Vol. 97, p. 214, 1975.
16. Bergeles, G., Gosman, A. D., and B. E. Launder, "The Prediction of Three-Dimensional Discrete-Hole Cooling Processes. Part 1 - Laminar Flow", J. Heat Transfer, Vol. 98, p. 379, 1966.
17. Bergeles, G., Gosman, A. D., and B. E. Launder, "The Turbulent Jet in a Cross Stream at Low Injection Rates: A Three-Dimensional Numerical Treatment", Numerical Heat Transfer, Vol. 1, p. 217, 1978.
18. Abramovich, G. N., The Theory of Turbulent Jets, MIT Press, Cambridge, MA, 1963.

Appendix A

Modifying STAN5 to Obtain STANCOOL

Program STAN5 is the two-dimensional boundary layer program described in the documentation report by Crawford and Kays [6]. Conversion of that program to STANCOOL involves appending several lines of FORTRAN coding to the main and supporting subroutines, and appending subroutine COOL. In this appendix we will present listings of the main and subrouting modifications, a listing of COOL, and a listing of a sample input deck and part of the resulting output.

In describing the conversion of STAN5, the identifying line numbers to the right of the FORTRAN coding correspond to those given in [6]. With one or two exceptions, all coding lines with line numbers remain unchanged, and they are supplied to mark the starting location for appending new lines.

Modifications to MAIN are given in Listing A. The added common lines will also be found in STEP, WALL, OUT, AUX, INPUT, and COOL. The call to Subrouting COOL is located in MAIN, and the XLOC (I) and STX (I) arrays are filled here. These arrays will be used in COOL to integrate $St(x)$ from $-P/2 \leq x \leq +P/2$; i.e. one-half pitch distance before and after the injection location, to obtain the average Stanton number associated with the area around a row of holes. In the output a table of the average values are printed after the last film cooling hole is passed. This table facilitates comparison to the spanwise-averaged experimental data for the full-coverage region.

When the program encounters a row of holes, the program stops, and COOL injects the coolant by altering the velocity and stagnation enthalpy (temperature) profiles. When the program restarts, a start-up stability problem exists. This problem is solved by iterating the finite-difference solution 4 times for the first few integration steps after re-start. The mechanics of this form the rest of the modifications to MAIN, and the modifications to STEP (Listing B), WALL (Listing C), and OUT (Listing D).

Augmentation of the mixing length occurs in AUX, and these modifications are given in Listing E. Equation (26) is programmed as the program variable DAMP. Equation (27) is the variable ALAME, and it is computed in COOL and transferred to AUX via the common. Equation (28) is the variable AL.

Subroutine INPUT is where the film-cooling variables are read. The AUX1(M) and AUX2(M) arrays are auxiliary arrays that already exist in STAN5, and they are used by STANCOOL to specify the M and θ parameter as a function of x for those $X(M)$ that locate film-cooling rows. (Recall that $X(M)$ is tied to $UG(M)$ and $FJ(J,M)$ for specifying U and I^* , as a function of x ; therefore for those $X(M)$ that are not film-cooling locations, AUX1 and AUX2 entries must be zeros). The block of appended lines in the INPUT routine consists of two read statements, several write statements, and comment lines. These are given in Listing F. ALAM is Eqn. (29); DELMR is Eqn. (20); and APLMOD is the modified A^+ for the blowing region (see Section V.D.). The film-cooling geometry variables include FNROW, the total number of rows of film cooling; PITCH, the lateral spacing between the holes (to calculate the injected mass per unit span, Eqn. (21); DIAM, the hole diameter; ANGLE, the angle between the hole axis and the surface; and SKEW, the angle the hole axis is turned from the downstream direction (e.g., for normal injection, ANGLE = 90, SKEW = 0; for in-line slant-hole injection ANGLE = 30, SKEW = 0; for compound-angled injection ANGLE = 30, SKEW = 45). Note that the dimensions on PITCH and DIAM must be consistent with GC (e.g., feet).

Subroutine COOL contains three major calculation blocks pertaining to the injection model, the augmented mixing-length constants, and the averaging algorithm for the Stanton numbers. If the input variable K1 equals 55, this routine is called at each integration step, and it is bypassed for K1 = 0 (STAN5 configuration).

The injection model is contained in the major block of the routine, and it is bypassed except when XU corresponds to the location of a row of holes. For a given DELMR, the velocity profile is modified according to Eqn. (17) and the stagnation enthalpy (temperature) profile is modified according to Eqn. (19). Injection ceases when Eqn. (21) is satisfied, and the resulting y -location is YPEN. It is never allowed to be greater than 80 percent of the boundary layer thickness.

The second block of COOL sets the effective mixing-length augmentation constant ALAME, according to Eqn. (26). The effective A^+ , APL0, is also calculated in this block using the lag equation described in [6], i.e., $A^+ = 26$ upstream, and it is exponentially decreased to about 23 at the start of the full-coverage region using the same PPLAG damping constant that is recommended in [6].

The third block of COOL implements the algorithm to compute stream-averaged Stanton numbers from the STX(I) and XLOC(I) arrays. The algorithm attempts to simulate the experimental conditions of the full-coverage surface where the average heat transfer for a plate is due to the effects of upstream injectants as well as those from the plate in question. For example with 11 rows of film cooling, 11 stream-averaged Stanton numbers would result for a given M , θ , geometry, and experimental initial conditions. These would then be compared to the experimental Stanton numbers for ease in determining the proper set of DELMR and ALAM.

Listing H contains a sample data set in the format described in [6]. The data set is that used to predict the $\theta = 0$ case in Fig. 20. Included also in the listing is the output from STANCOOL of the eleven stream-averaged Stanton numbers for the eleven rows of film cooling.

Listing A

MAIN Driver Program

C.....TURBULENT BOUNDARY LAYER PREDICTION---PATANKAR/SPALDING METHOD,	MAIN0000
C.....KAYS/STANFORD VERSION, DESIGNATION STAN5, DECEMBER, 1975	MAIN0010
C	COOL
C PROGRAM STANCOOL UTILIZES THE STAN5 PROGRAM WITH MODIFICATIONS	COOL
C AND AN APPENDED SUBROUTINE TO MODEL THE INJECTION PROCESS AND	COOL
C TURBULENCE AUGMENTATION. THE PROGRAM MARCHES IN THE STREAMWISE	COOL
C DIRECTION AND, WHEN A ROW OF HOLES IS ENCOUNTERED, IT STOPS AND	COOL
C INJECTS COOLANT INTO THE BOUNDARY LAYER. THE TURBULENCE LENGTH	COOL
C SCALE IS MODELED BY ALGEBRAICALLY AUGMENTING THE MIXING LENGTH.	COOL
C THE TURBULENCE VELOCITY SCALE IS THE DU/DY PRANDTL FORMULATION	COOL
3/ADD/RBOM(54),OMD(54),ROMD(54),ITKE	MAIN0290
4/FC1/ALAM,DELMR,APLMOD,FNROWS,PITCH,DIAM,ANGLE,SKEW	COOL
5/FC2/XLOC(600),STX(600),KTX,KADJ,APLO,YPEN,ALAME	COOL
C.....BY LINEAR INTERPOLATION OF INPUT DATA	MAIN0840
205 IF (LSUB.GT.0.OR.KADJ.GT.0) GO TO 35	COOL
CALL STEP(3)	MAIN1230
IF (KADJ.GT.0) GO TO 58	COOL
INTG=INTG+1	MAIN1960
IF (K1.EQ.55) CALL COOL(M)	COOL
IF (LVAR.EQ.6) GO TO 1000	COOL
1F(LVAR.GT.1)GO TO 1000	MAIN4130
IF (KTX.LE.2.AND.KADJ.LE.3) GO TO 70	COOL
NINTG=INTG-1	COOL
XLOC(INTG)=XU	COOL
STX(INTG)=ST(1)	COOL
70 CALL STEP(4)	MAIN4560
IF (KTX.LE.2) KADJ=KADJ+1	COOL
IF (KADJ.GT.4) KADJ=0	COOL
IF (KADJ.GT.0) GO TO 15	COOL

Listing B

Subroutine STEP

SUBROUTINE STEP(KSTEP)	STEP0000
3/ADD/RBOM(54),OMD(54),ROMD(54),ITKE	STEP0150
4/FC1/ALAM,DELMR,APLMD,FNROWS,PITCH,DIAM,ANGLE,SKEW	COOL
5/FC2/XLOC(600),STX(600),KTX,KADJ,APLO,YPEN,ALAME	COOL
DIMENSION CUTEMP(54),CTEMP(5,64)	COOL
CU(I)=-P1*U(I+1)-P2*U(I)-P3*U(I-1)	STEP2670
C G1,G2,G3 CONTAIN ENTRAINMENT TERM AND SHOULD NOT BE RE-CALC	COOL
C UNLESS ENTRAINMENT OR PRESSURE GRADIENT IS BEING ITERATED.	COOL
C G4 - CU(I) - IS UPSTREAM CONVECTION AND MUST NOT BE ITERATED.	COOL
IF (KADJ.GT.0) CU(I)=CUTEMP(I)	COOL
C(J,I)=-C(J,I)+SU(J,I)-F(J,I)*SD	STEP2710
C G4 -C(J,I) - IS UPSTREAM CONVECTION AND MUST NOT BE ITERATED.	COOL
IF (KADJ.EQ.0) CTEMP(J,I)=C(J,I)	COOL
IF (KADJ.GT.0) C(J,I)=CTEMP(J,I)	COOL
C.....SOURCE TERM FOR VELOCITY EQUATION	STEP2760
IF (KADJ.GT.0) GO TO 414	COOL
CU(I)=-CU(I)-2.*(S1+S2+S3)	STEP2810
C S4 - G4 - CU(I) TERM	COOL
CUTEMP(1)=CU(I)	COOL
S3=S3/U(I-1)	STEP2840
414 CONTINUE	COOL
C.....SETTING UP VELOCITIES AT A FREE BOUNDARY	STEP4030
471 IF(KEX.EQ.2.AND.KADJ.EQ.0)U(NP3)=SQRT(U(NP3)*U(NP3)	COOL
1-2.*DX*(DPDX-GC*BF(NP3))/RHO(NP3))	COOL
560 CONTINUE	STEP5220
KTX=1000	COOL
KADJ=0	COOL

Listing C

Subroutine WALL

SUBROUTINE WALL	WALL0000
2/CN/AXX,BXX,CXX,DXX,EXX,K1,K2,K3,SP(54),AUX1(100),AUX2(100),YPMAX	WALL0150
4/FC1/ALAM,DELMR,APLMOD,FNROWS,PITCH,DIAM,ANGLE,SKEW	COOL
5/FC2/XLOC(600),STX(600),KTX,KADJ,APLO,YPEN,ALAME	COOL
IF(MARKER.EQ.1)GO TO 170	WALL1580
IF (KADJ.GT.0) GO TO 170	COOL
MARKER=0	WALL3420
IF (LSUB.GT.0.AND.KTX.LT.5) LSUB=0	COOL

Listing D

Subroutine AUX

SUBROUTINE AUX	AUX00000
3/ADD/RBOM(54),OMD(54),ROMD(54),ITKE	AUX00150
4/FC1/ALAM,DELMR,APLMOD,FNROWS,PITCH,DIAM,ANGLE,SKEW	COOL
5/FC2/XLOC(600),STX(600),KTX,KADJ,APLO,YPEN,ALAME	COOL
IF (KEX.EQ.1)YTKE=(Y(NP3)-Y(1+1))*YPUT	AUX01054
IF (K1.NE.55)GO TO 34	COOL
AD=1.0E-5	COOL
YMSQ=(YM*YM)/(YPEN*YPEN)	COOL
IF (YMSQ.LT.18.) AD=EXP(-YMSQ)	COOL
DAMP=2.71828*YMSQ*AD	COOL
AL=AL+ALAME*YL*DAMP	COOL
34 CONTINUE	COOL

Listing E

Subroutine OUT

SUBROUTINE OUT	OUT00000
2/CN/AXX,BXX,CXX,DXX,EXX,K1,K2,K3,SP(54),AUX1(100),AUX2(100),YPMAX	OUT00140
4/FC1/ALAM,DELMR,APLMOD,FNROWS,PITCH,DIAM,ANGLE,SKEW	COOL
5/FC2/XLOC(600),STX(600),KTX,KADJ,APLO,YPEN,ALAME	COOL
IF(SOURCE(1).EQ.2.AND.NPH.GT.1)STA=ST(2)	OUT00410

IF (KADJ.GT.0) GO TO 210

COOL

WRITE(6,284)NINTG,XU,UGU,CAY,FAM,REM,CF2,H,REH,STA,F(1,1),CPL,AME OUT00540

IF (KADJ.GT.0) GO TO 278

COOL

Listing F

Subroutine INPUT

SUBROUTINE INPUT(KERROR)

INPU0000

2/CN/AXX,BXX,CXX,DXX,EXX,K1,K2,K3,SP(54),AUX1(100),AUX2(100),YPMAX INPU0140

4/FC1/ALAM,DELMR,APLMOD,FNROWS,PITCH,DIAM,ANGLE,SKEW

COOL

5/FC2/XLOC(600),STX(600),KTX,KADJ,APLO,YPEN,ALAME

COOL

C (DECIMAL NUMBERS, IN THE FORM OF A TABLE.)

INPU2140

C COOL

C FOR FILM COOLING AUX1(M) IS THE BLOWING RATIO. THE AUX2(M)

COOL

C ARRAY IS THE TEMPERATURE PARAMETER (STAG. ENTHALPY IF VARIABLE

COOL

C PROPERTIES) OR INJECTANT TEMPERATURE (STAG. ENTHALPY) IF THE WALL

COOL

C IS ADIABATIC. FOR THOSE X(M) THAT ARE NOT INJECTION LOCATIONS

COOL

C SPECIFY THE CORRESPONDING AUX1(M) AS ZERO. NOTE THAT X(1)

COOL

C MUST NOT BE AN INJECTION LOCATION.

COOL

WRITE(6,740)NUMRUN,SPACE,OUTPUT,K1,K2,K3

INPU4370

IF (K1.NE.55) GO TO 299

COOL

C COOL

C ***** K1=55 CALL COOL FOR FULL-COVERAGE FILM COOLING

COOL

C K3=55 PRINT FILM COOLING INJECTION PROCESS

COOL

C COOL

C ***** AUX1(M) BLOWING PARAMETER, (RHO2*U2)/(RHOINF*UINF)

COOL

C AUX2(M) TEMPERATURE PARAMETER, (T2-TINF)/(TWALL-TINF)

COOL

C OR, INJ TEMP, T2, IF WALL IS ADIABATIC

COOL

C COOL

C READ FILM COOLING PREDICTION CONSTANTS

COOL

C COOL

C ALAM LAMBDA AUGMENTED, TURBULENCE MODEL

COOL

C DELMR MASS FLOW RATIO, INJECTION MODEL

COOL

C APLMOD APLUS FOR BLOWING REGION

COOL

C COOL

READ (5,580) ALAM,DELMR,APLMOD

COOL

C COOL

C ***** READ FILM COOLING GEOMETRY

COOL

C COOL

C FNROWS NUMBER OF INJECTION LOCATIONS

COOL

C PITCH LATERAL CENTER-TO-CENTER HOLE SPACING

COOL

C DIAM JET DIAMETER

COOL

C ANGLE HOLE AXIS ANGLE

COOL

C SKEW HOLE AXIS SKEW ANGLE

COOL

C	READ (5,580) FNROWS,PITCH,DIAM,ANGLE,SKEW	COOL
	WRITE (6,405)	COOL
405	FORMAT (//5X,'FILM COOLING USING DISCRETE HOLE INJECTION'/)	COOL
	WRITE (6,406)	COOL
406	FORMAT (5X,'TURBULENCE MODEL IS AUGMENTED MIXING LENGTH'/)	COOL
	WRITE (6,410) ALAM,DELMR,APLMOD	COOL
410	FORMAT (5X,'ALAM=',F6.3,5X,'DELMR=',F6.3,5X,'APLMOD=',F4.0/)	COOL
	WRITE(6,415) FNROWS,PITCH,DIAM,ANGLE,SKEW	
415	FORMAT(5X,'NROWS=',F4.0,5X,'PITCH=',F7.5,5X,'DIAM=',F7.5,	COOL
	1 5X,'ANGLE=',F4.0,5X,'SKEW =' ,F4.0/)	COOL
299	CONTINUE	COOL

Listing G

Subroutine COOL

```

SUBROUTINE COOL(M)
C
C SUBROUTINE COOL CONTAINS THE INJECTION MODEL FOR SIMULATION OF
C FULL-COVERAGE FILM COOLING. AUGMENTED MIXING-LENGTH PARAMETERS
C ARE ALSO COMPUTED HERE, BUT THE MODEL ITSELF RESIDES IN SUB AUX.
C
C SUBROUTINE COOL IS CALLED CONTINUOUSLY IF K1=55. UNTIL THE FIRST
C INJECTION ROW IS ENCOUNTERED, CONTROL IS RETURNED TO THE DRIVER
C (MAIN). RECALL THAT X(1) MUST NOT BE A FILM COOLING LOCATION.
C WHEN XU=X(ROW OF HOLES), COOLANT IS INJECTED INTO THE B.L.
C FOR ALL OTHER VALUES OF XU, AND AFTER THE LAST FILM COOLING
C LOCATION IS ENCOUNTERED, THE INJECTION MODEL SECTION IS BYPASSED
C AND ONLY THE AUGMENTED MIXING-LENGTH PARAMETERS ARE COMPUTED.
C
C      K1=55  CALL COOL FOR FULL-COVERAGE FILM COOLING
C      K3=55  PRINT FILM COOLING INJECTION PROCESS
C
C      AUX1(M) BLOWING PARAMETER, (RHO2^U2)/(RHOINF*U1NF)
C      AUX2(M) TEMPERATURE PARAMETER, (T2-TINF)/(TWALL-TINF)
C              OR, INJ TEMP, T2, IF WALL IS ADIABATIC
C
C      ALAM    LAMBDA AUGMENTED, TURBULENCE MODEL
C      DELMR   MASS FLOW RATIO, INJECTION MODEL
C      APLMOD  APLUS FOR BLOWING REGION
C
C      FNROWS  NUMBER OF INJECTION LOCATIONS
C      PITCH   LATERAL CENTER-TO-CENTER HOLE SPACING
C      DIAM    JET DIAMETER
C      ANGLE   HOLE AXIS ANGLE
C      ANGLE   HOLE AXIS ANGLE
C
C      INTEGER GEOM,FLUID,SOURCE(5),SPACE,BODFOR,OUTPUT,TYPBC
C      COMMON/GEN/PEI,AMI,AME,DPDX,XU,XD,XL,DX,INTG,CSALFA,TYPBC(5),

```

```

1MODE,PRT(5),PRE,NKBC,X(100),RW(100),FJ(5,100),GC,CJ,AM(100),PRO,
2UG(100),PO,SOURCE,RETRAN,NUMRUN,SPACE,RWO,PPLAG,OUTPUT,DELTAX,GV
3/E/N,NP1,NP2,NP3,NEQ,NPH,KEX,KIN,KASE,KRAD,GEOM,FLUID,BODFOR,YPMIN
5/V/U(54),F(5,64),R(54),OM(54),Y(54),UGU,UGD,UI,FI(5),PMEAN,TAUW
7/L/AK,ALMG,ALMGG,FRA,APL,BPL,AQ,BQ,BMU(54),PREF(5,64),AUXM1
8/L1/YL,UMAX,UMIN,FR,YLP,YEM,ENFRA,KENT,AUXM2
9/P/RHO(54),VISC(54),PR(5,64),RHOC,VISCOC,PRC(5),T(54),RHOM,BF(54)
1/O/H,REM,CF2,ST(5),LSUB,LVAR,CAY,REH,PPL,GPL,QW(5),KD
2/CN/AXX,BXX,CXX,DXX,EXX,K1,K2,K3,SP(54),AUX1(100),AUX2(100),YPMAX
3/ADD/RBOM(54),OMD(54),ROMD(54),ITKE
4/PC1/ALAM,DELMR,APLMOD,FNROWS,PITCH,DIAM,ANGLE,SKEW
5/PC2/XLOC(600),STX(600),KTX,KADJ,APLO,YPEN,ALAME

```

```

C      IF(INTG.GT.1)GO TO 5
C      INITIALIZE VARIABLE5
      NROWS=IFIX(FNROWS+0.01)
      KCOUNT=0
      KTERM=0
      XPRINT=X(NROWS+1) + 0.75*PITCH
      IF(NROWS.EQ.6.AND.PITCH/DIAM.GT.6.)XPRINT=X(12)+0.75*PITCH/2.
      ANGLE=ANGLE*3.14159/180.
      SKEW=SKEW*3.14159/180.
      APLINL=APL
      APLE=APL
      UGU=1.
      DXMAX=0.25*DIAM
      YPEN=1.E-5
      YPENI=YPEN
      ALAME=0.
      XHOLE=X(1)
C
C      5 IF (KTERM.EQ.1) GO TO 900
      MM=M-1
      HLOC=X(MM)
      IF (XU.NE.HLOC) GO TO 105
C
C      A FILM COOLING OR BC LOCATION X(M) HAS BEEN ENCOUNTERED
      AUXM=AUX1(MM)
      AUXTH=AUX2(MM)
C
C      X-BOUNDARY CONDITION BUT NOT AN INJECTION LOCATION
C      REPORT THE "ALL
      IF(AUXM.E.0.AND.DELMR.NE.0.0) WRITE(6,121) MM,XU
121  FORMAT (/10X,'SUBROUTINE COOL CALLED AT LOCATION X(',12,
1  ') AND XU=',F7.4,' ; HOWEVER M=0 AT THIS LOCATION')
      IF(AUXM.EQ.0.0.AND.DELMR.NE.0.0) GO TO 105
C
      KCOUNT=KCOUNT+1
      IF(KCOUNT.EQ.NROWS) KTERM=1
C      REPORT THE CALL FOR FILM COOLING
      WRITE (6,120) MM,XU,KCOUNT,AUXM,AUXTH
120  FORMAT (///10X,'SUBROUTINE COOL HAS BEEN CALLED',/10X,
1  'INJECTION MODEL WITH AUGMENTED MIXING LENGTH',/10X,

```

```

2 'X(' ,12,') =' ,F7.4,3X,'ROW =' ,I3,3X,'M =' ,F5.2,3X,
3 'THETA =' ,F5.2///)
C
C SPECIAL PROVISION FOR ST AVG WITH NO FILM COOLING
IF(HLOC.EQ.X(1))KCOUNT=0
IF (AUXM.EQ.0.0.AND.ALAM.EQ.0.0) GO TO 105
KTX=0
C
C INJECTION TEMPERATURE (STAGNATION ENTHALPY IF VAR PROP)
FCOOLT=AUXTH*(F(1,1)-F(1,NP3))+F(1,NP3)
C
C MODIFICATION FOR ADIABATIC WALL CONDITION
IF ADIABATIC WALL, AUXTH IS INJ TEMP (STAG ENTHALPY IF VAR PROP)
IF (TYPBC(1).EQ.2) FCOOLT=AUXTH
FCOOL=FCOOLT
C
C OBTAIN DENSITY OF INJECTANT
IF(FLUID.NE.2) GO TO 125
C FIRST ITERATION, FCOOL=FCOOLT
CALL PROP2(1,FCOOL,TCOOL,VISC2,PR2,RHO2)
C SECOND ITERATION
U2=AUXM*U(NP3)*RHO(NP3)/RHO2
FCOOL=FCOOLT-(U2*U2)/(2.*GC*CJ)
CALL PROP2(1,FCOOL,TCOOL,VISC2,PR2,RHO2)
C THIRD ITERATION
FCOOL=FCOOLT-(U2*U2)/(2.*GC*CJ)
CALL PROP2(1,FCOOL,TCOOL,VISC2,PR2,RHO2)
C
125 IF (FLUID.NE.2) RHO2=RHO(NP3)
C
C ***** INJECTION MODEL *****
C
C INITIALIZE
COOLR=3.14159*DIAM*DIAM*AUXM*U(NP3)*RHO(NP3)/(4.*PITCH)
COOLR1=COOLR*R(1)
PEIO=PEI
PEI=PEI+COOLR1
VJET=AUXM*U(NP3)*RHO(NP3)/RHO2
VCOST=VJET*COS(ANGLE)*COS(SKEW)
XHO..E=HLOC
ILL=3
C
IF (NPH.EQ.0) GO TO 99
J=1
FOLD=F(J,ILL-1)
99 UOLD=U(ILL-1)
ILLM=ILL-1
OMA=OM(ILL-1)
C
C COMMENCE INJECTING COOLANT
DO 70 I=ILL,NP1
IF (I.EQ.NP1) GO TO 109
UBAR=(U(1)+UOLD)*0.5
OMB=OMA

```

```

OLDM=(OM(I)-OMB)*PEIO
DELM=DELMR*OLDM
IF(DELM.LT.COOLR) GO TO 10
C FLUID INJECTED NOW EQUALS COOLR, EXIT DO LOOP
DELM=COOLR
II=I-1
GO TO 80
C SET NEW AVERAGE VELOCITY, ENTHALPY, AND TKE
10 UBN=(OLDM*UBAR+DELM*VCOST)/(OLDM+DELM)
IF(NPH.EQ.0) GO TO 30
J=1
FBAR=(F(J,I)+FOLD)*0.5
FBN=(OLDM*FBAR+DELM*FCOOL)/(OLDM+DELM)
30 IF(I.EQ.ILL) GO TO 40
IF(I.EQ.ILL+1) GO TO 50
C MODIFY VELOCITY, ENTHALPY TO CONSERVE MOMENTUM & STAG. ENTHALPY
C STAGNATION ENTHALPY, AND MECHANICAL ENERGY
UOLD=U(I)
U(I)=2.*UBN-U(I-1)
OMA=OM(I)
OM(I)=OM(I-1)+(DELM+OLDM)/PEI
IF(NPH.EQ.0) GO TO 60
J=1
FOLD=F(J,I)
F(J,I)=2.*FBN-F(J,I-1)
59 IF(K3.GE.55)WRITE (6,44) I,UOLD,U(I),FOLD,F(1,I),DELM,OLDM
GO TO 60
C SPECIAL HANDLING FOR NODES ILL AND ILL+1
40 OMA=OM(ILL)
OLDM3=OLDM
DELM3=DELM
UBN3=UBN
UOLD=U(ILL)
IF (NPH.EQ.0) GO TO 60
J=1
FBN3=FBN
FOLD=F(J,ILL)
GO TO 60
50 UBN4=UBN
UO2=U(ILL-1)
UO3=U(ILL)
DELY=(Y(ILL)-Y(ILL-1))/(Y(ILL+1)-Y(ILL-1))
U(ILL-1)=UBN3-(UBN4-UBN3)*DELY
U(ILL)=2.*UBN3-U(ILL-1)
UOLD=U(ILL+1)
U(ILL+1)=2.*UBN4-U(ILL)
OM(ILL)=OM(ILL-1)+DELM3/PEI+(OM(ILL)-OM(ILL-1))*PEIO/PEI
OMA=OM(ILL+1)
OM(ILL+1)=OM(ILL)+(DELM+OLDM)/PEI
IF (NPH.EQ.0) GO TO 60
J=1
FBN4=FBN
FO2=F(J,ILL-1)
FO3=F(J,ILL)

```

```

      F(J, ILL-1)=FBN3-(FBN4-FBN3)*DELY
      F(J, ILL)=2.*FBN3-F(J, ILL-1)
      FOLD=F(J, ILL+1)
      F(J, ILL+1)=2.*FBN4-F(J, ILL)
42  IF(K3.GE.55)WRITE(6,43)
43  FORMAT (6X,'I',4X,'UOLD',4X,'UNEW',6X,'FOLD',4X,'FNEW',
      ' 8X','DELM',10X,'OLDM',/)
      ITWO=ILL-1
      ITHREE=ILL
      IF(K3.GE.55)WRITE (6,44) ITWO,UO2,U(ILL-1),FO2,F(1,ILL-1)
      IF(K3.GE.55)WRITE (6,44) ITHREE,UO3,U(ILL),FO3,F(1,ILL),DELM3,OLDM3
      IF(K3.GE.55)WRITE (6,44) I,UOLD,U(I),FOLD,F(1,I),DELM,OLDM
44  FORMAT (5X,I2,2F8.2,2X,2F8.2,2X,2E14.5)
C
60  COOLR1=COOLR1-DELM
70  CONTINUE
80  FLOW1=(OM(II+1)-OMA)*PEIO
      FLOW2=(OM(II+2)-OM(II+1))*PEIO
      AMOMIN=0.5*(FLOW2*(U(II+2)+U(II+1))+FLOW1*(U(II+1)+UOLD))
      E1N=FLOW2*((U(II+2)+U(II+1))/2.)*2/2.+FLOW1*((U(II+1)+UOLD)/2.)*2/2.
      +DELM*VJET*VJET/2.
      UOLDII=UOLD
      UOLD=U(II+1)
      U(II+1)=(2.*AMOMIN-FLOW2*U(II+2)-(FLOW1+DELM)*U(II))/
      (FLOW2+FLOW1+DELM)
      ECUT=FLOW2*((U(II+2)+U(II+1))/2.)*2/2.+(FLOW1+DELM)*((U(II+1)+
      U(II))/2.)*2/2.
      OMB=OM(II+1)
      OM(II+1)=OM(II)+(FLOW1+DELM)/PEI
      IIP2=II+2
      DO 300 K=IIP2,NP1
        OMA=OM(K)
        OM(K)=OM(K-1)+(OMA-OMB)*PEIO/PEI
300  OMB=OMA
      DO 330 I=2,NP1
        RBOI(I)=1./(OM(I+1)-OM(I-1))
        OMD(I)=OM(I+1)-OM(I)
330  ROMD(I)=1./OMD(I)
      IF(NPH.EQ.0)GO TO 350
      J=1
      ENIN=FLOW2*0.5*(F(J,II+2)+F(J,II+1))+FLOW1*0.5*(F(J,II+1)
      +FOLD)+DELM*FCOOL
      FOLD=F(J,II+1)
      F(J,II+1)=(2.*ENIN-FLOW2*F(J,II+2)-(FLOW1+DELM)*F(J,II))/
      (FLOW2+FLOW1+DELM)
349  I=II+1
      IF(K3.GE.55)WRITE (6,44) I,UOLD,U(I),FOLD,F(1,I),DELM,OLDM
C
350  IF (FLUID.NE.2) GO TO 360
      DO 355 K=2,I
355  CALL PROP2(K,F(1,K),T(K),VISCO(K),PR(1,K),RHO(K))
360  CALL STEP(3)
      IF(K3.GE.55) WRITE (6,909) YL

```

Table of Contents

Chapter		Page	
I.	INTRCDUCTION AND OVERVIEW	1	1/A7
II.	EXPERIMENTAL METHODOLOGY AND PROCEDURES	3	1/A9
II.A.	Heat Transfer with Full-Coverage Film Cooling . .	3	1/A9
II.B.	Stanford Experimental Program	5	1/A11
II.C.	Experimental Facility	6	1/A12
II.D.	Heat-Flux Data Acquisition	7	1/A13
II.D.1.	Spanwise-averaged data	7	1/A13
II.D.2.	Local heat flux data	8	1/A14
III.	HEAT TRANSFER FOR THREE INJECTION GEOMETRIES	11	1/B4
III.A.	Temperature Parameter	11	1/B4
III.B.	Mass Flux Ratio	11	1/B4
III.C.	Initial Conditions	13	1/B6
III.D.	Number of Rows of Holes	14	1/B7
III.E.	Hole Spacing	15	1/B8
III.F.	Concluding Remarks	16	1/B9
IV.	LOCAL HEAT FLUX DATA	20	1/B13
IV.A.	Experimental Test Conditions	20	1/B13
IV.A.1.	Presentation of the data	20	1/B13
IV.A.2.	Symmetry of the data	22	1/C3
IV.A.3.	Comparison of third and fifth blowing row data	22	1/C3
IV.A.4.	Low-M data	24	1/C5
IV.A.5.	High-M data	25	1/C6
IV.A.6.	Comparison to spanwise-averaged data . .	26	1/C7
IV.C.	Concluding Remarks	27	1/C8
V.	NUMERICAL PREDICTION PROGRAM	34	1/D7
V.A.	Introduction	34	1/D7
V.B.	The STANCOOL Program	34	1/D7
V.C.	Injection Model	36	1/D9
V.C.1.	Model development	36	1/D9
V.C.2.	STANCOOL injection model	37	1/D10
V.D.	Turbulence-Augmentation Model	40	1/D13
V.D.1.	Model development	40	1/D13
V.D.2.	STANCOOL turbulence model	41	1/D14
V.E.	Summary and Constants for the Model	43	1/E2
V.F.	Prediction of the Data Bases	44	1/E3
References	69	1/G1

A	MODIFYING STAN5 TO OBTAIN STANCOOL	71	1/G3
B	PREVIOUSLY UNREPORTED SLANT-INJECTION DATA	87	2/A7
B.1.	Data with 11 rows blowing, heated starting length	89	2/A9
B.1.a.	Initial profiles of temperature and velocity	89	2/A9
B.1.b.	M = 0.20; $\theta \approx 1$	90	2/A11
	M = 0.20; $\theta \approx 0$	91	2/A13
	M = 0.20; $\theta \approx 1$, $\theta = 0$ by superposition	92	2/B1
B.1.c.	M = 0.6; $\theta \approx 1$	93	2/B3
	M = 0.6; $\theta \approx 0$	94	2/B5
	M = 0.6; $\theta \approx 1$, $\theta = 0$ by superposition	95	2/B7
B.1.d.	M = 0.75; $\theta \approx 1$	96	2/B9
	M = 0.75; $\theta \approx 0$	97	2/B11
	M = 0.75; $\theta \approx 1$, $\theta = 0$ by superposition	98	2/B13
B.1.e.	M = 0.90; $\theta \approx 1$	99	2/C1
	M = 0.90; $\theta \approx 0$	100	2/C3
	M = 0.90; $\theta \approx 1$, $\theta = 0$ by superposition	101	2/C5
B.1.f.	M = 1.33; $\theta \approx 1$	102	2/C7
	M = 1.33; $\theta \approx 0$	103	2/C9
	M = 1.33; $\theta \approx 1$, $\theta = 0$ by superposition	104	2/C11
B.2.	Data with 6 rows blowing, heated starting length	105	2/C13
B.2.a.	Initial profiles of temperature and velocity	105	2/C13
B.2.b.	M = 0.4; $\theta \approx 1$	106	2/D1
	M = 0.4; $\theta \approx 0$	107	2/D3
	M = 0.4; $\theta \approx 1$, $\theta = 0$ by superposition	108	2/D5
B.2.c.	M = 0.9; $\theta \approx 1$	109	2/D7
	M = 0.9; $\theta \approx 0$	110	2/D9
	M = 0.9; $\theta \approx 1$, $\theta = 0$ by superposition	111	2/D11

```

909 FORMAT (/10X,'YL=',F9.5/)
C
  YPEN=Y(II)+DELM*(Y(II+1)-Y(II))/(DELMR*OLDM)
  YPENI=YPEN
  IF (YPEN.GT.YL)YL=YPEN
  IF(YPEN/YL.GT.0.8)YPEN=0.8*YL
C
C *****
105 CONTINUE
  IF (KCOUNT.EQ.0) RETURN
C
  GO TO 950
C
C INITIALIZE RECOVERY REGION
900 APLO=APLINL
  IF (KTX.GT.25)DELTAX=0.2
  IF (KTX.GT.25) DXMAX=1000.
  GO TO 951
C
C DAMP APLMOD IN FILM COOLING REGION
950 APLO=APLMOD
951 KTX=KTX+1
  IF (KTX.LE.5) DX=0.5*DX
  IF(DX.GT.DXMAX) DX=DXMAX
  IF(YL.LT.YPENI)YL=YPENI
  XPYL=(XU-XHOLE)/YL
  UTAUG=SQRT(GC*TAUW/RHO(NP3))
  IF (UTAUG.LT.0.01*UGU.OR.UTAUG.GT.0.1*UGU) UTAUG=0.05*UGU
  DAMP=EXP(-(DX*UTAUG*RHO(1))/(VISCO(1)*PPLAG))
  APLE=APLO-(APLO-APLE)*DAMP
  APLO=APLE
  IF (KD.EQ.1.OR.KD.EQ.3) APL=APLE
  IF (DELMR.EQ.0.0.AND.ALAM.EQ.0.0) GO TO 955
  ALAME=ALAM*EXP(-1.*XPYL/2.)
C
  IF (KTX.NE.1) GO TO 955
952 AL2D=ALMG*YL
  IF (YPEN.LT.AL2D/AK) AL2D=AK*YPEN
  ALAUG=ALAME*YL
  ALTOT=AL2D+ALAUG
  IF(K3.NE.55)WRITE (6,130)
130 FORMAT (1H1)
  WRITE (6,954) ALAME,YPEN,AL2D,ALAUG,ALTOT,YL
954 FORMAT(/5X,'ALAME=',F6.4,5X,'YPEN=',F6.4,3X,'L2D1=',F6.4,3X,
1'LAUG=',F6.4,3X,'LTOT=',F6.4,3X,'YL=',F6.4,3X,
2 'IF YPEN WAS .GT. YL, YL=YPEN'/)
  IF(K3.NE.55.AND.OUTPUT.EQ.2) WRITE (6,140)
140 FORMAT(/,115H INTG XU UGU K F REM
1 CF2 H REH ST F(1,WALL) APL OR BPL AME)
C
955 SP(1)=YPEN/YL
  SP(2)=YL
  SP(3)=ALAME
  IF (TYPBC(1).EQ.2)SP(5)=(F(1,1)-F(1,NP3))/(AUXTH-F(1,NP3))

```

```

      IF (XU.LE.XPRINT) RETURN
C
C   COMPUTE AVERAGE STANTON NUMBERS
      XPRINT=X(NXBC) +1.
      WRITE (6,405)
405  FORMAT(/,10X,'STANTON NUMBER AVERAGE OVER DISTANCE FROM 0.5*PITCH
      1 BEFORE A HOLE LOCATION TO 0.5*PITCH AFTER THAT LOCATION'/)
      JHI=1
      DELTA=PITCH/2.
      IF(NROWS.EQ.6.AND.PITCH/DIAM.GT.6.)DELTA=PITCH/4.
      IF(NROWS.EQ.6.AND.PITCH/DIAM.GT.6.)NROWS=11
      NROWP1=NROWS+1
      DO 470 I=2,NROWP1
      XLO=X(I)-DELTA
      XHI=X(I)+DELTA
      DO 410 J=JHI,1000
      IF(XLOC(J).GE.XLO) GO TO 420
410  CONTINUE
420  JLO=J
      DO 430 J=JLO,1000
      IF (XLOC(J).GE.XHI) GO TO 440
430  CONTINUE
440  JHI=J-1
C   TRAPEZOIDAL RULE
      LLO=JLO+1
      LHI=JHI-1
      STAVG=STX(JLO)*(XLOC(JLO+1)-XLOC(JLO))
      DO 450 J=LLO,LHI
450  STAVG=STAVG+STX(J)*(XLOC(J+1)-XLOC(J-1))
      STAVG=0.5*(STAVG+STX(JHI)*(XLOC(JHI)-XLOC(JHI-1)))/(XLOC(JHI)-
      1 XLOC(JLO))
      WRITE (6,460) X(I),STAVG
460  FORMAT (10X,'XLOCATION=',F7.4,5X,'STANTON NUMBER AVERAGE=',E12.5/)
470  CONTINUE
      RETURN
C
109  WRITE (6,110)
      LVAR=6
110  FORMAT(' PROGRAM TERMINATED BECAUSE PD WAS OUTSIDE OF THE E-SURFAC
      1E')
      RETURN
540  WRITE (6,113)
113  FORMAT (/,10X,'DELMR CALCULATION DID NOT CONVERGE IN 15 ITER')
      LVAR=6
      RETURN
      END

```

Listing H

Sample Input Data

2700HSL40

1	2	1	2	21	2	1	1			
0.0	4.5		0.10		200.		0.01	0.006	0.	
0	0	2								
2117.	0.0742		0.00001229	0.715		1.0				
14	1	1								
0.0	1.0									
0.1667	1.0		0.40		0.0					
0.3333	1.0		0.40		0.0					
0.5	1.0		0.40		0.0					
0.6667	1.0		0.40		0.0					
0.8333	1.0		0.40		0.0					
1.0	1.0		0.40		0.0					
1.1667	1.0		0.40		0.0					
1.3333	1.0		0.40		0.0					
1.5	1.0		0.40		0.0					
1.6667	1.0		0.40		0.0					
1.8333	1.0		0.40		0.0					
1.9167	1.0									
4.5	1.0									
55.2	0.		97.6							
55.2	0.		97.6							
55.2	0.		97.6							
55.2	0.		97.6							
55.2	0.		97.6							
55.2	0.		97.6							
55.2	0.		97.6							
55.2	0.		97.6							
55.2	0.		97.6							
55.2	0.		97.6							
55.2	0.		97.6							
55.2	0.		97.6							
55.2	0.		97.6							
0.	0.		97.6							
0.000769	22.5		88.5							
0.000954	25.		86.7							
0.001195	27.2		85.							
0.001508	29.		83.8							
0.001914	30.5		82.6							
0.0025	32.0		81.6							
0.0032	33.		80.7							
0.0040	33.9		80.							
0.0051	35.		79.4							
0.0065	36.2		78.8							
0.0083	37.3		78.3							
0.0108	38.8		77.6							
0.0135	40.1		77.							

0.017	41.8	76.2				
0.0215	43.5	75.4				
0.0275	45.8	74.6				
0.035	48.1	73.7				
0.044	50.8	73.				
0.056	53.3	72.3				
0.071	55.0	71.8				
0.087	55.2	71.7				
0.41	.085	.01	0.	0.	1.0	0.
25.	0.	1.				
4000.	0.86					
32.2	778.	0.8				
1	11	2	55	00	55	
0.085	0.15	22.				
11.	0.166666	0.03333	30.	0.		

STANTON NUMBER AVERAGE

XLOCATION= 0.1667	STANTON NUMBER AVERAGE= 0.22895e-02
XLOCATION= 0.3333	STANTON NUMBER AVERAGE= 0.25046e-02
XLOCATION= 0.5000	STANTON NUMBER AVERAGE= 0.25233e-02
XLOCATION= 0.6667	STANTON NUMBER AVERAGE= 0.25305e-02
XLOCATION= 0.8333	STANTON NUMBER AVERAGE= 0.25049e-02
XLOCATION= 1.0000	STANTON NUMBER AVERAGE= 0.25025e-02
XLOCATION= 1.1667	STANTON NUMBER AVERAGE= 0.24759e-02
XLOCATION= 1.3333	STANTON NUMBER AVERAGE= 0.24528e-02
XLOCATION= 1.5000	STANTON NUMBER AVERAGE= 0.24333e-02
XLOCATION= 1.6667	STANTON NUMBER AVERAGE= 0.24363e-02
XLOCATION= 1.8333	STANTON NUMBER AVERAGE= 0.24105e-02

Appendix B

PREVIOUSLY UNREPORTED SLANT-INJECTION DATA

This appendix is a tabulation of the Stanton number data for a heated starting length and six and eleven rows of film-cooling. Initial velocity and temperature profiles precede the data. For the Stanton number data at each blowing ratio the experimental data at $\theta \approx 1$ and $\theta \approx 0$ are given first, followed by a sheet with the superposition-adjusted data to values at $\theta = 0, 1$.

Nomenclature

CF/2	$C_f/2$, friction coefficient.
CP	c , specific heat.
DEL	Velocity or thermal boundary layer thickness (see DEL99 or DELT99).
DEL1	δ_1 , displacement thickness.
DEL2	δ_2 , momentum thickness.
DEL99	Velocity boundary layer thickness.
DELT99	Thermal boundary layer thickness.
DREEN	Uncertainty in Re_{Δ_2} .
DST	Uncertainty in St .
DTM	Uncertainty in θ .
ETA	$\{1 - St(\theta = 1)\}/St(\theta = 0)$.
F	Blowing fraction.
F-COL	F at $\theta = 0$.
F-HOT	F at $\theta = 1$.
H	Velocity shape factor.
LOG B	ϕ function in $\theta = 1$ data correlation.
M	Blowing parameter.
PORT	Topwall location where profile is obtained.
PR	Pr , Prandtl number.
RE DEL2	
REENTH	Re_{Δ_2} , enthalpy thickness Reynolds number.
REH	
REM	Re_{δ_2} , momentum thickness Reynolds number.

REX	Re_x , x-Reynolds number.
RHO	Density.
ST	Stanton number.
STCR	$St(\theta = 0)/St_0$. Note: St_0 is defined at bottom of each summary data sheet.
STHR	$St(\theta = 1)/St_0$.
T	Recovery temperature of temperature probe.
T2	T_2 , secondary air temperature.
TADB	T_∞ , r, temperature to define Stanton number.
TBAR	$(T_0 - T)/(T_0 - T_\infty)$ (or one minus that quantity in the second tabulated data column).
THETA	θ , temperature parameter.
TINF	Mainstream static temperature.
TO	T_0 , plate temperature.
TPLATE	
U	Velocity.
U+	U^+ , non-dimensional velocity.
UINF	U_∞ , mainstream velocity.
VISC	ν , kinematic viscosity.
XLOC	x , distance from nozzle exit to probe tip.
XVO	x_{vo} , distance from nozzle exit to virtual origin, turbulent boundary layer.
Y	y , distance normal to surface.
Y+	y^+ , non-dimensional y distance.

REX = 0.13721E 07	REM = 3007.	REN = 2078.
XVD = 0.03 CM	DEL2 = 0.267 CM	DEM2 = 0.104 CM
UINF = 16.03 M/S	DEL99 = 3.152 CM	DEL99 = 2.229 CM
VISC = 0.14951E-04 M2/S	DEL1 = 0.363 CM	UINF = 16.02 M/S
PORT = 1	H = 1.433	VISC = 0.14933E-04 M2/S
XLDC = 121.92 CM	CF/2 = 0.16423E-02	TINF = 20.12 DEG C
		TPLATE = 37.96 DEG C

89

90

PUR: 020177 *** DISCRETE HOLE RIG *** HAS-3-14336

STANTON NUMBER DATA

TADN= 21.28 DEG C UINF= 17.10 M/S TINF= 21.15 DEG C
PHO= 1.200 KG/M3 VISC= 0.15097E-04 M2/S XYO= 0.0 CM
CP= 1009. J/KGK FR= 0.714

HEATED STARTING LENGTH, 11 PWMS OF BLOWING M=0.20, THETA=1.0

PLATE	X	REX	TO	PEENTH	STANTON NO	DST	DREEN	M	F	T2	THETA	OTH
1	127.8	0.14468E 07	35.10	0.20885E 04	0.24369E-02	0.448E-04	29.					
2	132.8	0.15043E 07	35.15	0.22167E 04	0.20140E-02	0.425E-04	30.	0.18	0.0059	36.3	1.011	0.018
3	137.9	0.15619E 07	35.15	0.26646E 04	0.16503E-02	0.410E-04	33.	0.20	0.0066	39.0	1.048	0.018
4	143.0	0.16194E 07	35.11	0.31529E 04	0.15575E-02	0.407E-04	36.	0.16	0.0051	36.6	1.027	0.018
5	148.1	0.16770E 07	35.13	0.35405E 04	0.14950E-02	0.404E-04	38.	0.18	0.0059	38.9	1.044	0.018
6	153.2	0.17345E 07	35.11	0.39809E 04	0.14750E-02	0.404E-04	40.	0.16	0.0053	37.9	0.985	0.018
7	158.2	0.17920E 07	35.15	0.43624E 04	0.14134E-02	0.401E-04	42.	0.17	0.0056	38.1	1.000	0.018
8	163.3	0.18495E 07	35.15	0.47644E 04	0.13303E-02	0.398E-04	43.	0.14	0.0046	38.5	1.018	0.018
9	168.4	0.19071E 07	35.17	0.51064E 04	0.12934E-02	0.396E-04	45.	0.19	0.0062	38.5	1.017	0.018
10	173.5	0.19647E 07	35.17	0.55390E 04	0.12266E-02	0.394E-04	47.	0.16	0.0051	37.3	0.951	0.018
11	178.6	0.20222E 07	35.15	0.59872E 04	0.11914E-02	0.393E-04	48.	0.17	0.0055	37.5	0.962	0.018
12	183.6	0.20797E 07	35.15	0.62597E 04	0.11558E-02	0.392E-04	49.	0.14	0.0044	37.5	0.963	0.018
13	187.5	0.21235E 07	35.78	0.65529E 04	0.10695E-02	0.376E-04	50.					
14	190.1	0.21531E 07	35.27	0.65069E 04	0.12237E-02	0.446E-04	50.					
15	192.7	0.21827E 07	35.63	0.66231E 04	0.12160E-02	0.462E-04	50.					
16	195.4	0.22125E 07	35.65	0.66595E 04	0.12448E-02	0.461E-04	50.					
17	198.0	0.22423E 07	35.67	0.66967E 04	0.12605E-02	0.466E-04	50.					
18	200.6	0.22719E 07	35.69	0.67335E 04	0.12400E-02	0.466E-04	50.					
19	203.2	0.23015E 07	35.52	0.67700E 04	0.12506E-02	0.454E-04	50.					
20	205.8	0.23312E 07	35.59	0.68080E 04	0.12970E-02	0.475E-04	50.					
21	208.5	0.23600E 07	35.57	0.68459E 04	0.12173E-02	0.453E-04	50.					
22	211.1	0.23904E 07	35.50	0.68829E 04	0.12807E-02	0.474E-04	50.					
23	213.7	0.24201E 07	35.46	0.69204E 04	0.12455E-02	0.460E-04	50.					
24	216.3	0.24490E 07	35.63	0.69570E 04	0.12770E-02	0.485E-04	50.					
25	218.9	0.24795E 07	35.44	0.69963E 04	0.13153E-02	0.489E-04	50.					
26	221.6	0.25093E 07	35.17	0.70343E 04	0.12436E-02	0.483E-04	50.					
27	224.2	0.25395E 07	35.37	0.70713E 04	0.12500E-02	0.437E-04	50.					
28	226.8	0.25605E 07	35.34	0.71092E 04	0.13106E-02	0.513E-04	50.					
29	229.4	0.25931E 07	35.31	0.71492E 04	0.13802E-02	0.496E-04	50.					
30	232.0	0.26278E 07	35.57	0.71901E 04	0.13007E-02	0.515E-04	50.					
31	234.6	0.26574E 07	35.57	0.72300E 04	0.13063E-02	0.489E-04	50.					
32	237.3	0.26872E 07	35.33	0.72695E 04	0.13565E-02	0.497E-04	50.					
33	239.9	0.27170E 07	35.31	0.73091E 04	0.13159E-02	0.493E-04	50.					
34	242.5	0.27466E 07	35.00	0.73491E 04	0.13089E-02	0.472E-04	50.					
35	245.1	0.27762E 07	35.19	0.73874E 04	0.13422E-02	0.517E-04	50.					
36	247.8	0.28059E 07	35.83	0.74161E 04	0.59663E-03	0.353E-04	50.					

UNCERTAINTY IN REX=23440.

UNCERTAINTY IN F=0.05032 IN RATIO

RUM 013177-1 *** DISCRETE HOLE RIG *** HAS-3-14336

STANTON NUMBER DATA

TADS= 18.63 DEG C UINF= 16.99 M/S TINF= 18.50 DEG C
 PHO= 1.216 KG/M3 VISC= 0.14806E-04 M2/S XYD= 0.0 CM
 CP= 1009. J/KGK PR= 0.714

HEATED STARTING LENGTH, 11 POMS OF BLOWING, M=0.20, THETA=0.0

PLATE	X	REX	TO	REENTH	STANTON NO	DST	OREEN	M	F	T2	THETA	DTH
1	127.8	0.14659E 07	34.15	0.21161E 04	0.23772E-02	0.476E-04	29.					
2	132.8	0.15241E 07	34.15	0.22524E 04	0.22994E-02	0.472E-04	29.	0.19	0.0061	21.4	0.188	0.019
3	137.9	0.15824E 07	34.11	0.24531E 04	0.22913E-02	0.473E-04	30.	0.23	0.0075	21.7	0.206	0.019
4	143.0	0.16407E 07	34.13	0.26770E 04	0.22977E-02	0.473E-04	31.	0.20	0.0064	21.8	0.209	0.019
5	149.1	0.16990E 07	34.13	0.28061E 04	0.22139E-02	0.468E-04	32.	0.24	0.0078	21.6	0.197	0.019
6	153.2	0.17573E 07	34.09	0.31066E 04	0.22944E-02	0.474E-04	32.	0.19	0.0061	21.8	0.209	0.019
7	158.2	0.18156E 07	34.15	0.33117E 04	0.21767E-02	0.466E-04	33.	0.24	0.0078	21.6	0.198	0.019
8	163.3	0.18739E 07	34.13	0.35269E 04	0.21023E-02	0.462E-04	34.	0.19	0.0062	21.6	0.198	0.019
9	168.4	0.19321E 07	34.09	0.37213E 04	0.21144E-02	0.464E-04	34.	0.24	0.0078	21.5	0.195	0.019
10	173.5	0.19904E 07	34.11	0.39314E 04	0.20656E-02	0.461E-04	35.	0.19	0.0061	21.6	0.201	0.019
11	178.6	0.20477E 07	34.13	0.41221E 04	0.20093E-02	0.458E-04	35.	0.23	0.0076	21.6	0.196	0.019
12	183.6	0.21070E 07	34.15	0.43244E 04	0.19670E-02	0.455E-04	36.	0.19	0.0060	21.7	0.202	0.019
13	187.5	0.21513E 07	32.81	0.44789E 04	0.17665E-02	0.586E-04	36.					
14	190.1	0.21814E 07	32.35	0.45337E 04	0.18333E-02	0.642E-04	36.					
15	192.7	0.22114E 07	32.87	0.45894E 04	0.18239E-02	0.652E-04	36.					
16	195.4	0.22415E 07	32.93	0.46435E 04	0.17819E-02	0.627E-04	36.					
17	198.0	0.22717E 07	32.97	0.46968E 04	0.17626E-02	0.621E-04	36.					
18	200.6	0.23017E 07	32.99	0.47495E 04	0.17507E-02	0.618E-04	36.					
19	203.2	0.23317E 07	33.00	0.48011E 04	0.16732E-02	0.589E-04	36.					
20	205.8	0.23618E 07	33.06	0.48518E 04	0.17001E-02	0.599E-04	36.					
21	208.5	0.23918E 07	33.00	0.49017E 04	0.16196E-02	0.571E-04	36.					
22	211.1	0.24210E 07	33.05	0.49505E 04	0.16293E-02	0.585E-04	36.					
23	213.7	0.24510E 07	33.00	0.49999E 04	0.15945E-02	0.568E-04	36.					
24	216.3	0.24820E 07	33.04	0.50477E 04	0.16480E-02	0.595E-04	37.					
25	218.9	0.25122E 07	32.87	0.50967E 04	0.16174E-02	0.581E-04	37.					
26	221.6	0.25422E 07	32.64	0.51443E 04	0.15473E-02	0.586E-04	37.					
27	224.2	0.25722E 07	31.57	0.51934E 04	0.17224E-02	0.566E-04	37.					
28	226.8	0.26022E 07	32.83	0.52437E 04	0.16207E-02	0.619E-04	37.					
29	229.4	0.26323E 07	32.81	0.52939E 04	0.17187E-02	0.595E-04	37.					
30	232.0	0.26623E 07	33.31	0.53444E 04	0.16473E-02	0.604E-04	37.					
31	234.6	0.26923E 07	33.23	0.53934E 04	0.16095E-02	0.576E-04	37.					
32	237.3	0.27225E 07	33.10	0.54419E 04	0.16169E-02	0.579E-04	37.					
33	239.9	0.27526E 07	33.00	0.54900E 04	0.15870E-02	0.574E-04	37.					
34	242.5	0.27827E 07	32.64	0.55375E 04	0.15715E-02	0.549E-04	37.					
35	245.1	0.28127E 07	32.87	0.55851E 04	0.15986E-02	0.596E-04	37.					
36	247.8	0.28427E 07	32.49	0.56318E 04	0.15075E-02	0.619E-04	37.					

UNCERTAINTY IN REX=23959.

UNCERTAINTY IN F=0.05032 IN RATIO

RUN 013177-1 *** DISCRETE HOLE RIG *** NAS-3-14336 STANTON NUMBER DATA

HEATED STARTING LENGTH, 11 POWS OF BLOWING, M=0.20, THETA=0.0

RUN 020177 *** DISCRETE HOLE RIG *** NAS-3-14336 STANTON NUMBER DATA

HEATED STARTING LENGTH, 11 POWS OF BLOWING M=0.20, THETA=1.0

LINEAR SUPERPOSITION IS APPLIED TO STANTON NUMBER DATA FROM
RUN NUMBERS 013177-1 AND 020177 TO OBTAIN STANTON NUMBER DATA AT TH=0 AND TH=1

PLATE	PEXCOL	PE DEL2	ST(TH=0)	REXHOT	RE DEL2	ST(TH=1)	ETA	STCR	F-COL	STHR	F-HOT	LOGB
1	1465796.0	2116.1	0.002377	1446804.0	2088.6	0.002437	0.0000	1.000	0.0000	1.000	0.0000	1.000
2	1524099.0	2254.3	0.002354	1504342.0	2216.8	0.002018	0.147	1.208	0.0061	1.028	0.0059	2.196
3	1592393.0	2394.3	0.002441	1561881.0	2661.8	0.001681	0.312	1.256	0.0075	0.863	0.0066	2.119
4	1640677.0	2537.8	0.002483	1619419.0	3133.7	0.001591	0.359	1.287	0.0064	0.823	0.0051	1.831
5	1698971.0	2679.8	0.002389	1676958.0	3515.2	0.001526	0.361	1.247	0.0078	0.794	0.0059	1.942
6	1757265.0	2822.3	0.002500	1734496.0	3941.9	0.001490	0.404	1.314	0.0061	0.781	0.0053	1.826
7	1815558.0	2964.4	0.002374	1792034.0	4328.0	0.001406	0.408	1.256	0.0078	0.742	0.0056	1.843
8	1873852.0	3103.3	0.002291	1849573.0	4730.2	0.001339	0.416	1.220	0.0062	0.711	0.0046	1.631
9	1932146.0	3234.5	0.002311	1907111.0	5058.3	0.001311	0.433	1.238	0.0078	0.700	0.0062	1.890
10	1990440.0	3365.2	0.002277	1964650.0	5494.9	0.001210	0.469	1.227	0.0061	0.650	0.0051	1.658
11	2048733.0	3499.4	0.002224	2022108.0	5855.5	0.001145	0.485	1.205	0.0076	0.619	0.0055	1.692
12	2107027.0	3627.7	0.002178	2079727.0	6237.4	0.001116	0.488	1.187	0.0060	0.607	0.0044	1.498
13	2165331.0	3720.4	0.001948	2123456.0	6538.4	0.001035	0.468	1.066		0.565		
14	2181352.0	3760.5	0.002051	2153088.0	6571.4	0.001192	0.419	1.126		0.652		
15	2211373.0	3841.2	0.001952	2182721.0	6666.7	0.001187	0.401	1.091		0.652		
16	2241540.0	3899.8	0.001922	2212496.0	6642.4	0.001219	0.366	1.060		0.671		
17	2271707.0	3957.2	0.001893	2242273.0	6678.8	0.001236	0.347	1.048		0.682		
18	2301729.0	4013.9	0.001864	2271905.0	6715.1	0.001215	0.355	1.045		0.672		
19	2331749.0	4069.0	0.001783	2301537.0	6751.4	0.001230	0.310	0.992		0.682		
20	2361771.0	4123.0	0.001805	2331169.0	6788.6	0.001278	0.292	1.006		0.711		
21	2391792.0	4176.0	0.001724	2360802.0	6825.3	0.001198	0.305	0.964		0.668		
22	2421814.0	4227.8	0.001720	2390434.0	6861.8	0.001264	0.265	0.964		0.706		
23	2451835.0	4278.9	0.001685	2420067.0	6898.8	0.001228	0.271	0.947		0.688		
24	2481856.0	4330.5	0.001745	2449843.0	6935.7	0.001259	0.278	0.982		0.707		
25	2511879.0	4382.2	0.001696	2479619.0	6973.7	0.001301	0.233	0.957		0.732		
26	2541899.0	4432.1	0.001626	2509251.0	7011.2	0.001229	0.244	0.920		0.693		
27	2571921.0	4484.3	0.001845	2538893.0	7047.6	0.001228	0.335	1.047		0.695		
28	2601942.0	4537.6	0.001701	2568516.0	7085.0	0.001295	0.239	0.967		0.735		
29	2631964.0	4593.3	0.001807	2598148.0	7124.5	0.001364	0.245	1.030		0.775		
30	2661985.0	4643.3	0.001717	2627781.0	7165.0	0.001368	0.203	0.980		0.779		
31	2692007.0	4694.5	0.001688	2657413.0	7204.4	0.001291	0.235	0.966		0.737		
32	2722028.0	4745.2	0.001685	2687189.0	7243.5	0.001344	0.202	0.966		0.769		
33	2752050.0	4795.4	0.001658	2716965.0	7282.8	0.001303	0.214	0.953		0.747		
34	2782072.0	4844.9	0.001640	2746597.0	7321.3	0.001296	0.210	0.945		0.745		
35	2812093.0	4894.6	0.001665	2776229.0	7360.3	0.001330	0.202	0.962		0.766		
36	2842115.0	4945.9	0.001745	2805862.0	7388.2	0.000552	0.684	1.010		0.319		

STANTON NUMBER RATIO BASED ON ST*PR**0.4=0.0295*REX**(-.2)

STANTON NUMBER RATIO FOR TH=1 IS CONVERTED TO COMPARABLE TRANSPIRATION VALUE
USING $\text{ALOG}(1 + B)/B$ EXPRESSION IN THE BLOWN SECTION

RUN 020377 *** DISCRETE HOLE RIG *** NAS-3-14336

STANTON NUMBER DATA

TABD= 20.45 DEG C UINF= 16.93 M/S TINF= 20.32 DEG C
 PHD= 1.206 KG/M3 VISC= 0.14986E-04 M2/S XYD= 0.0 CM
 CP= 1009. J/KGK FR= 0.714

HEATED STARTING LENGTH, 11 ROWS OF BLOWING M=0.60, THETA=1.0

PLATE	X	PEX	TO	PEENTH	STANTON NO	DST	DREN	M	F	T2	THETA	DTH
1	127.8	0.14434E 07	38.51	0.20837E 04	0.24519E-02	0.423E-04	29.					
2	132.8	0.15000E 07	38.48	0.22146E 04	0.21090E-02	0.497E-04	39.	0.55	0.0179	38.2	0.985	0.017
3	137.9	0.15580E 07	38.51	0.33455E 04	0.19979E-02	0.401E-04	55.	0.54	0.0176	38.6	1.005	0.017
4	143.0	0.16154E 07	38.48	0.44652E 04	0.17181E-02	0.359E-04	67.	0.55	0.0177	39.0	1.028	0.017
5	148.1	0.16730E 07	38.49	0.56011E 04	0.15590E-02	0.383E-04	77.	0.52	0.0170	38.7	1.012	0.017
6	153.2	0.17304E 07	38.51	0.66751E 04	0.14908E-02	0.360E-04	86.	0.53	0.0171	38.3	0.990	0.017
7	158.2	0.17878E 07	38.49	0.77278E 04	0.14361E-02	0.372E-04	93.	0.54	0.0175	38.4	0.993	0.017
8	163.3	0.18452E 07	38.49	0.88047E 04	0.13857E-02	0.377E-04	101.	0.57	0.0183	38.9	1.024	0.017
9	168.4	0.19026E 07	38.51	0.99616E 04	0.13606E-02	0.375E-04	109.	0.53	0.0173	38.4	0.992	0.017
10	173.5	0.19600E 07	38.51	0.11023E 05	0.13180E-02	0.374E-04	115.	0.56	0.0182	38.0	0.970	0.017
11	178.6	0.20174E 07	38.53	0.12108E 05	0.12617E-02	0.372E-04	121.	0.53	0.0173	37.7	0.953	0.017
12	183.6	0.20748E 07	38.55	0.13125E 05	0.12669E-02	0.372E-04	126.	0.55	0.0177	37.7	0.952	0.017
13	187.5	0.21164E 07	38.80	0.14145E 05	0.10613E-02	0.354E-04	129.					
14	190.1	0.21400E 07	38.46	0.14177E 05	0.10601E-02	0.397E-04	129.					
15	192.7	0.21775E 07	38.82	0.14208E 05	0.10567E-02	0.409E-04	129.					
16	195.4	0.22072E 07	38.84	0.14239E 05	0.10517E-02	0.399E-04	129.					
17	198.0	0.22369E 07	38.86	0.14270E 05	0.10405E-02	0.396E-04	129.					
18	200.6	0.22665E 07	38.88	0.14301E 05	0.10123E-02	0.388E-04	129.					
19	203.2	0.22961E 07	38.93	0.14330E 05	0.96554E-03	0.369E-04	129.					
20	205.8	0.23258E 07	37.03	0.14359E 05	0.93050E-03	0.374E-04	129.					
21	208.5	0.23555E 07	37.05	0.14387E 05	0.91638E-03	0.357E-04	129.					
22	211.1	0.23848E 07	37.03	0.14414E 05	0.92983E-03	0.365E-04	129.					
23	213.7	0.24143E 07	37.03	0.14441E 05	0.89652E-03	0.354E-04	129.					
24	216.3	0.24440E 07	37.16	0.14468E 05	0.90207E-03	0.367E-04	129.					
25	218.9	0.24737E 07	37.01	0.14494E 05	0.89058E-03	0.357E-04	129.					
26	221.5	0.25033E 07	38.80	0.14520E 05	0.83959E-03	0.354E-04	129.					
27	224.2	0.25329E 07	38.17	0.14544E 05	0.82296E-03	0.318E-04	129.					
28	226.8	0.25624E 07	37.01	0.14570E 05	0.88417E-03	0.373E-04	129.					
29	229.4	0.25920E 07	37.03	0.14596E 05	0.92725E-03	0.357E-04	129.					
30	232.0	0.26215E 07	37.33	0.14623E 05	0.90064E-03	0.367E-04	129.					
31	234.6	0.26511E 07	37.31	0.14650E 05	0.86913E-03	0.351E-04	129.					
32	237.3	0.26807E 07	37.18	0.14676E 05	0.88151E-03	0.353E-04	129.					
33	239.9	0.27103E 07	37.14	0.14701E 05	0.86198E-03	0.350E-04	129.					
34	242.5	0.27401E 07	38.90	0.14727E 05	0.84566E-03	0.332E-04	129.					
35	245.1	0.27694E 07	37.01	0.14752E 05	0.86530E-03	0.366E-04	129.					
36	247.8	0.27992E 07	38.69	0.14777E 05	0.80060E-03	0.376E-04	129.					

UNCERTAINTY IN REX=23592.

UNCERTAINTY IN F=0.05033 IN RATIO

94

RUN 020277 *** DISCRETE HOLE PIG *** NAS-3-14336

STANTON NUMBER DATA

TACB= 20.54 DEG C UINF= 16.96 M/S TINF= 20.41 DEG C
 PHO= 1.202 KG/M3 VISC= 0.15046E-04 M2/S XYO= 0.0 CM
 CP= 1009. J/KGK PR= 0.714

HEATED STARTING LENGTH, 11 ROWS OF BLOWING, M=0.60, THETA=0.0

PLATE	X	REX	TO	REENTH	STANTON NO	DST	DREEN	M	F	T2	THETA	DTH
1	127.8	0.14401E 07	35.43	0.20789E 04	0.24648E-02	0.505E-04	29.					
2	132.8	0.14973E 07	35.41	0.22191E 04	0.24319E-02	0.504E-04	31.	0.61	0.0198	22.1	0.110	0.020
3	137.9	0.15546E 07	35.39	0.24561E 04	0.25335E-02	0.511E-04	36.	0.62	0.0201	22.3	0.123	0.020
4	143.0	0.16119E 07	35.41	0.27725E 04	0.25343E-02	0.510E-04	40.	0.62	0.0201	22.2	0.119	0.020
5	148.1	0.16691E 07	35.41	0.30543E 04	0.25322E-02	0.510E-04	43.	0.60	0.0194	22.1	0.115	0.020
6	153.2	0.17264E 07	35.39	0.33277E 04	0.25652E-02	0.513E-04	46.	0.60	0.0195	22.2	0.119	0.020
7	158.2	0.17837E 07	35.43	0.36045E 04	0.24689E-02	0.506E-04	49.	0.61	0.0197	22.1	0.111	0.020
8	163.3	0.18409E 07	35.43	0.38708E 04	0.24655E-02	0.505E-04	52.	0.61	0.0198	22.0	0.105	0.020
9	168.4	0.18982E 07	35.39	0.41310E 04	0.24624E-02	0.506E-04	55.	0.61	0.0197	22.0	0.105	0.020
10	173.5	0.19555E 07	35.39	0.43919E 04	0.24928E-02	0.508E-04	57.	0.61	0.0196	22.0	0.106	0.020
11	178.6	0.20128E 07	35.41	0.46528E 04	0.24548E-02	0.505E-04	60.	0.63	0.0194	22.0	0.107	0.020
12	183.6	0.20700E 07	35.43	0.49124E 04	0.24728E-02	0.506E-04	62.	0.62	0.0199	22.0	0.106	0.020
13	188.5	0.21135E 07	33.31	0.51356E 04	0.20916E-02	0.669E-04	63.					
14	190.1	0.21430E 07	32.83	0.51977E 04	0.21147E-02	0.730E-04	63.					
15	192.7	0.21725E 07	33.31	0.52590E 04	0.20526E-02	0.740E-04	63.					
16	195.4	0.22020E 07	33.35	0.53196E 04	0.20361E-02	0.721E-04	63.					
17	198.0	0.22315E 07	33.39	0.53791E 04	0.19976E-02	0.709E-04	63.					
18	200.6	0.22613E 07	33.43	0.54371E 04	0.19310E-02	0.689E-04	63.					
19	203.2	0.22908E 07	33.48	0.54931E 04	0.18606E-02	0.661E-04	63.					
20	205.8	0.23203E 07	33.60	0.55482E 04	0.18683E-02	0.657E-04	63.					
21	208.5	0.23490E 07	33.54	0.56021E 04	0.17856E-02	0.635E-04	63.					
22	211.1	0.23793E 07	33.65	0.56546E 04	0.17653E-02	0.643E-04	63.					
23	213.7	0.24090E 07	33.58	0.57060E 04	0.17187E-02	0.619E-04	63.					
24	216.3	0.24384E 07	33.65	0.57571E 04	0.17460E-02	0.641E-04	63.					
25	218.9	0.24680E 07	33.50	0.58079E 04	0.16908E-02	0.610E-04	63.					
26	221.6	0.24975E 07	33.29	0.58562E 04	0.15828E-02	0.610E-04	63.					
27	224.2	0.25270E 07	32.35	0.59040E 04	0.16551E-02	0.564E-04	63.					
28	226.8	0.25565E 07	33.56	0.59530E 04	0.16644E-02	0.647E-04	63.					
29	229.4	0.25860E 07	33.56	0.60034E 04	0.17484E-02	0.617E-04	63.					
30	232.0	0.26155E 07	34.04	0.60537E 04	0.16571E-02	0.620E-04	63.					
31	234.6	0.26450E 07	34.00	0.61020E 04	0.16132E-02	0.590E-04	63.					
32	237.3	0.26746E 07	33.92	0.61494E 04	0.15969E-02	0.588E-04	63.					
33	239.9	0.27043E 07	33.83	0.61960E 04	0.15612E-02	0.579E-04	64.					
34	242.5	0.27335E 07	33.52	0.62420E 04	0.15499E-02	0.556E-04	64.					
35	245.1	0.27633E 07	33.71	0.62879E 04	0.15644E-02	0.599E-04	64.					
36	247.8	0.27920E 07	33.39	0.63323E 04	0.14420E-02	0.613E-04	64.					

UNCERTAINTY IN REX=23538.

UNCERTAINTY IN F=0.05033 IN RATIO

RUN 020277 *** DISCRETE HOLE RIG *** HAS-3-14336 STANTON NUMBER DATA

HEATED STARTING LENGTH, 11 POWS OF BLOWING, M=0.60, THETA=0.0

RUN 020377 *** DISCRETE HOLE RIG *** HAS-3-14336 STANTON NUMBER DATA

HEATED STARTING LENGTH, 11 POWS OF BLOWING M=0.60, THETA=1.0

LINEAR SUPERPOSITION IS APPLIED TO STANTON NUMBER DATA FROM
RUN NUMBERS 020277 AND 020377 TO OBTAIN STANTON NUMBER DATA AT TH=0 AND TH=1

PLATE	REXCOL	RE DEL2	ST(TH=0)	REXHOT	RE DEL2	ST(TH=1)	ETA	STCR	F-COL	STHR	F-HOT	LOGS
1	1440051.0	2070.9	0.002465	1443365.0	2083.7	0.002452	0.0000	1.000	0.0000	1.000	0.0000	1.000
2	1497321.0	2220.3	0.002472	1500767.0	2214.4	0.002104	0.149	1.259	0.0198	1.072	0.0179	4.051
3	1554591.0	2355.6	0.002604	1558169.0	3360.8	0.001995	0.234	1.336	0.0201	1.024	0.0176	3.948
4	1611861.0	2515.9	0.002644	1615570.0	4475.8	0.001733	0.345	1.366	0.0201	0.896	0.0177	3.700
5	1669131.0	2667.8	0.002659	1672972.0	5584.7	0.001580	0.406	1.383	0.0194	0.822	0.0170	3.509
6	1726401.0	2821.4	0.002707	1730374.0	6648.0	0.001491	0.449	1.418	0.0195	0.782	0.0171	3.346
7	1783671.0	2973.5	0.002684	1787776.0	7710.7	0.001426	0.453	1.373	0.0197	0.752	0.0175	3.567
8	1840941.0	3122.4	0.002595	1845177.0	8795.8	0.001395	0.462	1.377	0.0198	0.741	0.0183	3.676
9	1898211.0	3270.9	0.002591	1902579.0	9927.7	0.001370	0.471	1.383	0.0197	0.732	0.0173	3.536
10	1955481.0	3420.5	0.002635	1959981.0	10996.8	0.001292	0.510	1.415	0.0196	0.694	0.0182	3.599
11	2012751.0	3570.5	0.002603	2017382.0	12111.3	0.001208	0.536	1.406	0.0194	0.653	0.0173	3.419
12	2070021.0	3720.1	0.002622	2074784.0	13171.4	0.001220	0.535	1.424	0.0199	0.663	0.0177	3.510
13	2113546.0	3870.0	0.002221	2118410.0	14237.8	0.001003	0.548	1.211		0.547		
14	2143040.0	3993.9	0.002247	2147971.0	14267.5	0.001001	0.555	1.229		0.548		
15	2172534.0	3959.3	0.002178	2177533.0	14297.1	0.001001	0.541	1.194		0.549		
16	2202171.0	4023.3	0.002160	2207238.0	14326.6	0.000996	0.539	1.188		0.548		
17	2231806.0	4086.5	0.002118	2236944.0	14356.0	0.000987	0.534	1.168		0.544		
18	2261302.0	4148.0	0.002047	2266506.0	14384.8	0.000961	0.531	1.132		0.531		
19	2290796.0	4207.4	0.001973	2296067.0	14412.6	0.000915	0.536	1.094		0.507		
20	2320290.0	4265.7	0.001900	2325629.0	14439.9	0.000931	0.530	1.100		0.517		
21	2349784.0	4323.0	0.001895	2355192.0	14466.5	0.000867	0.542	1.056		0.483		
22	2379278.0	4378.6	0.001871	2384753.0	14492.4	0.000883	0.528	1.045		0.493		
23	2408772.0	4433.1	0.001822	2414315.0	14518.0	0.000850	0.533	1.020		0.476		
24	2438409.0	4487.3	0.001852	2444020.0	14543.2	0.000855	0.539	1.040		0.480		
25	2468046.0	4541.1	0.001792	2473726.0	14568.4	0.000846	0.528	1.008		0.476		
26	2497540.0	4592.3	0.001676	2503288.0	14592.7	0.000798	0.524	0.945		0.450		
27	2527034.0	4643.1	0.001760	2532850.0	14616.0	0.000776	0.559	0.995		0.439		
28	2556528.0	4695.1	0.001763	2562411.0	14639.9	0.000840	0.523	0.999		0.476		
29	2586023.0	4748.4	0.001952	2591974.0	14665.4	0.000881	0.524	1.052		0.501		
30	2615517.0	4801.6	0.001752	2621536.0	14691.1	0.000858	0.510	0.997		0.489		
31	2645011.0	4852.7	0.001707	2651097.0	14716.1	0.000827	0.515	0.974		0.472		
32	2674646.0	4902.8	0.001687	2680802.0	14740.8	0.000841	0.501	0.964		0.481		
33	2704285.0	4952.1	0.001649	2710508.0	14765.4	0.000823	0.501	0.945		0.472		
34	2733779.0	5000.6	0.001639	2740070.0	14789.5	0.000806	0.508	0.941		0.463		
35	2763273.0	5049.2	0.001652	2769632.0	14813.6	0.000826	0.500	0.951		0.475		
36	2792767.0	5096.1	0.001523	2799193.0	14837.2	0.000764	0.498	0.878		0.441		

STANTON NUMBER RATIO BASED ON ST*PR**0.4=0.0295*REX**(-.2)

STANTON NUMBER RATIO FOR TH=1 IS CONVERTED TO COMPARABLE TRANSPIRATION VALUE
USING ALG011 + B1/B EXPRESSION IN THE BLOWN SECTION

PUR 012677 *** DISCRETE HOLE FIG *** NAS-3-14336 STANTON NUMBER DATA

TACO= 20.91 DEG C UINF= 16.84 M/S TINF= 20.78 DEG C
 PHO= 1.207 KG/M3 VISC= 0.14913E-04 M2/S XFD= 0.0 CM
 CP= 1010. J/KGK PR= 0.714

HEATED STARTING LENGTH, 11 POWS OF BLOWING M=0.75, THETA=1.0

PLATE	X	REX	TO	WEENTH	STANTON NO	DST	DREEN	M	F	T2	THETA	DTH
1	127.8	0.14350E 07	35.02	0.20716E 04	0.24346E-02	0.445E-04	29.					
2	132.8	0.14921E 07	35.02	0.22024E 04	0.21569E-02	0.431E-04	46.	0.76	0.8246	37.2	0.953	0.010
3	137.9	0.15491E 07	35.00	0.23667E 04	0.22434E-02	0.435E-04	67.	0.65	0.8219	37.1	0.945	0.010
4	143.0	0.16062E 07	37.98	0.49719E 04	0.20197E-02	0.425E-04	81.	0.67	0.8218	37.3	0.962	0.010
5	145.1	0.16633E 07	33.00	0.62003E 04	0.10679E-02	0.417E-04	93.	0.67	0.8216	37.1	0.940	0.010
6	153.2	0.17203E 07	35.00	0.75554E 04	0.17561E-02	0.416E-04	102.	0.65	0.8212	36.8	0.930	0.010
7	159.2	0.17774E 07	37.96	0.87790E 04	0.17277E-02	0.412E-04	111.	0.65	0.8219	36.8	0.930	0.010
8	163.3	0.18345E 07	37.96	0.10039E 05	0.16694E-02	0.410E-04	120.	0.71	0.8228	37.1	0.952	0.010
9	165.4	0.18915E 07	37.98	0.11373E 05	0.16404E-02	0.408E-04	129.	0.66	0.8215	36.7	0.925	0.010
10	173.5	0.19486E 07	37.94	0.12601E 05	0.16102E-02	0.408E-04	136.	0.71	0.8229	36.5	0.919	0.010
11	178.6	0.20057E 07	37.94	0.13889E 05	0.15566E-02	0.406E-04	143.	0.69	0.8223	36.2	0.898	0.010
12	183.6	0.20627E 07	37.98	0.15120E 05	0.15709E-02	0.406E-04	150.	0.70	0.8226	36.2	0.896	0.010
13	187.5	0.21201E 07	26.42	0.16341E 05	0.12970E-02	0.436E-04	153.					
14	190.1	0.21755E 07	26.00	0.16379E 05	0.13146E-02	0.473E-04	153.					
15	192.7	0.21649E 07	26.40	0.16417E 05	0.12036E-02	0.401E-04	153.					
16	195.4	0.21944E 07	26.48	0.16455E 05	0.12731E-02	0.469E-04	153.					
17	195.0	0.22040E 07	26.55	0.16490E 05	0.12353E-02	0.457E-04	153.					
18	200.6	0.22534E 07	26.61	0.16527E 05	0.11954E-02	0.440E-04	153.					
19	203.2	0.22027E 07	26.63	0.16562E 05	0.11499E-02	0.427E-04	153.					
20	205.8	0.23121E 07	26.71	0.16596E 05	0.11904E-02	0.440E-04	153.					
21	208.5	0.23415E 07	26.72	0.16629E 05	0.10645E-02	0.404E-04	153.					
22	211.1	0.23779E 07	26.74	0.16661E 05	0.10759E-02	0.412E-04	153.					
23	213.7	0.24003E 07	26.74	0.16690E 05	0.10263E-02	0.396E-04	153.					
24	216.5	0.24290E 07	26.84	0.16720E 05	0.10489E-02	0.411E-04	153.					
25	219.9	0.24594E 07	26.76	0.16752E 05	0.10150E-02	0.398E-04	153.					
26	221.6	0.24970E 07	26.61	0.16783E 05	0.10042E-02	0.400E-04	153.					
27	224.2	0.25181E 07	25.92	0.16811E 05	0.93500E-03	0.351E-04	153.					
28	226.8	0.25475E 07	26.80	0.16839E 05	0.98647E-03	0.409E-04	153.					
29	229.4	0.25769E 07	26.89	0.16869E 05	0.10317E-02	0.390E-04	153.					
30	232.0	0.26063E 07	27.11	0.16900E 05	0.10652E-02	0.418E-04	153.					
31	234.6	0.26357E 07	27.12	0.16930E 05	0.95131E-03	0.379E-04	153.					
32	237.3	0.26652E 07	26.99	0.16950E 05	0.96597E-03	0.381E-04	153.					
33	239.9	0.26940E 07	26.97	0.16926E 05	0.92499E-03	0.373E-04	153.					
34	242.5	0.27242E 07	26.72	0.17012E 05	0.90517E-03	0.352E-04	153.					
35	245.1	0.27536E 07	26.98	0.17039E 05	0.92294E-03	0.386E-04	153.					
36	247.8	0.27829E 07	26.61	0.17065E 05	0.85978E-03	0.395E-04	153.					

UNCERTAINTY IN REX=23455.

UNCERTAINTY IN F=0.05034 IN RATIO

RGN 012777 *** DISCRETE HOLE RIG *** NAS-3-14336

STANTON NUMBER DATA

TACD= 18.49 DEG C UINF= 16.90 M/S TINF= 18.36 DEG C
 PHD= 1.211 KG/M3 VISC= 0.14861E-04 M2/S XTD= 0.0 CM
 CP= 1009. J/KGK PR= 0.715

HEATED STARTING LENGTH, 11 ROWS OF BLOWING, M=0.75, THETA=0.0

PLATE	X	REX	TO	REENTH	STANTON NO	DST	DREEN	H	F	T2	THETA	DTM
1	127.8	0.14530E 07	33.08	0.20976E 04	0.23031E-02	0.504E-04	29.					
2	132.8	0.15107E 07	33.10	0.22322E 04	0.23553E-02	0.507E-04	33.	0.76	0.0247	21.5	0.214	0.020
3	137.9	0.15675E 07	33.14	0.26794E 04	0.25644E-02	0.518E-04	41.	0.75	0.0243	21.6	0.221	0.020
4	143.0	0.16263E 07	33.16	0.31403E 04	0.26331E-02	0.521E-04	47.	0.75	0.0243	21.6	0.219	0.020
5	148.1	0.16841E 07	33.12	0.35976E 04	0.25318E-02	0.516E-04	52.	0.76	0.0245	21.6	0.222	0.020
6	153.2	0.17419E 07	33.12	0.40542E 04	0.25270E-02	0.516E-04	57.	0.74	0.0241	21.7	0.229	0.020
7	159.2	0.17997E 07	33.16	0.45233E 04	0.25025E-02	0.512E-04	62.	0.74	0.0241	21.7	0.226	0.020
8	163.3	0.18575E 07	33.12	0.49815E 04	0.24833E-02	0.513E-04	66.	0.76	0.0247	21.6	0.220	0.020
9	168.4	0.19153E 07	33.12	0.54397E 04	0.25071E-02	0.515E-04	70.	0.74	0.0240	21.7	0.223	0.020
10	173.5	0.19730E 07	33.10	0.58934E 04	0.25147E-02	0.516E-04	74.	0.76	0.0247	21.6	0.220	0.020
11	178.6	0.20308E 07	33.16	0.63530E 04	0.25091E-02	0.514E-04	77.	0.75	0.0244	21.6	0.218	0.020
12	183.6	0.20915E 07	33.14	0.68042E 04	0.24556E-02	0.511E-04	81.	0.75	0.0244	21.6	0.218	0.020
13	187.5	0.21325E 07	32.07	0.72181E 04	0.23393E-02	0.770E-04	82.					
14	190.1	0.21623E 07	31.00	0.72874E 04	0.23082E-02	0.779E-04	82.					
15	192.7	0.21920E 07	32.43	0.73544E 04	0.21904E-02	0.771E-04	82.					
16	195.4	0.22219E 07	32.53	0.74190E 04	0.21470E-02	0.742E-04	82.					
17	193.0	0.22512E 07	32.62	0.74323E 04	0.21020E-02	0.728E-04	82.					
18	200.6	0.22216E 07	32.72	0.75441E 04	0.20430E-02	0.711E-04	82.					
19	203.2	0.23114E 07	32.74	0.76040E 04	0.19766E-02	0.683E-04	82.					
20	205.8	0.23411E 07	32.83	0.76631E 04	0.19930E-02	0.692E-04	82.					
21	208.5	0.23709E 07	32.79	0.77205E 04	0.18576E-02	0.646E-04	82.					
22	211.1	0.24006E 07	32.85	0.77759E 04	0.18534E-02	0.657E-04	82.					
23	213.7	0.24304E 07	32.81	0.78303E 04	0.17896E-02	0.628E-04	82.					
24	216.3	0.24603E 07	32.91	0.78842E 04	0.18288E-02	0.651E-04	82.					
25	218.9	0.24902E 07	32.79	0.79383E 04	0.17973E-02	0.635E-04	82.					
26	221.6	0.25200E 07	32.66	0.79914E 04	0.17716E-02	0.658E-04	82.					
27	224.2	0.25497E 07	31.53	0.80435E 04	0.17254E-02	0.565E-04	82.					
28	226.8	0.25795E 07	32.81	0.80950E 04	0.17302E-02	0.651E-04	82.					
29	229.4	0.26092E 07	32.85	0.81476E 04	0.18006E-02	0.622E-04	82.					
30	232.0	0.26390E 07	33.31	0.82001E 04	0.17254E-02	0.624E-04	82.					
31	234.6	0.26688E 07	33.31	0.82505E 04	0.16567E-02	0.593E-04	82.					
32	237.3	0.26987E 07	33.14	0.82999E 04	0.16553E-02	0.588E-04	82.					
33	239.9	0.27285E 07	33.12	0.83484E 04	0.16005E-02	0.579E-04	82.					
34	242.5	0.27583E 07	32.79	0.83957E 04	0.15764E-02	0.549E-04	82.					
35	245.1	0.27881E 07	33.06	0.84420E 04	0.15865E-02	0.591E-04	82.					
36	247.8	0.28178E 07	32.74	0.84886E 04	0.14885E-02	0.608E-04	82.					

UNCERTAINTY IN REX=23749.

UNCERTAINTY IN F=0.05033 IN RATIO

98

RUN 012777 *** DISCRETE HOLE RIG *** HAS-3-14336 STANTON NUMBER DATA

HEATED STARTING LENGTH, 11 ROWS OF BLOWING, M=0.75, THETA=0.0

RUN 012877 *** DISCRETE HOLE RIG *** HAS-3-14336 STANTON NUMBER DATA

HEATED STARTING LENGTH, 11 ROWS OF BLOWING M=0.75, THETA=1.0

LINEAR SUPERPOSITION IS APPLIED TO STANTON NUMBER DATA FROM
RUN NUMBERS 012777 AND 012877 TO OBTAIN STANTON NUMBER DATA AT TH=0 AND TH=1

PLATE	PEXCOL	RE DELZ	ST(TH=0)	REXHOT	RE DELZ	ST(TH=1)	ETA	STCR	F-COL	STHR	F-HOT	LOGB
1	1452782.0	2097.6	0.002303	1434988.0	2071.6	0.002435	0.000	1.000	0.0000	1.000	0.0000	1.000
2	1510766.0	2233.8	0.002413	1490057.0	2202.2	0.002144	0.111	1.230	0.0247	1.091	0.0246	4.961
3	1560550.0	2377.4	0.002660	1549125.0	3731.7	0.002221	0.165	1.367	0.0243	1.138	0.0219	4.713
4	1626335.0	2535.6	0.002918	1606194.0	5104.2	0.001981	0.297	1.458	0.0243	1.022	0.0218	4.531
5	1684119.0	2697.0	0.002732	1663262.0	6458.1	0.001827	0.331	1.424	0.0245	0.950	0.0216	4.407
6	1741903.0	2857.6	0.002760	1720331.0	7794.7	0.001733	0.372	1.448	0.0241	0.907	0.0212	4.294
7	1799687.0	3016.9	0.002754	1777399.0	9100.0	0.001650	0.401	1.454	0.0241	0.869	0.0219	4.338
8	1857471.0	3175.5	0.002736	1834468.0	10441.7	0.001602	0.414	1.454	0.0247	0.849	0.0228	4.445
9	1915255.0	3334.7	0.002775	1891537.0	11836.0	0.001566	0.436	1.484	0.0240	0.835	0.0215	4.262
10	1973040.0	3495.0	0.002801	1948605.0	13150.2	0.001509	0.461	1.507	0.0247	0.810	0.0229	4.409
11	2030824.0	3658.0	0.002812	2005674.0	14538.2	0.001430	0.491	1.521	0.0244	0.772	0.0223	4.280
12	2088608.0	3818.3	0.002738	2062742.0	15890.7	0.001446	0.472	1.490	0.0244	0.785	0.0226	4.366
13	2146392.0	3937.3	0.002675	2106114.0	17239.5	0.001139	0.574	1.461		0.621		
14	2162203.0	4016.3	0.002628	2135505.0	17273.4	0.001164	0.557	1.460		0.636		
15	2192042.0	4092.4	0.002482	2164895.0	17307.3	0.001146	0.538	1.364		0.628		
16	2221945.0	4165.5	0.002428	2194428.0	17341.0	0.001141	0.530	1.338		0.627		
17	2251048.0	4237.2	0.002384	2223961.0	17373.9	0.001098	0.539	1.317		0.605		
18	2281607.0	4307.2	0.002316	2253351.0	17405.8	0.001067	0.539	1.282		0.590		
19	2311366.0	4375.1	0.002243	2282741.0	17436.6	0.001025	0.543	1.245		0.568		
20	2341124.0	4442.1	0.002252	2312132.0	17467.4	0.001069	0.525	1.254		0.593		
21	2370884.0	4507.1	0.002113	2341522.0	17497.0	0.000944	0.553	1.179		0.526		
22	2400642.0	4570.1	0.002117	2370912.0	17525.0	0.000957	0.548	1.184		0.534		
23	2430401.0	4632.0	0.002035	2400303.0	17552.4	0.000911	0.552	1.141		0.510		
24	2460160.0	4693.3	0.002080	2429835.0	17579.5	0.000930	0.553	1.169		0.522		
25	2490008.0	4754.6	0.002049	2459366.0	17606.4	0.000897	0.562	1.155		0.505		
26	2519966.0	4815.4	0.002018	2488759.0	17632.7	0.000888	0.560	1.140		0.500		
27	2549925.0	4874.9	0.001980	2518149.0	17657.8	0.000815	0.588	1.121		0.461		
28	2579884.0	4933.8	0.001969	2547539.0	17682.6	0.000874	0.556	1.118		0.495		
29	2609843.0	4993.6	0.002048	2576930.0	17708.9	0.000915	0.553	1.165		0.519		
30	2639802.0	5053.0	0.001938	2606320.0	17736.6	0.000966	0.501	1.105		0.549		
31	2669761.0	5109.9	0.001804	2635711.0	17763.2	0.000845	0.552	1.076		0.481		
32	2699720.0	5165.9	0.001877	2665243.0	17788.3	0.000862	0.541	1.075		0.492		
33	2729679.0	5221.0	0.001818	2694776.0	17813.1	0.000823	0.547	1.043		0.471		
34	2759638.0	5274.7	0.001792	2724267.0	17837.0	0.000804	0.552	1.031		0.461		
35	2789597.0	5328.3	0.001880	2753757.0	17861.0	0.000822	0.543	1.038		0.473		
36	2819556.0	5380.3	0.001694	2783247.0	17884.1	0.000754	0.555	0.978		0.435		

STANTON NUMBER RATIO BASED ON ST*PR**0.4=0.0295*REX**(-.2)

STANTON NUMBER RATIO FOR TH=1 IS CONVERTED TO COMPARABLE TRANSPARATION VALUE
USING LOG(1 + B1/B) EXPRESSION IN THE BLOWN SECTION

RUN 011777-2 *** DISCPETE HOLE PIG *** HAS-3-14336

STANTON NUMBER DATA

TAOS= 18.20 DEG C UINF= 16.90 M/S TINF= 18.07 DEG C
 PHO= 1.219 KG/M3 VISC= 0.14754E-04 M2/S XYO= -0.4 CM
 CP= 1000. J/KGK FR= 0.714

*** HEATED STARTING LENGTH, 12 ROWS OF BLOWING, M=0.9, THEATA=1.0 ***

PLATE	X	REX	TO	REENTH	STANTON NO	DST	DREEN	M	F	T2	THETA	DTH
1	127.8	0.14679E 07	34.51	0.21498E 04	0.22320E-02	0.449E-04	29.					
2	132.8	0.15261E 07	34.48	0.22763E 04	0.21187E-02	0.444E-04	52.	0.82	0.0264	35.0	1.029	0.019
3	137.9	0.15942E 07	34.44	0.23900E 04	0.23327E-02	0.456E-04	79.	0.81	0.0261	34.8	1.024	0.019
4	143.0	0.16424E 07	34.48	0.26758E 04	0.22129E-02	0.449E-04	99.	0.81	0.0262	35.0	1.032	0.019
5	148.1	0.17206E 07	34.46	0.27371E 04	0.20590E-02	0.442E-04	116.	0.82	0.0267	34.9	1.027	0.019
6	153.2	0.17501E 07	34.55	0.29032E 04	0.19601E-02	0.435E-04	130.	0.80	0.0258	34.4	0.993	0.019
7	158.2	0.18170E 07	34.57	0.10655E 05	0.19137E-02	0.432E-04	142.	0.81	0.0262	34.4	0.993	0.019
8	163.3	0.18751E 07	34.44	0.12310E 05	0.19027E-02	0.435E-04	153.	0.79	0.0257	34.6	1.011	0.019
9	168.4	0.19333E 07	34.48	0.13931E 05	0.18255E-02	0.430E-04	164.	0.80	0.0260	34.4	0.994	0.019
10	173.5	0.19915E 07	34.48	0.15543E 05	0.18245E-02	0.430E-04	173.	0.79	0.0256	34.0	0.973	0.019
11	178.6	0.20497E 07	34.49	0.17093E 05	0.17657E-02	0.427E-04	182.	0.80	0.0259	33.5	0.941	0.019
12	183.6	0.21079E 07	34.49	0.18612E 05	0.17695E-02	0.428E-04	190.	0.79	0.0257	33.5	0.941	0.019
13	187.5	0.21521E 07	33.63	0.20091E 05	0.15420E-02	0.522E-04	194.					
14	190.1	0.21820E 07	33.35	0.20138E 05	0.15686E-02	0.545E-04	194.					
15	192.7	0.22120E 07	33.65	0.20184E 05	0.15207E-02	0.550E-04	194.					
16	195.4	0.22421E 07	33.92	0.20229E 05	0.14840E-02	0.527E-04	194.					
17	198.0	0.22722E 07	34.00	0.20273E 05	0.14334E-02	0.512E-04	194.					
18	200.6	0.23022E 07	34.07	0.20315E 05	0.13815E-02	0.497E-04	194.					
19	203.2	0.23321E 07	34.13	0.20356E 05	0.13232E-02	0.473E-04	194.					
20	205.8	0.23621E 07	34.27	0.20396E 05	0.13210E-02	0.476E-04	194.					
21	208.5	0.23921E 07	34.25	0.20434E 05	0.12380E-02	0.449E-04	194.					
22	211.1	0.24220E 07	34.28	0.20471E 05	0.12362E-02	0.455E-04	194.					
23	213.7	0.24520E 07	34.28	0.20507E 05	0.11717E-02	0.432E-04	194.					
24	216.3	0.24821E 07	34.40	0.20543E 05	0.11965E-02	0.449E-04	194.					
25	218.9	0.25122E 07	34.32	0.20579E 05	0.11842E-02	0.439E-04	194.					
26	221.6	0.25422E 07	34.23	0.20613E 05	0.11379E-02	0.446E-04	194.					
27	224.2	0.25721E 07	33.35	0.20647E 05	0.11255E-02	0.393E-04	194.					
28	226.8	0.26021E 07	34.28	0.20682E 05	0.11731E-02	0.459E-04	194.					
29	229.4	0.26321E 07	34.30	0.20718E 05	0.12097E-02	0.435E-04	194.					
30	232.0	0.26620E 07	34.68	0.20753E 05	0.11412E-02	0.436E-04	194.					
31	234.6	0.26920E 07	34.68	0.20786E 05	0.10962E-02	0.415E-04	194.					
32	237.3	0.27221E 07	34.53	0.20819E 05	0.10986E-02	0.413E-04	194.					
33	239.9	0.27522E 07	34.51	0.20851E 05	0.10497E-02	0.404E-04	194.					
34	242.5	0.27822E 07	34.23	0.20883E 05	0.10294E-02	0.378E-04	194.					
35	245.1	0.28121E 07	34.44	0.20914E 05	0.10505E-02	0.418E-04	194.					
36	247.8	0.28421E 07	34.17	0.20944E 05	0.97433E-03	0.424E-04	194.					

UNCERTAINTY IN REX=20712.

UNCERTAINTY IN F=0.05033 IN RATIO

RUN 011777-1 *** DISCRETE HOLE PIG *** NAS-3-14336

STANTON NUMBER DATA

TADB= 19.13 DEG C UINF= 16.93 M/S TINF= 19.00 DEG C
 PHO= 1.215 KG/M3 VISC= 0.14837E-04 M2/S XYO= -0.4 CM
 CP= 1009. J/KGK PR= 0.714

*** HEATED STARTING LENGTH, 12 ROWS OF BLOWING, M=0.9, THEATA=0.0 ***

PLATE	X	REX	TO	REENTH	STANTON NO	DST	DREEN	M	F	T2	THETA	DTH
1	127.8	0.14522E 07	34.15	0.21414E 04	0.22974E-02	0.489E-04	29.					
2	132.8	0.15201E 07	34.11	0.22768E 04	0.23763E-02	0.494E-04	34.	0.92	0.0299	20.1	0.075	0.020
3	137.9	0.15781E 07	34.13	0.25544E 04	0.27070E-02	0.513E-04	42.	0.88	0.0263	20.3	0.084	0.020
4	143.0	0.16361E 07	34.13	0.26547E 04	0.26855E-02	0.524E-04	49.	0.90	0.0292	20.2	0.082	0.020
5	143.1	0.16940E 07	34.11	0.31602E 04	0.26702E-02	0.525E-04	55.	0.89	0.0287	20.2	0.077	0.020
6	153.2	0.17520E 07	34.13	0.34570E 04	0.29183E-02	0.527E-04	60.	0.87	0.0281	20.2	0.080	0.020
7	159.2	0.18099E 07	34.13	0.37547E 04	0.26359E-02	0.521E-04	64.	0.88	0.0284	20.2	0.078	0.020
8	163.3	0.18679E 07	34.09	0.40480E 04	0.26553E-02	0.524E-04	69.	0.88	0.0285	20.1	0.072	0.020
9	168.4	0.19258E 07	34.13	0.43310E 04	0.28159E-02	0.520E-04	73.	0.89	0.0288	20.1	0.070	0.020
10	173.5	0.19837E 07	34.15	0.46132E 04	0.26640E-02	0.522E-04	77.	0.86	0.0280	20.1	0.073	0.020
11	178.6	0.20417E 07	34.17	0.48964E 04	0.26550E-02	0.521E-04	80.	0.88	0.0284	20.1	0.074	0.020
12	183.6	0.20997E 07	34.21	0.51817E 04	0.28013E-02	0.517E-04	84.	0.88	0.0284	20.1	0.074	0.020
13	187.5	0.21437E 07	32.91	0.54661E 04	0.27640E-02	0.896E-04	86.					
14	190.1	0.21734E 07	32.66	0.55075E 04	0.26829E-02	0.894E-04	86.					
15	192.7	0.22034E 07	33.35	0.5563E 04	0.25860E-02	0.896E-04	86.					
16	195.4	0.22334E 07	33.44	0.56623E 04	0.25067E-02	0.854E-04	86.					
17	198.0	0.22634E 07	33.52	0.57342E 04	0.24351E-02	0.831E-04	86.					
18	200.6	0.22933E 07	33.53	0.58978E 04	0.23578E-02	0.807E-04	86.					
19	203.2	0.23231E 07	33.63	0.58767E 04	0.22510E-02	0.768E-04	86.					
20	205.8	0.23530E 07	33.77	0.59444E 04	0.22621E-02	0.782E-04	86.					
21	208.5	0.23828E 07	33.73	0.60111E 04	0.21805E-02	0.744E-04	86.					
22	211.1	0.24126E 07	33.85	0.60758E 04	0.21529E-02	0.747E-04	86.					
23	213.7	0.24425E 07	33.77	0.61393E 04	0.20960E-02	0.710E-04	86.					
24	216.3	0.24725E 07	33.94	0.62022E 04	0.21167E-02	0.740E-04	86.					
25	218.9	0.25025E 07	33.83	0.62655E 04	0.21202E-02	0.731E-04	86.					
26	221.6	0.25323E 07	33.75	0.63276E 04	0.20358E-02	0.746E-04	86.					
27	224.2	0.25622E 07	32.34	0.63894E 04	0.20970E-02	0.664E-04	86.					
28	226.8	0.25920E 07	33.77	0.64523E 04	0.21162E-02	0.773E-04	86.					
29	229.4	0.26219E 07	33.79	0.65159E 04	0.21391E-02	0.723E-04	86.					
30	232.0	0.26517E 07	34.32	0.65783E 04	0.20353E-02	0.719E-04	86.					
31	234.6	0.26816E 07	34.32	0.66380E 04	0.19613E-02	0.684E-04	86.					
32	237.3	0.27115E 07	34.15	0.66965E 04	0.19526E-02	0.676E-04	86.					
33	239.9	0.27415E 07	34.13	0.67540E 04	0.18971E-02	0.670E-04	86.					
34	242.5	0.27714E 07	33.71	0.68100E 04	0.18529E-02	0.627E-04	86.					
35	245.1	0.28012E 07	34.06	0.68661E 04	0.18981E-02	0.685E-04	86.					
36	247.8	0.28311E 07	33.73	0.69209E 04	0.17755E-02	0.700E-04	86.					

UNCERTAINTY IN REX=20632.

UNCERTAINTY IN F=0.05033 IN RATIO

RUN 011777-1 *** DISCRETE HOLE RIG *** NAS-3-14336 STANTON NUMBER DATA

*** HEATED STARTING LENGTH, 12 ROWS OF BLOWING, M=0.9, THEATA=0.0 ***

RUN 011777-2 *** DISCRETE HOLE RIG *** NAS-3-14336 STANTON NUMBER DATA

*** HEATED STARTING LENGTH, 12 ROWS OF BLOWING, M=0.9, THEATA=1.0 ***

LINEAR SUPERPOSITION IS APPLIED TO STANTON NUMBER DATA FROM
RUN NUMBERS 011777-1 AND 011777-2 TO OBTAIN STANTON NUMBER DATA AT TH=0 AND TH=1

PLATE	REXCOL	RE DEL2	ST (TH=0)	REXHOT	RE DEL2	ST (TH=1)	ETA	STCR	F-COL	STHR	F-HOT	LOGB
1	1462192.0	2141.4	0.002297	1467083.0	2149.8	0.002233	0.0000	1.000	0.0000	1.000	0.0000	1.000
2	1520147.0	2277.4	0.002397	1526063.0	2276.6	0.002127	0.113	1.223	0.0209	1.087	0.0264	5.202
3	1579101.0	2426.2	0.002738	1584243.0	3945.4	0.002343	0.144	1.409	0.0283	1.206	0.0261	5.380
4	1636056.0	2590.9	0.002945	1642424.0	5596.3	0.002233	0.242	1.526	0.0292	1.158	0.0262	5.336
5	1694010.0	2761.6	0.002947	1700604.0	7244.7	0.002085	0.293	1.537	0.0207	1.038	0.0267	5.308
6	1751955.0	2933.9	0.003320	1756784.0	8915.2	0.001970	0.343	1.575	0.0261	1.036	0.0253	5.124
7	1809920.0	3105.4	0.002916	1816964.0	10528.3	0.001906	0.346	1.541	0.0284	1.009	0.0262	5.153
8	1867874.0	3274.8	0.002932	1875144.0	12164.3	0.001904	0.351	1.560	0.0285	1.014	0.0257	5.121
9	1925829.0	3443.6	0.002892	1933324.0	13769.7	0.001828	0.368	1.548	0.0288	0.979	0.0260	5.119
10	1983783.0	3612.7	0.002945	1991504.0	15390.1	0.001805	0.387	1.586	0.0280	0.973	0.0256	5.066
11	2041738.0	3783.4	0.002945	2049684.0	16979.2	0.001712	0.419	1.595	0.0284	0.928	0.0259	5.044
12	2099692.0	3952.5	0.002839	2107864.0	18583.1	0.001699	0.412	1.573	0.0284	0.926	0.0257	5.033
13	2143738.0	4079.0	0.002968	2152081.0	20147.2	0.001459	0.491	1.568		0.799		
14	2173584.0	4163.4	0.002778	2182044.0	20191.5	0.001493	0.463	1.523		0.819		
15	2203431.0	4244.9	0.002677	2212007.0	20235.6	0.001448	0.459	1.472		0.797		
16	2233422.0	4323.7	0.002594	2242115.0	20278.5	0.001415	0.455	1.430		0.781		
17	2263414.0	4400.1	0.002521	2272223.0	20320.2	0.001365	0.458	1.393		0.755		
18	2293406.0	4474.2	0.002441	2302186.0	20360.4	0.001315	0.461	1.353		0.730		
19	2323107.0	4545.5	0.002330	2332148.0	20399.1	0.001260	0.459	1.295		0.701		
20	2352953.0	4615.6	0.002364	2362111.0	20436.8	0.001256	0.469	1.317		0.700		
21	2382800.0	4684.7	0.002261	2392074.0	20473.3	0.001174	0.481	1.263		0.656		
22	2412647.0	4751.8	0.002231	2422037.0	20508.5	0.001174	0.474	1.249		0.658		
23	2442493.0	4817.7	0.002175	2452000.0	20542.7	0.001109	0.490	1.221		0.623		
24	2472484.0	4883.0	0.002195	2482108.0	20576.4	0.001134	0.483	1.235		0.639		
25	2502476.0	4948.6	0.002200	2512216.0	20610.2	0.001121	0.491	1.241		0.633		
26	2532323.0	5013.1	0.002112	2542179.0	20643.1	0.001077	0.490	1.194		0.609		
27	2562169.0	5077.2	0.002180	2572141.0	20675.2	0.001060	0.514	1.235		0.601		
28	2592016.0	5142.6	0.002197	2602104.0	20707.7	0.001109	0.495	1.248		0.630		
29	2621863.0	5208.6	0.002218	2632067.0	20741.5	0.001146	0.484	1.263		0.653		
30	2651709.0	5273.2	0.002112	2662030.0	20774.9	0.001081	0.488	1.205		0.617		
31	2681556.0	5335.2	0.002035	2691993.0	20806.7	0.001038	0.490	1.164		0.594		
32	2711547.0	5395.9	0.002025	2722100.0	20837.9	0.001041	0.486	1.161		0.597		
33	2741539.0	5455.6	0.001969	2752209.0	20868.3	0.000992	0.496	1.131		0.570		
34	2771385.0	5513.7	0.001924	2782171.0	20897.7	0.000964	0.499	1.108		0.555		
35	2801232.0	5571.9	0.001970	2812134.0	20927.0	0.000993	0.496	1.137		0.573		
36	2831078.0	5628.9	0.001844	2842097.0	20955.7	0.000920	0.501	1.066		0.532		

STANTON NUMBER RATIO BASED ON ST*PR**0.4=0.0295*REX**(-.2)

STANTON NUMBER RATIO FOR TH=1 IS CONVERTED TO COMPARABLE TRANSPIRATION VALUE
USING $\text{LOG}(1 + B/D)$ EXPRESSION IN THE BLOWN SECTION

RUN 012177 *** DISCRETE HOLE RIG *** HAS-3-14336

STANTON NUMBER DATA

TADB= 22.09 DEG C UINF= 17.29 M/S TINF= 21.96 DEG C
 PHO= 1.191 KG/M3 VISC= 0.15232E-04 M2/S XYO= -0.4 CM
 CP= 1011. J/KGK FR= 0.715

HEATED STARTING LENGTH,11 ROWS OF BLOWING M=1.33,THETA=1.0

PLATE	X	REX	TO	PEENTH	STANTON NO	DST	DREEN	M	F	T2	THETA	OTH
1	127.0	0.14548E 07	36.06	0.21305E 04	0.23243E-02	0.522E-04	29.					
2	132.0	0.15124E 07	36.06	0.22504E 04	0.21277E-02	0.512E-04	77.	1.36	0.0440	36.4	1.025	0.022
3	137.9	0.15701E 07	36.06	0.49944E 04	0.25300E-02	0.536E-04	125.	1.32	0.0429	35.9	0.993	0.022
4	143.0	0.16277E 07	36.04	0.76051E 04	0.28604E-02	0.556E-04	157.	1.27	0.0413	36.1	1.004	0.022
5	148.1	0.16854E 07	36.08	0.10157E 05	0.20308E-02	0.553E-04	182.	1.25	0.0405	36.1	1.004	0.022
6	153.2	0.17431E 07	36.06	0.12663E 05	0.26764E-02	0.544E-04	204.	1.27	0.0410	36.0	0.995	0.022
7	158.2	0.18007E 07	36.06	0.15163E 05	0.25072E-02	0.533E-04	223.	1.27	0.0412	35.9	0.987	0.022
8	163.3	0.18584E 07	36.08	0.17646E 05	0.23847E-02	0.525E-04	241.	1.25	0.0405	36.1	1.005	0.022
9	168.4	0.19160E 07	36.08	0.20127E 05	0.23083E-02	0.521E-04	259.	1.30	0.0421	35.9	0.989	0.022
10	173.5	0.19737E 07	36.08	0.22650E 05	0.22306E-02	0.517E-04	274.	1.26	0.0406	35.7	0.976	0.022
11	178.6	0.20314E 07	36.08	0.25070E 05	0.21462E-02	0.512E-04	288.	1.23	0.0399	35.4	0.951	0.022
12	183.6	0.20890E 07	36.06	0.27303E 05	0.21053E-02	0.510E-04	301.	1.25	0.0404	35.4	0.952	0.022
13	187.5	0.21320E 07	35.12	0.29687E 05	0.17741E-02	0.607E-04	307.					
14	192.1	0.21625E 07	34.86	0.29740E 05	0.17734E-02	0.629E-04	307.					
15	192.7	0.21902E 07	35.35	0.29792E 05	0.17218E-02	0.633E-04	307.					
16	195.4	0.22221E 07	35.45	0.29842E 05	0.16544E-02	0.600E-04	307.					
17	198.0	0.22519E 07	35.52	0.29891E 05	0.16305E-02	0.592E-04	307.					
18	200.6	0.22816E 07	35.60	0.29935E 05	0.15780E-02	0.577E-04	307.					
19	203.2	0.23113E 07	35.66	0.29984E 05	0.15034E-02	0.547E-04	307.					
20	205.8	0.23410E 07	35.77	0.30027E 05	0.14972E-02	0.548E-04	307.					
21	208.5	0.23707E 07	35.73	0.30072E 05	0.13984E-02	0.514E-04	307.					
22	211.1	0.24004E 07	35.79	0.30113E 05	0.13874E-02	0.521E-04	307.					
23	213.7	0.24301E 07	35.77	0.30154E 05	0.13343E-02	0.500E-04	307.					
24	216.3	0.24598E 07	35.87	0.30194E 05	0.13612E-02	0.518E-04	307.					
25	218.9	0.24895E 07	35.77	0.30234E 05	0.13357E-02	0.504E-04	307.					
26	221.6	0.25192E 07	35.70	0.30273E 05	0.12933E-02	0.514E-04	307.					
27	224.2	0.25490E 07	34.89	0.30311E 05	0.12591E-02	0.452E-04	307.					
28	226.8	0.25787E 07	35.77	0.30350E 05	0.13678E-02	0.535E-04	307.					
29	229.4	0.26085E 07	35.79	0.30391E 05	0.13775E-02	0.504E-04	307.					
30	232.0	0.26382E 07	36.15	0.30431E 05	0.13320E-02	0.513E-04	307.					
31	234.6	0.26679E 07	36.15	0.30470E 05	0.12710E-02	0.465E-04	307.					
32	237.3	0.26976E 07	36.04	0.30507E 05	0.12670E-02	0.433E-04	307.					
33	239.9	0.27273E 07	36.00	0.30544E 05	0.12258E-02	0.473E-04	307.					
34	242.5	0.27570E 07	35.79	0.30580E 05	0.11792E-02	0.445E-04	307.					
35	245.1	0.27867E 07	35.94	0.30615E 05	0.12081E-02	0.483E-04	307.					
36	247.8	0.28164E 07	35.73	0.30650E 05	0.11042E-02	0.483E-04	307.					

UNCERTAINTY IN REX=20527.

UNCERTAINTY IN F=0.05031 IN RATIO

PLN 012077 *** DISCRETE HOLE RIG *** MAS-3-14336

STANTON NUMBER DATA

TADB= 21.80 DEG C UINF= 17.33 M/S TINF= 21.74 DEG C
 RHO= 1.193 PG/M3 VISC= 0.15205E-04 M2/S KYD= -0.4 CM
 CP= 1009. J/KGK PR= 0.714

HEATED STARTING LENGTH, 11 PWS OF BLOWING, M=1.33, THETA=0.0

PLATE	X	PEX	TO	PEENTH	STANTON NO	DST	DPREN	M	F	T2	THETA	DTH
1	127.8	0.14507E 07	36.44	0.21392E 04	0.23056E-02	0.500E-04	29.					
2	132.8	0.15165E 07	36.44	0.22757E 04	0.24037E-02	0.506E-04	40.	1.42	0.0459	22.7	0.064	0.021
3	137.9	0.15765E 07	36.48	0.25930E 04	0.27186E-02	0.523E-04	56.	1.39	0.0450	22.8	0.070	0.021
4	143.0	0.16344E 07	36.44	0.29531E 04	0.34540E-02	0.574E-04	69.	1.39	0.0450	22.8	0.071	0.021
5	148.1	0.16923E 07	36.46	0.33442E 04	0.36819E-02	0.590E-04	79.	1.35	0.0437	22.8	0.071	0.021
6	153.2	0.17502E 07	36.46	0.37351E 04	0.35702E-02	0.502E-04	80.	1.41	0.0458	22.8	0.075	0.021
7	158.2	0.18081E 07	36.44	0.41400E 04	0.35502E-02	0.501E-04	96.	1.38	0.0448	22.9	0.077	0.021
8	163.3	0.18660E 07	36.44	0.45421E 04	0.34654E-02	0.575E-04	104.	1.40	0.0454	22.8	0.074	0.021
9	168.4	0.19237E 07	36.42	0.49396E 04	0.35396E-02	0.581E-04	111.	1.40	0.0453	22.9	0.076	0.021
10	173.5	0.19816E 07	36.42	0.53433E 04	0.35505E-02	0.502E-04	118.	1.37	0.0445	22.8	0.075	0.021
11	178.6	0.20397E 07	36.46	0.57432E 04	0.35840E-02	0.583E-04	124.	1.35	0.0436	22.9	0.079	0.021
12	183.6	0.20976E 07	36.42	0.61500E 04	0.35525E-02	0.502E-04	130.	1.36	0.0441	22.9	0.080	0.021
13	187.5	0.21416E 07	34.35	0.65267E 04	0.33736E-02	0.105E-03	132.					
14	190.1	0.21714E 07	33.88	0.66000E 04	0.34130E-02	0.114E-03	132.					
15	192.7	0.22012E 07	34.59	0.67073E 04	0.32442E-02	0.112E-03	132.					
16	195.4	0.22312E 07	34.70	0.68030E 04	0.31613E-02	0.108E-03	132.					
17	198.0	0.22611E 07	34.82	0.68961E 04	0.30800E-02	0.105E-03	132.					
18	200.6	0.22909E 07	34.93	0.69867E 04	0.29891E-02	0.102E-03	132.					
19	203.2	0.23207E 07	34.97	0.70747E 04	0.29075E-02	0.990E-04	132.					
20	205.8	0.23506E 07	35.09	0.71615E 04	0.29066E-02	0.996E-04	132.					
21	208.5	0.23804E 07	35.01	0.72457E 04	0.27339E-02	0.934E-04	132.					
22	211.1	0.24102E 07	35.07	0.73279E 04	0.27735E-02	0.956E-04	133.					
23	213.7	0.24400E 07	35.01	0.74091E 04	0.26719E-02	0.915E-04	133.					
24	216.3	0.24700E 07	35.14	0.74976E 04	0.27186E-02	0.946E-04	133.					
25	218.9	0.24999E 07	34.97	0.75705E 04	0.27041E-02	0.930E-04	133.					
26	221.6	0.25298E 07	34.83	0.76506E 04	0.26577E-02	0.965E-04	133.					
27	224.2	0.25596E 07	33.37	0.77309E 04	0.27254E-02	0.870E-04	133.					
28	226.8	0.25894E 07	34.64	0.78134E 04	0.28040E-02	0.101E-03	133.					
29	229.4	0.26192E 07	34.89	0.78969E 04	0.27838E-02	0.942E-04	133.					
30	232.0	0.26490E 07	35.49	0.79766E 04	0.26831E-02	0.940E-04	133.					
31	234.6	0.26787E 07	35.52	0.80570E 04	0.25680E-02	0.891E-04	133.					
32	237.3	0.27085E 07	35.31	0.81333E 04	0.25467E-02	0.875E-04	133.					
33	239.9	0.27383E 07	35.30	0.82001E 04	0.24603E-02	0.861E-04	133.					
34	242.5	0.27681E 07	34.89	0.82810E 04	0.24233E-02	0.819E-04	133.					
35	245.1	0.27984E 07	35.24	0.83535E 04	0.24373E-02	0.870E-04	133.					
36	247.8	0.28282E 07	34.91	0.84242E 04	0.23014E-02	0.891E-04	133.					

UNCERTAINTY IN REX=20611.

UNCERTAINTY IN F=0.05031 IN RATIO

104

RUN 012077 *** DISCRETE HOLE RIG *** HAS-3-14336 STANTON NUMBER DATA

HEATED STARTING LENGTH, 11 ROWS OF BLOWING, $M=1.33$, $\theta=0.0$

RUN 012177 *** DISCRETE HOLE RIG *** HAS-3-14336 STANTON NUMBER DATA

HEATED STARTING LENGTH, 11 ROWS OF BLOWING $M=1.33$, $\theta=1.0$

LINEAR SUPERPOSITION IS APPLIED TO STANTON NUMBER DATA FROM
RUN NUMBERS 012077 AND 012177 TO OBTAIN STANTON NUMBER DATA AT $\theta=0$ AND $\theta=1$

PLATE	REXCOL	RE DEL2	ST(TH=0)	REXHOT	RE DEL2	ST(TH=1)	ETA	STCR	F-COL	STHR	F-HOT	LOGS
1	1450708.0	2139.2	0.002309	1454765.0	2130.5	0.002324	UUUUU	1.000	0.0000	1.000	0.0000	1.000
2	1511604.0	2276.2	0.002422	1512426.0	2259.1	0.002135	0.119	1.237	0.0459	1.089	0.0440	7.306
3	1576500.0	2425.4	0.002731	1570086.0	4931.0	0.002540	0.070	1.405	0.0450	1.306	0.0429	7.642
4	1634395.0	2605.7	0.003499	1627746.0	7558.0	0.002860	0.183	1.813	0.0450	1.481	0.0413	7.807
5	1692291.0	2815.5	0.003747	1685406.0	10100.8	0.002034	0.244	1.955	0.0437	1.478	0.0405	7.750
6	1750187.0	3029.6	0.003649	1743066.0	12597.7	0.002676	0.267	1.917	0.0450	1.405	0.0410	7.704
7	1802093.0	3240.5	0.003639	1800726.0	15109.5	0.002497	0.314	1.924	0.0448	1.319	0.0412	7.600
8	1865978.0	3463.7	0.003554	1850387.0	17623.4	0.002300	0.330	1.891	0.0454	1.265	0.0405	7.447
9	1923574.0	3657.0	0.003640	1916047.0	20093.0	0.002305	0.367	1.949	0.0453	1.233	0.0421	7.609
10	1981770.0	3868.5	0.003669	1973707.0	22648.5	0.002205	0.399	1.976	0.0445	1.187	0.0406	7.370
11	2039665.0	4082.1	0.003709	2031367.0	25114.5	0.002007	0.437	2.009	0.0436	1.130	0.0399	7.199
12	2097561.0	4296.1	0.003684	2039027.0	27535.7	0.002025	0.450	2.007	0.0441	1.102	0.0404	7.227
13	2141562.0	4455.3	0.003519	2132849.0	29948.0	0.001605	0.521	1.925		0.921		
14	2171373.0	4561.0	0.003563	2162544.0	29970.0	0.001682	0.520	1.955		0.922		
15	2201195.0	4664.7	0.003303	2192239.0	30047.3	0.001637	0.516	1.861		0.900		
16	2231155.0	4764.4	0.003299	2222078.0	30095.0	0.001571	0.524	1.819		0.866		
17	2261116.0	4861.6	0.003212	2251917.0	30141.4	0.001550	0.517	1.776		0.856		
18	2293933.0	4956.1	0.003117	2281612.0	30186.7	0.001500	0.519	1.728		0.831		
19	2320749.0	5047.9	0.003035	2311307.0	30230.2	0.001425	0.530	1.687		0.792		
20	2350565.0	5133.5	0.003035	2341002.0	30272.4	0.001419	0.532	1.691		0.790		
21	2380382.0	5206.4	0.002856	2370697.0	30313.2	0.001324	0.536	1.595		0.739		
22	2410198.0	5312.3	0.002900	2400392.0	30352.4	0.001310	0.543	1.624		0.733		
23	2440014.0	5397.3	0.002794	2430087.0	30390.6	0.001260	0.549	1.569		0.707		
24	2469875.0	5481.4	0.002842	2459926.0	30428.4	0.001266	0.546	1.600		0.723		
25	2499936.0	5566.1	0.002929	2489765.0	30466.2	0.001240	0.555	1.596		0.710		
26	2529752.0	5649.8	0.002782	2519460.0	30503.0	0.001217	0.562	1.573		0.688		
27	2559569.0	5734.0	0.002859	2549155.0	30538.6	0.001177	0.588	1.621		0.666		
28	2589385.0	5820.5	0.002935	2578850.0	30575.2	0.001208	0.561	1.668		0.731		
29	2619202.0	5907.9	0.002917	2608546.0	30613.7	0.001299	0.555	1.661		0.739		
30	2649018.0	5993.3	0.002836	2638241.0	30651.7	0.001257	0.552	1.602		0.717		
31	2678834.0	6075.3	0.002686	2667935.0	30688.1	0.001199	0.554	1.537		0.685		
32	2708795.0	6155.1	0.002663	2697774.0	30723.7	0.001196	0.551	1.527		0.685		
33	2738756.0	6233.3	0.002573	2727614.0	30758.7	0.001157	0.550	1.478		0.664		
34	2768672.0	6309.5	0.002537	2757308.0	30792.4	0.001110	0.562	1.461		0.639		
35	2798589.0	6385.5	0.002549	2787003.0	30825.8	0.001140	0.553	1.471		0.657		
36	2828205.0	6459.5	0.002411	2816698.0	30858.2	0.001038	0.570	1.394		0.690		

STANTON NUMBER RATIO BASED ON $ST \cdot PR^{0.4} = 0.0295 \cdot REX^{0.2}$

STANTON NUMBER RATIO FOR $\theta=1$ IS CONVERTED TO COMPARABLE TRANSPIRATION VALUE
USING $ALOG(1 + B/D)$ EXPRESSION IN THE BLOWN SECTION

REK	=	0.15570E-07	REM	=	3327.	REN	=	1409.
IND	=	12.89 CM	DELZ	=	0.305 CM	DEHZ	=	0.129 CM
UINF	=	16.31 M/S	DEL99	=	2.746 CM	DEL799	=	1.715 CM
VISC	=	0.14956E-04 MZ/S	DELI	=	0.417 CM	UINF	=	16.31 M/S
PIPT	=	1	H	=	1.368	VISC	=	0.14978E-04 MZ/S
XLOC	=	155.70 CM	CF/2	=	0.17451E-02	TINF	=	18.04 DEG C
					TPLATE	=	33.58 DEG C	

YICH1	Y/DEL	UIM/S1	U/USHF	Y*	U*	YICH1	T(DEC C)	TBAR	TBAR
0.005	0.009	8.73	0.536	11.6	12.82	0.0546	27.06	0.442	0.558
0.005	0.010	8.79	0.539	12.7	12.90	0.0572	26.94	0.451	0.549
0.030	0.011	8.90	0.546	13.9	13.06	0.0622	26.87	0.455	0.545
0.036	0.013	9.16	0.562	16.2	13.44	0.0699	26.18	0.502	0.498
0.043	0.016	9.45	0.579	19.7	13.67	0.0775	25.30	0.562	0.438
0.053	0.019	9.75	0.598	24.3	14.31	0.0876	24.57	0.611	0.389
0.056	0.024	9.93	0.609	30.1	14.58	0.1029	23.87	0.659	0.341
0.031	0.030	10.14	0.622	37.0	14.88	0.1232	23.27	0.699	0.301
0.099	0.036	10.31	0.632	45.1	15.14	0.1406	22.65	0.728	0.272
0.119	0.043	10.53	0.646	54.4	15.46	0.1791	22.54	0.749	0.251
0.145	0.053	10.66	0.654	65.9	15.65	0.2146	22.20	0.772	0.228
0.175	0.064	10.85	0.666	79.8	15.94	0.2553	21.92	0.791	0.209
0.211	0.077	11.09	0.680	96.0	16.28	0.3051	21.60	0.813	0.187
0.262	0.095	11.34	0.695	119.2	16.65	0.3670	21.28	0.834	0.166
0.323	0.117	11.58	0.710	146.9	17.00	0.4432	20.96	0.856	0.144
0.399	0.145	11.87	0.728	181.6	17.43	0.5448	20.59	0.881	0.119
0.500	0.182	12.20	0.748	227.9	17.91	0.6464	20.27	0.902	0.098
0.627	0.228	12.58	0.772	285.7	18.47	0.7734	19.99	0.922	0.078
0.780	0.284	12.94	0.794	355.2	19.00	0.9204	19.74	0.938	0.062
0.932	0.339	13.35	0.819	426.6	19.60	1.0274	19.54	0.952	0.048
1.055	0.395	13.69	0.840	494.0	20.10	1.1544	19.40	0.962	0.038
1.262	0.460	14.07	0.863	575.0	20.66	1.2814	19.28	0.970	0.030
1.440	0.525	14.40	0.883	655.9	21.14	1.4084	19.18	0.976	0.024
1.618	0.599	14.73	0.904	735.9	21.63	1.5354	19.10	0.982	0.018
1.796	0.654	15.06	0.923	817.9	22.10	1.6624	19.05	0.986	0.014
1.974	0.719	15.34	0.941	898.9	22.52	1.7894	19.01	0.988	0.012
2.151	0.784	15.61	0.957	979.9	22.91	1.9164	18.98	0.990	0.010
2.329	0.848	15.81	0.970	1060.8	23.21	2.0434	18.95	0.992	0.008
2.507	0.913	16.00	0.981	1141.8	23.49	2.1704	18.92	0.994	0.006
2.685	0.978	16.11	0.988	1222.8	23.66	2.2974	18.91	0.995	0.005
2.863	1.043	16.23	0.995	1303.8	23.82	2.4244	18.89	0.996	0.004
3.040	1.107	16.29	0.999	1384.8	23.91	2.5514	18.87	0.998	0.002
3.218	1.172	16.31	1.000	1465.7	23.94	2.6784	18.86	0.998	0.002
						2.805	18.85	0.999	0.001
						2.932	18.84	1.000	0.000

COMPILE TIME= 0.51 SEC, EXECUTION TIME= 0.15 SEC, 22.40.50 FRIDAY 13 APR 79 MATFIV - JAN 1976 VIL5

106

RUN 123076 *** DISCRETE HOLE RIG *** HAS-3-14336 STANTON NUMBER DATA

TADB= 18.35 DEG C UINF= 16.39 M/S TINF= 18.23 DEG C
PHO= 1.204 KG/M3 VISC= 0.14924E-04 M2/S XYD= 12.9 CM
CP= 1010. J/KGK PR= 0.715

HEATED STARTING LENGTH, M=0.4, SIX BLOWING ROWS, THEAT=1.0

PLATE	X	REX	TO	REENTH	STANTON NO	DST	DREEN	M	F	T2	THETA	DTM
1	127.8	0.12614E 07	34.51	0.10000E 01	0.34419E-02	0.545E-04	0.					
2	132.8	0.13172E 07	34.53	0.10000E 01	0.27337E-02	0.498E-04	0.	0.00	0.0000	34.5	1.000	0.019
3	137.9	0.13730E 07	34.49	0.10000E 01	0.26465E-02	0.494E-04	0.	0.00	0.0000	34.5	1.000	0.019
4	143.0	0.14288E 07	34.51	0.10000E 01	0.25253E-02	0.486E-04	0.	0.00	0.0000	34.5	1.000	0.019
5	143.1	0.14846E 07	34.55	0.10000E 01	0.24637E-02	0.482E-04	0.	0.00	0.0000	34.6	1.000	0.019
6	153.2	0.15404E 07	34.57	0.10000E 01	0.24036E-02	0.478E-04	0.	0.00	0.0000	34.6	1.000	0.019
7	153.2	0.15962E 07	34.63	0.14817E 04	0.22153E-02	0.466E-04	28.	0.39	0.0125	32.8	0.886	0.019
8	163.3	0.16519E 07	34.53	0.22129E 04	0.18194E-02	0.449E-04	29.	0.37	0.0119	33.9	0.962	0.019
9	168.4	0.17077E 07	34.53	0.29485E 04	0.15690E-02	0.439E-04	31.	0.38	0.0122	33.6	0.941	0.019
10	173.5	0.17635E 07	34.49	0.36767E 04	0.14908E-02	0.437E-04	32.	0.39	0.0127	33.4	0.934	0.019
11	178.6	0.18193E 07	34.53	0.44198E 04	0.14263E-02	0.433E-04	34.	0.38	0.0124	33.3	0.927	0.019
12	183.6	0.18751E 07	34.49	0.51409E 04	0.13767E-02	0.433E-04	35.	0.38	0.0124	33.3	0.929	0.019
13	187.5	0.19175E 07	34.42	0.58450E 04	0.15010E-02	0.534E-04	36.					
14	190.1	0.19462E 07	34.21	0.58890E 04	0.15528E-02	0.545E-04	36.					
15	192.7	0.19750E 07	34.61	0.59337E 04	0.15566E-02	0.563E-04	36.					
16	195.4	0.20038E 07	34.55	0.59788E 04	0.15802E-02	0.557E-04	36.					
17	198.0	0.20327E 07	34.55	0.60243E 04	0.15804E-02	0.559E-04	36.					
18	200.6	0.20614E 07	34.57	0.60694E 04	0.15550E-02	0.554E-04	36.					
19	203.2	0.20902E 07	34.51	0.61135E 04	0.15169E-02	0.533E-04	36.					
20	205.8	0.21189E 07	34.61	0.61579E 04	0.15605E-02	0.554E-04	36.					
21	208.5	0.21476E 07	34.55	0.62019E 04	0.14961E-02	0.531E-04	36.					
22	211.1	0.21764E 07	34.51	0.62455E 04	0.15318E-02	0.546E-04	36.					
23	213.7	0.22051E 07	34.49	0.62891E 04	0.14980E-02	0.532E-04	36.					
24	216.3	0.22340E 07	34.63	0.63328E 04	0.15444E-02	0.556E-04	36.					
25	218.9	0.22629E 07	34.59	0.63771E 04	0.15332E-02	0.551E-04	36.					
26	221.6	0.22916E 07	34.40	0.64210E 04	0.15200E-02	0.570E-04	36.					
27	224.2	0.23203E 07	33.27	0.64644E 04	0.14953E-02	0.493E-04	36.					
28	226.8	0.23490E 07	34.42	0.65079E 04	0.15330E-02	0.580E-04	36.					
29	229.4	0.23778E 07	34.36	0.65521E 04	0.15302E-02	0.537E-04	36.					
30	232.0	0.24065E 07	34.72	0.65966E 04	0.15549E-02	0.565E-04	36.					
31	234.6	0.24352E 07	34.70	0.66408E 04	0.15194E-02	0.547E-04	36.					
32	237.3	0.24641E 07	34.49	0.66847E 04	0.15326E-02	0.545E-04	36.					
33	239.9	0.24930E 07	34.46	0.67286E 04	0.15168E-02	0.549E-04	36.					
34	242.5	0.25217E 07	34.09	0.67722E 04	0.15151E-02	0.525E-04	36.					
35	245.1	0.25504E 07	34.36	0.68157E 04	0.15110E-02	0.562E-04	36.					
36	247.8	0.25792E 07	34.04	0.68585E 04	0.14656E-02	0.597E-04	36.					

UNCERTAINTY IN REX=27895.

UNCERTAINTY IN F=0.00000 IN RATIO

RUN 122976 *** DISCRETE HOLE RIG *** NAS-3-14336

STANTON NUMBER DATA

TADB= 10.72 DEG C UINF= 16.52 M/S TINF= 18.60 DEG C
PHO= 1.199 KG/M3 VISC= 0.14995E-04 M2/S XYD= 12.9 CM
CP= 1010. J/KGK PR= 0.715

HEATED STARTING LENGTH, M=0.4, SIX BLOWING ROWS, THEAT=0.0

PLATE	X	PEX	TO	PEENTH	STANTON NO	DST	DREEN	M	F	T2	THETA	DTN
1	127.8	0.12656E 07	33.48	0.10000E 01	0.34794E-02	0.589E-04	0.					
2	132.8	0.13216E 07	33.50	0.10000E 01	0.27635E-02	0.540E-04	0.	0.00	0.0000	33.5	1.000	0.021
3	137.9	0.13776E 07	33.50	0.10000E 01	0.26505E-02	0.532E-04	0.	0.00	0.0000	33.5	1.000	0.021
4	143.0	0.14336E 07	33.54	0.10000E 01	0.25457E-02	0.525E-04	0.	0.00	0.0000	33.5	1.000	0.021
5	148.1	0.14895E 07	33.50	0.10000E 01	0.25046E-02	0.524E-04	0.	0.00	0.0000	33.5	1.000	0.021
6	153.2	0.15455E 07	33.50	0.10000E 01	0.24714E-02	0.522E-04	0.	0.00	0.0000	33.5	1.000	0.021
7	158.2	0.16015E 07	33.50	0.14942E 04	0.24870E-02	0.523E-04	28.	0.41	0.0132	20.6	0.131	0.020
8	163.3	0.16575E 07	33.48	0.17317E 04	0.25387E-02	0.526E-04	30.	0.41	0.0133	20.4	0.120	0.020
9	168.4	0.17134E 07	33.52	0.19612E 04	0.24499E-02	0.520E-04	32.	0.41	0.0132	20.4	0.121	0.020
10	173.5	0.17694E 07	33.52	0.21669E 04	0.24290E-02	0.519E-04	34.	0.41	0.0132	20.4	0.121	0.020
11	178.6	0.18254E 07	33.50	0.24123E 04	0.24200E-02	0.519E-04	35.	0.41	0.0131	20.4	0.120	0.020
12	183.6	0.18814E 07	33.54	0.26331E 04	0.23257E-02	0.512E-04	37.	0.41	0.0132	20.4	0.120	0.020
13	187.5	0.19239E 07	33.02	0.28200E 04	0.22873E-02	0.768E-04	38.					
14	190.1	0.19527E 07	32.91	0.28851E 04	0.22207E-02	0.756E-04	38.					
15	192.7	0.19816E 07	33.50	0.29483E 04	0.21606E-02	0.762E-04	38.					
16	195.4	0.20105E 07	33.50	0.30103E 04	0.21381E-02	0.738E-04	38.					
17	198.0	0.20395E 07	33.50	0.30719E 04	0.21265E-02	0.735E-04	38.					
18	200.6	0.20683E 07	33.50	0.31327E 04	0.20893E-02	0.724E-04	38.					
19	203.2	0.20972E 07	33.52	0.31916E 04	0.19923E-02	0.608E-04	38.					
20	205.8	0.21260E 07	33.63	0.32499E 04	0.20493E-02	0.710E-04	38.					
21	208.5	0.21548E 07	33.62	0.33077E 04	0.19516E-02	0.675E-04	38.					
22	211.1	0.21836E 07	33.69	0.33641E 04	0.19581E-02	0.686E-04	38.					
23	213.7	0.22125E 07	33.67	0.34195E 04	0.19083E-02	0.664E-04	38.					
24	216.3	0.22414E 07	33.81	0.34753E 04	0.19317E-02	0.682E-04	38.					
25	218.9	0.22704E 07	33.75	0.35309E 04	0.19220E-02	0.672E-04	38.					
26	221.6	0.22992E 07	33.67	0.35850E 04	0.18839E-02	0.698E-04	38.					
27	224.2	0.23281E 07	32.35	0.36403E 04	0.18912E-02	0.606E-04	38.					
28	226.8	0.23569E 07	33.73	0.36948E 04	0.18819E-02	0.703E-04	38.					
29	229.4	0.23857E 07	33.63	0.37491E 04	0.18851E-02	0.644E-04	38.					
30	232.0	0.24145E 07	34.09	0.38034E 04	0.18779E-02	0.671E-04	38.					
31	234.6	0.24434E 07	34.09	0.38570E 04	0.18308E-02	0.646E-04	38.					
32	237.3	0.24723E 07	33.94	0.39096E 04	0.18142E-02	0.638E-04	38.					
33	239.9	0.25013E 07	33.86	0.39620E 04	0.18210E-02	0.647E-04	38.					
34	242.5	0.25301E 07	33.48	0.40145E 04	0.18185E-02	0.621E-04	38.					
35	245.1	0.25590E 07	33.77	0.40667E 04	0.17943E-02	0.655E-04	38.					
36	247.8	0.25878E 07	33.44	0.41174E 04	0.17206E-02	0.695E-04	39.					

UNCERTAINTY IN REX=27988.

UNCERTAINTY IN F=0.00000 IN RATIO

108

RUN 122976 *** DISCRETE HOLE RIG *** NAS-3-14336 STANTON NUMBER DATA

HEATED STARTING LENGTH, M=0.4, SIX BLOWING ROWS, THEAT=1.0

RUN 123076 *** DISCRETE HOLE RIG *** NAS-3-14336 STANTON NUMBER DATA

HEATED STARTING LENGTH, M=0.4, SIX BLOWING ROWS, THEAT=1.0

LINEAR SUPERPOSITION IS APPLIED TO STANTON NUMBER DATA FROM

RUN NUMBERS 122976 AND 123076 TO OBTAIN STANTON NUMBER DATA AT TH=0 AND TH=1

PLATE	REXCOL	RE DEL2	ST(TH=0)	REXHOT	RE DEL2	ST(TH=1)	ETA	STCR	F-COL	STHR	F-HOT	LOGB
1	1265624.0	1.0	UUUUUUUU	1261416.0	1.0	UUUUUUUU	UUUU	UUUU	0.0000	UUUUUU	UUUUUUUUUUUUUUUU	
2	1321600.0	1.0	UUUUUUUU	1317206.0	1.0	UUUUUUUU	UUUU	UUUU	0.0000	UUUUUU	UUUUUUUUUUUUUUUU	
3	1377576.0	1.0	UUUUUUUU	1372996.0	1.0	UUUUUUUU	UUUU	UUUU	0.0000	UUUUUU	UUUUUUUUUUUUUUUU	
4	1433553.0	1.0	UUUUUUUU	1428787.0	1.0	UUUUUUUU	UUUU	UUUU	0.0000	UUUUUU	UUUUUUUUUUUUUUUU	
5	1489529.0	1.0	UUUUUUUU	1484577.0	1.0	UUUUUUUU	UUUU	UUUU	0.0000	UUUUUU	UUUUUUUUUUUUUUUU	
6	1545505.0	1.0	UUUUUUUU	1540367.0	1.0	UUUUUUUU	UUUU	UUUU	0.0000	UUUUUU	UUUUUUUUUUUUUUUU	
7	1601482.0	1494.2	0.002407	1595157.0	1481.7	0.002215	UUUU	1.000	0.0132	1.000	0.0125	1.000
8	1657458.0	1637.7	0.002642	1651947.0	2291.6	0.001787	0.324	1.373	0.0133	0.928	0.0119	3.043
9	1713434.0	1783.8	0.002578	1707738.0	3050.4	0.001517	0.411	1.349	0.0132	0.793	0.0122	2.904
10	1769411.0	1927.8	0.002568	1763528.0	3815.6	0.001419	0.448	1.352	0.0132	0.747	0.0127	2.909
11	1825387.0	2071.6	0.002568	1819318.0	4601.3	0.001341	0.478	1.361	0.0131	0.710	0.0124	2.826
12	1881363.0	2212.5	0.002466	1875108.0	5368.2	0.001292	0.476	1.315	0.0132	0.689	0.0124	2.802
13	1937340.0	2316.2	0.002404	1917509.0	6118.1	0.001431	0.405	1.287		0.766		
14	1993317.0	2384.4	0.002320	1946241.0	6160.1	0.001493	0.356	1.246		0.802		
15	2049294.0	2450.3	0.002250	1974973.0	6203.2	0.001503	0.332	1.212		0.809		
16	2010518.0	2514.8	0.002221	2003544.0	6246.9	0.001531	0.311	1.200		0.826		
17	2039496.0	2578.7	0.002207	2032715.0	6290.9	0.001532	0.306	1.196		0.829		
18	2068324.0	2641.9	0.002168	2061447.0	6334.6	0.001508	0.305	1.178		0.819		
19	2097152.0	2702.9	0.002063	2090179.0	6377.5	0.001475	0.285	1.124		0.803		
20	2125979.0	2763.3	0.002121	2118911.0	6420.6	0.001524	0.282	1.159		0.832		
21	2154808.0	2823.1	0.002019	2147644.0	6463.5	0.001456	0.279	1.106		0.797		
22	2183635.0	2881.4	0.002021	2176375.0	6505.9	0.001494	0.261	1.110		0.820		
23	2212463.0	2939.0	0.001969	2205107.0	6548.4	0.001462	0.258	1.084		0.804		
24	2241290.0	2996.1	0.001909	2233978.0	6591.2	0.001510	0.241	1.098		0.833		
25	2270118.0	3053.4	0.001980	2262850.0	6634.4	0.001499	0.243	1.096		0.829		
26	2298946.0	3109.9	0.001938	2291582.0	6677.4	0.001488	0.232	1.075		0.825		
27	2327774.0	3166.0	0.001950	2320314.0	6719.8	0.001460	0.251	1.085		0.812		
28	2356602.0	3222.0	0.001934	2349046.0	6762.4	0.001502	0.223	1.078		0.837		
29	2385430.0	3277.9	0.001937	2377778.0	6805.7	0.001507	0.222	1.083		0.842		
30	2414258.0	3333.6	0.001926	2406510.0	6849.3	0.001526	0.208	1.079		0.855		
31	2443086.0	3389.5	0.001877	2435242.0	6892.7	0.001492	0.205	1.054		0.837		
32	2471914.0	3442.4	0.001856	2464113.0	6935.9	0.001508	0.188	1.045		0.843		
33	2500742.0	3496.1	0.001866	2492985.0	6979.0	0.001490	0.202	1.053		0.840		
34	2529570.0	3549.9	0.001863	2521717.0	7021.8	0.001488	0.201	1.054		0.841		
35	2558398.0	3603.3	0.001836	2550448.0	7064.6	0.001486	0.191	1.041		0.842		
36	2587226.0	3655.2	0.001758	2579180.0	7106.7	0.001443	0.179	0.999		0.819		

STANTON NUMBER RATIO BASED ON ST*PR**0.4=0.0295*REX**(-.2)

STANTON NUMBER RATIO FOR TH=1 IS CONVERTED TO COMPARABLE TRANSPIRATION VALUE
USING $\text{A LOG}(1 + B)/B$ EXPRESSION IN THE BLOWN SECTION

RUN 010777 *** DISCRETE HOLE RIG *** HAS-3-14336

STANTON NUMBER DATA

TABO= 19.07 DEG C UIHF= 16.43 M/S TINF= 18.95 DEG C
PHO= 1.208 KG/M3 VISC= 0.14916E-04 MZ/S XYD= 12.9 CM
CP= 1009. J/KGK PR= 0.714

HEATED STARTING LENGTH, BLOWING FROM 7 TO 12 ROWS, M=0.9, THETA=0.0

PLATE	X	REX	TO	REENTH	STANTON NO	DST	DREN	M	F	T2	THETA	OTH
1	127.8	0.12651E 07	33.85	0.10000E 01	0.33271E-02	0.578E-04	0.					
2	132.8	0.13010E 07	33.79	0.10000E 01	0.27974E-02	0.544E-04	0.	0.00	0.0000	33.8	1.000	0.021
3	137.9	0.13770E 07	33.81	0.10000E 01	0.27014E-02	0.537E-04	0.	0.00	0.0000	33.8	1.000	0.021
4	143.0	0.14329E 07	33.81	0.10000E 01	0.25427E-02	0.527E-04	0.	0.00	0.0000	33.8	1.000	0.021
5	148.1	0.14889E 07	33.85	0.10000E 01	0.25401E-02	0.526E-04	0.	0.00	0.0000	33.8	1.000	0.021
6	153.2	0.15448E 07	33.86	0.10000E 01	0.25006E-02	0.523E-04	0.	0.00	0.0000	33.9	1.000	0.021
7	158.2	0.16008E 07	33.88	0.14937E 04	0.24921E-02	0.522E-04	28.	0.92	0.0297	20.0	0.069	0.021
8	163.3	0.16567E 07	33.85	0.17578E 04	0.28343E-02	0.544E-04	37.	0.91	0.0295	19.9	0.061	0.021
9	168.4	0.17127E 07	33.86	0.20208E 04	0.29779E-02	0.553E-04	44.	0.90	0.0292	19.9	0.061	0.021
10	173.5	0.17686E 07	33.83	0.22805E 04	0.30265E-02	0.558E-04	50.	0.91	0.0294	19.8	0.059	0.021
11	178.6	0.18246E 07	33.83	0.25536E 04	0.29836E-02	0.555E-04	56.	0.90	0.0292	19.9	0.062	0.021
12	183.6	0.18805E 07	33.86	0.28204E 04	0.29290E-02	0.550E-04	61.	0.91	0.0296	19.9	0.062	0.021
13	187.5	0.19230E 07	32.49	0.30474E 04	0.29200E-02	0.947E-04	63.					
14	190.1	0.19519E 07	32.24	0.31302E 04	0.28224E-02	0.946E-04	63.					
15	192.7	0.19807E 07	32.89	0.32100E 04	0.27058E-02	0.940E-04	63.					
16	195.4	0.20076E 07	32.99	0.32868E 04	0.26187E-02	0.898E-04	63.					
17	199.0	0.20376E 07	32.99	0.33618E 04	0.25858E-02	0.886E-04	63.					
18	200.6	0.20674E 07	32.99	0.34352E 04	0.25445E-02	0.870E-04	63.					
19	203.2	0.20962E 07	33.01	0.35071E 04	0.23987E-02	0.822E-04	63.					
20	205.8	0.21250E 07	33.21	0.35773E 04	0.24649E-02	0.847E-04	63.					
21	208.5	0.21530E 07	33.16	0.36467E 04	0.23438E-02	0.802E-04	63.					
22	211.1	0.21822E 07	33.23	0.37143E 04	0.23452E-02	0.816E-04	63.					
23	213.7	0.22115E 07	33.10	0.37824E 04	0.23774E-02	0.811E-04	63.					
24	216.3	0.22404E 07	33.29	0.38511E 04	0.23844E-02	0.829E-04	63.					
25	218.9	0.22694E 07	33.31	0.39192E 04	0.23354E-02	0.807E-04	63.					
26	221.6	0.22982E 07	33.31	0.39849E 04	0.22219E-02	0.817E-04	63.					
27	224.2	0.23270E 07	31.84	0.40496E 04	0.22580E-02	0.716E-04	63.					
28	226.8	0.23558E 07	33.31	0.41143E 04	0.22329E-02	0.822E-04	63.					
29	229.4	0.23846E 07	33.25	0.41786E 04	0.22212E-02	0.753E-04	63.					
30	232.0	0.24134E 07	33.75	0.42425E 04	0.22110E-02	0.781E-04	64.					
31	234.6	0.24423E 07	33.75	0.43052E 04	0.21365E-02	0.746E-04	64.					
32	237.3	0.24712E 07	33.60	0.43664E 04	0.21047E-02	0.731E-04	64.					
33	239.9	0.25002E 07	33.56	0.44267E 04	0.20751E-02	0.731E-04	64.					
34	242.5	0.25290E 07	33.20	0.44857E 04	0.20138E-02	0.684E-04	64.					
35	245.1	0.25578E 07	33.54	0.45441E 04	0.20327E-02	0.734E-04	64.					
36	247.8	0.25866E 07	33.25	0.46012E 04	0.19303E-02	0.762E-04	64.					

UNCERTAINTY IN REX=27976.

UNCERTAINTY IN F=0.00000 IN RATIO

109

RUN 010977 *** DISCRETE HOLE RIG *** HAS-3-14336

STANTON NUMBER DATA

TADB= 17.64 DEG C UINF= 16.39 M/S TINP= 17.52 DEG C
 PHO= 1.220 KG/M3 VISC= 0.14714E-04 M2/S XYD= 12.9 CM
 CP= 1009. J/KGK FR= 0.715

HEATED STARTING LENGTH, BLOWING FROM 7 TO 12 ROWS, M=0.9, THETA=1.0

PLATE	X	REX	TO	REENTH	STANTON NO	DST	DREEN	M	F	T2	THETA	DTM
1	127.8	0.12790E 07	34.63	0.10000E 01	0.34382E-02	0.518E-04	0.					
2	132.8	0.13355E 07	34.63	0.10000E 01	0.27421E-02	0.473E-04	0.	0.00	0.0000	34.6	1.000	0.018
3	137.9	0.13921E 07	34.63	0.10000E 01	0.26411E-02	0.467E-04	0.	0.00	0.0000	34.6	1.000	0.018
4	143.0	0.14487E 07	34.65	0.10000E 01	0.25143E-02	0.459E-04	0.	0.00	0.0000	34.6	1.000	0.018
5	148.1	0.15052E 07	34.65	0.10000E 01	0.24725E-02	0.457E-04	0.	0.00	0.0000	34.6	1.000	0.018
6	153.2	0.15618E 07	34.68	0.10000E 01	0.23986E-02	0.452E-04	0.	0.00	0.0000	34.7	1.000	0.018
7	159.2	0.16104E 07	34.72	0.15053E 04	0.23213E-02	0.447E-04	28.	1.03	0.0334	33.8	0.947	0.018
8	163.3	0.16750E 07	34.67	0.34292E 04	0.23828E-02	0.452E-04	39.	1.22	0.0396	35.1	1.025	0.018
9	168.4	0.17315E 07	34.63	0.58591E 04	0.23707E-02	0.452E-04	49.	1.08	0.0348	34.6	0.996	0.018
10	173.5	0.17891E 07	34.67	0.79504E 04	0.22003E-02	0.442E-04	56.	1.16	0.0375	34.4	0.986	0.018
11	178.6	0.18447E 07	34.61	0.10164E 05	0.21477E-02	0.441E-04	61.	0.93	0.0302	34.2	0.975	0.018
12	183.6	0.19012E 07	34.61	0.11953E 05	0.21518E-02	0.441E-04	66.	1.08	0.0349	34.2	0.975	0.018
13	187.5	0.19442E 07	34.06	0.13973E 05	0.21497E-02	0.716E-04	69.					
14	190.1	0.19733E 07	33.86	0.14035E 05	0.21064E-02	0.704E-04	69.					
15	192.7	0.20025E 07	34.51	0.14095E 05	0.20404E-02	0.709E-04	69.					
16	195.4	0.20317E 07	34.63	0.14154E 05	0.19721E-02	0.677E-04	69.					
17	198.0	0.20610E 07	34.63	0.14211E 05	0.19406E-02	0.667E-04	69.					
18	200.6	0.20902E 07	34.63	0.14267E 05	0.19067E-02	0.651E-04	69.					
19	203.2	0.21193E 07	34.76	0.14321E 05	0.17914E-02	0.616E-04	69.					
20	205.8	0.21484E 07	34.88	0.14374E 05	0.18245E-02	0.628E-04	69.					
21	208.5	0.21775E 07	34.84	0.14426E 05	0.17332E-02	0.595E-04	69.					
22	211.1	0.22067E 07	34.91	0.14476E 05	0.17224E-02	0.600E-04	69.					
23	213.7	0.22358E 07	34.89	0.14525E 05	0.16592E-02	0.573E-04	69.					
24	216.3	0.22651E 07	35.07	0.14574E 05	0.16974E-02	0.596E-04	69.					
25	218.9	0.22944E 07	35.05	0.14624E 05	0.16790E-02	0.585E-04	69.					
26	221.6	0.23235E 07	34.97	0.14671E 05	0.15791E-02	0.587E-04	69.					
27	224.2	0.23526E 07	33.62	0.14718E 05	0.16496E-02	0.524E-04	69.					
28	226.8	0.23818E 07	34.89	0.14767E 05	0.17220E-02	0.630E-04	69.					
29	229.4	0.24109E 07	34.91	0.14817E 05	0.16580E-02	0.566E-04	69.					
30	232.0	0.24400E 07	35.39	0.14865E 05	0.16371E-02	0.583E-04	69.					
31	234.6	0.24692E 07	35.41	0.14911E 05	0.15550E-02	0.550E-04	69.					
32	237.3	0.24984E 07	35.22	0.14957E 05	0.15516E-02	0.543E-04	69.					
33	239.9	0.25277E 07	35.20	0.15002E 05	0.15299E-02	0.544E-04	69.					
34	242.5	0.25568E 07	34.86	0.15045E 05	0.14753E-02	0.506E-04	69.					
35	245.1	0.25860E 07	35.14	0.15089E 05	0.14990E-02	0.546E-04	69.					
36	247.8	0.26151E 07	34.89	0.15131E 05	0.13903E-02	0.562E-04	69.					

UNCERTAINTY IN REX=28284.

UNCERTAINTY IN F=0.00000 IN RATIO

///

1. Report No. NASA CR-3219	2. Government Accession No.	3. Recipient's Catalog No.	
4. Title and Subtitle FULL-COVERAGE FILM COOLING ON FLAT, ISOTHERMAL SURFACES: A SUMMARY REPORT ON DATA AND PREDICTIONS		5. Report Date January 1980	
		6. Performing Organization Code	
7. Author(s) M. E. Crawford, W. M. Kays, and R. J. Moffat		8. Performing Organization Report No. HMT-23	
		10. Work Unit No.	
9. Performing Organization Name and Address Stanford University Stanford, California 94305		11. Contract or Grant No. NAS 3-14336	
		13. Type of Report and Period Covered Contractor Report	
12. Sponsoring Agency Name and Address National Aeronautics and Space Administration Washington, D.C. 20546		14. Sponsoring Agency Code	
15. Supplementary Notes Final report. Project Manager, Raymond E. Gaugler, Fluid System Components Division, NASA Lewis Research Center, Cleveland, Ohio 44135.			
16. Abstract An experimental and analytical study of the heat transfer and fluid mechanics characteristics of full-coverage film cooling has been under way since 1971. This report summarizes the results for flat, isothermal plates for three injection geometries (normal-, slant-, and compound-angle) and presents some new data concerning the spanwise distribution of the heat transfer coefficient within the blowing region. Data are also presented for two different numbers of rows of holes (6 and 11). The experimental results summarized herein can be predicted with a two-dimensional boundary layer code, STANCOOL, by providing descriptors of the injection parameters as inputs. STANCOOL is a modification of a published program, STAN5, and the necessary modifications are described in this report.			
17. Key Words (Suggested by Author(s)) Boundary layer Numerical Heat transfer Film cooling Computer program Turbine blade cooling Turbulence		18. Distribution Statement Unclassified - unlimited STAR Category 34	
19. Security Classif. (of this report) Unclassified	20. Security Classif. (of this page) Unclassified	21. No. of Pages 113	22. Price* A06

* For sale by the National Technical Information Service, Springfield, Virginia 22161

NASA-Langley, 1980

112

90 %

50 %

END

6-11-81